UNIVERSITÀ DEGLI STUDI DI PADOVA
Department of Industrial Engineering
Doctoral program in Industrial Engineering
Curriculum: Energy Engineering
XXXV Cohort

SIZING AND CONTROL OF A HYBRID HYDRO-BATTERY-FLYWHEEL STORAGE SYSTEM FOR FREQUENCY REGULATION SERVICES

Thesis for the degree of Doctor of Philosophy

Coordinator:
prof. Giulio Rosati

Supervisor:
prof. Giovanna Cavazzini

Co-Supervisors:
prof. Juan Ignacio Pérez-Díaz
prof. Guido Ardizzon

Ph.D. Candidate:
Stefano Casarin

Padova, March 2023

Stefano Casarin: *Sizing and control of a Hybrid hydro-battery-flywheel storage system for frequency regulation services*, Thesis for the degree of Doctor of Philosophy. © Padova, March 2023

Supervisor: *prof.* Giovanna Cavazzini

Template by Jacopo Schiavon: github.com/jschiavon/clean-thesis.

Abstract

Energy security and environmental challenges are some of the drivers for increasing the electricity generation from non-programmable Renewable Energy Source (RES), adding pressure to the grid, especially if located in weakly connected (or isolated) islands, like Sardinia. Variable-speed Pumped Storage Hydro Power (PSHP) can offer a high degree of flexibility in providing ancillary services (namely primary and secondary regulations), but due to the hydro-mechanical nature of the equipment, sudden variations in the power output cause wear and tear. Other energy storage devices can not compete with PSHP in terms of energy and power availability. This work aims to assess the potential benefits derived from the hybridization of a PSHP with Battery Energy Storage System (BESS) and Flywheel Energy Storage System (FESS) in providing frequency regulation services to the grid of the Sardinia island (Italy). The focus of the study tries to cross both the plant owner point of view, whose aim is to have a smooth PSHP operation and the economic incentive to hybridize the plant, and the Transmission System Operator's, whose aim is to have a fast reacting plant that better stabilizes the grid frequency. This is done by simulations of a detailed dynamic model of the PSHP(whose hydraulic machine has been characterized from real experimental data), BESS and FESS, considering different power ratings of these last two technologies. Moreover, two power management strategies are presented, based on different criteria, to effectively coordinate the devices making up the Hybrid Energy Storage System (HESS). First the simulations are performed open-loop, to assess the impact of various combinations of installed BESS and FESS powers over the wear and tear of the equipment. Later the model is

used in an optimization procedure to find the combination of installed BESS and FESS powers and the respective control parameters that would guarantee the maximum economic return at the end of the investment life. Last, the model is included into a Sardinian power system model and simulated in a future scenario with high RES penetration, assessing the plant capabilities to effectively contain and restore the frequency. Results show that there is not a catch-all solution in terms of hybridization and that a trade-off must be made between the plant owner's urge to smoothly operate the plant in order to reduce the equipment degradation, and the TSO's objective to have fast responsive plants providing high quality frequency regulation services. If on one hand open-loop simulations show that the hybridization reduce the main wear and tear indicators, on the other the optimal hybrid system limits the plant ability to contain the frequency excursions in closed-loop simulations, as the optimization problem was formulated over the plant owner's interests. The results show that there much potential for frequency stabilization and wear and tear reduction, but more techno-economic data is required to fully investigate the benefits of this configuration.

μή φατε κακά
Non dite cose malvagie

Contents

List of Figures

List of Tables

1 Introduction

In the age of Anthropocene, the most compelling challenge humanity faces is the containment of global warming, the driving force of climate change, whose initial effects are already affecting large portions of the ecosystem.

A 1.5 °C temperature increase to preindustrial levels target was established by the international community [1], which is only achievable by rapidly and drastically reducing greenhouse gas (GHG) emissions, as the mean global temperature increase is already 1.1 °C [2]. In 2019 the energy sector was responsible for 34 % (20 $GtCO_{2eq}$) of global GHG emissions [3], showing an increasing trend that was only slowed down thanks to the 2020 pandemic.

In this context, Renewable Energy Sources (RESs) have seen an exponential growth in the last 20 years, with wind electricity generation increasing from 104 TWh in 2005 to 1427 TWh in 2019, and solar Photovoltaic (PV) generation from 4 TWh to 681 TWh for the same period [4]. Even so, global RES generation is expected to expand by almost 75 % (2400 GW) between 2022 and 2027, showing an 85 % acceleration with respect to the previous five-year trend [5]. High fossil fuel and electricity prices resulting from the global energy crises made RES generation more economically attractive, and Russia's invasion of Ukraine highlighted the strategic value of self-sufficiency and energy security, all of which can be guaranteed by RES generation.

If on one hand wind and PV generation contribute in the reduction of fossil fuels dependence – a matter of strategic importance for net importers such as Europe – on the other it introduces new challenges in the energy

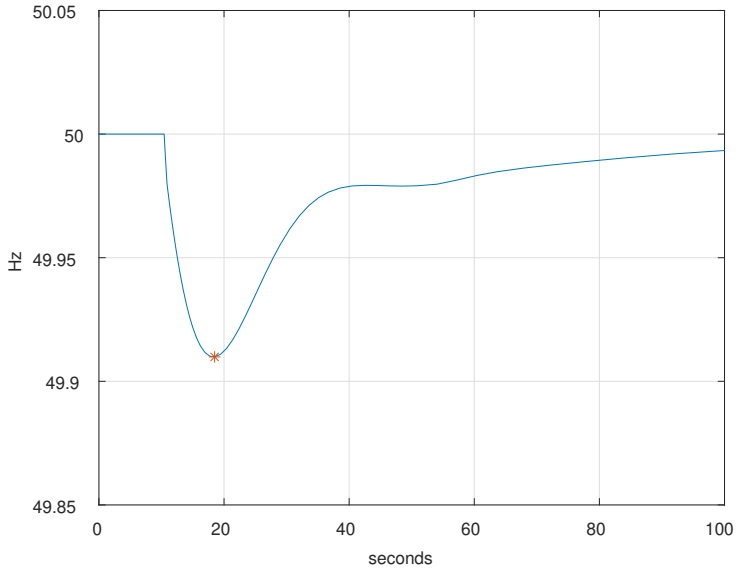

FIGURE 1.1: Frequency deviation following a step-like generation loss. A red asterisk marks the frequency nadir.

management, especially regarding the stability of the electric grid [6]. The next section outlines some key concepts regarding the electric power system and its stability.

1 HINTS OF GRID FREQUENCY STABILITY

In Europe and much of the world, AC power is transmitted and delivered to utilities at 50 Hz. The instantaneous value of the grid frequency results from the balance of total active power inputs, i.e. the sum of all the instantaneous powers from each generation node, and the sum of all the outputs, i.e. all the instantaneous power consumed by each connected load. If perfect active powers' balance is achieved, the frequency maintains its value constant over time at the reference value. Whenever a power imbalance occurs, due to either supply or demand-side, during the transient a change in the kinetic energy stored in motors and generators connected to the grid occurs. The detectable effect is a variation in the

frequency with respect to the reference value, decreasing if the demand exceeds the supply (Figure 1.1) and vice-versa [7].

Non-dispatchable RESs as wind and solar PV are characterized by high variability and unpredictability in power generation, resulting in more frequent and more intense power imbalances – hence frequency deviations – which, in extreme cases, could lead to catastrophic consequences [9]. Such variability in RES generation spans both intra-day and intra-hour time periods, as can be seen from Figure 1.2, reporting five representative days of wind power generation in two sites [8]. No information is provided about the location of the sites, but their mean generated power is 25 % and 30 % of the installed power, respectively, and in both cases the standard deviation equates the mean generated power. Moreover RESs are most of the time connected to the grid via power electronics, not contributing to the grid inertia unless additional measures are undertaken, which will be discussed later [10].

On an European level, regulations exist to coordinate and harmonize protocols, interventions, and the respective markets for maintaining the frequency stability in the different synchronous areas[1] [11, 12].

"Ancillary services" refer to the range of services that are necessary to maintain the stability and security of the electric system [13]. These services normally include active and reactive power control: the frequency stability depends on the balance of active powers, whereas voltage stability on the balance of reactive powers. Under normal operating conditions, voltage control and frequency control are decoupled and managed separately. As this study focuses on frequency stability and control, reactive powers and voltage stability will not be discussed in the rest of the work.

Among the ancillary services, two are of particular interest in this work: Primary Regulation, i.e. the provision of Frequency Containment Reserve (FCR), and Secondary Regulation, i.e. the provision of Frequency

[1] Five synchronous areas are defined within European Network of Transmission System Operators for Electricity (ENTSO-E) geographical area, being: Continental Europe, Nordic, Great Britain, Ireland and Northern Ireland, and Baltic [11].

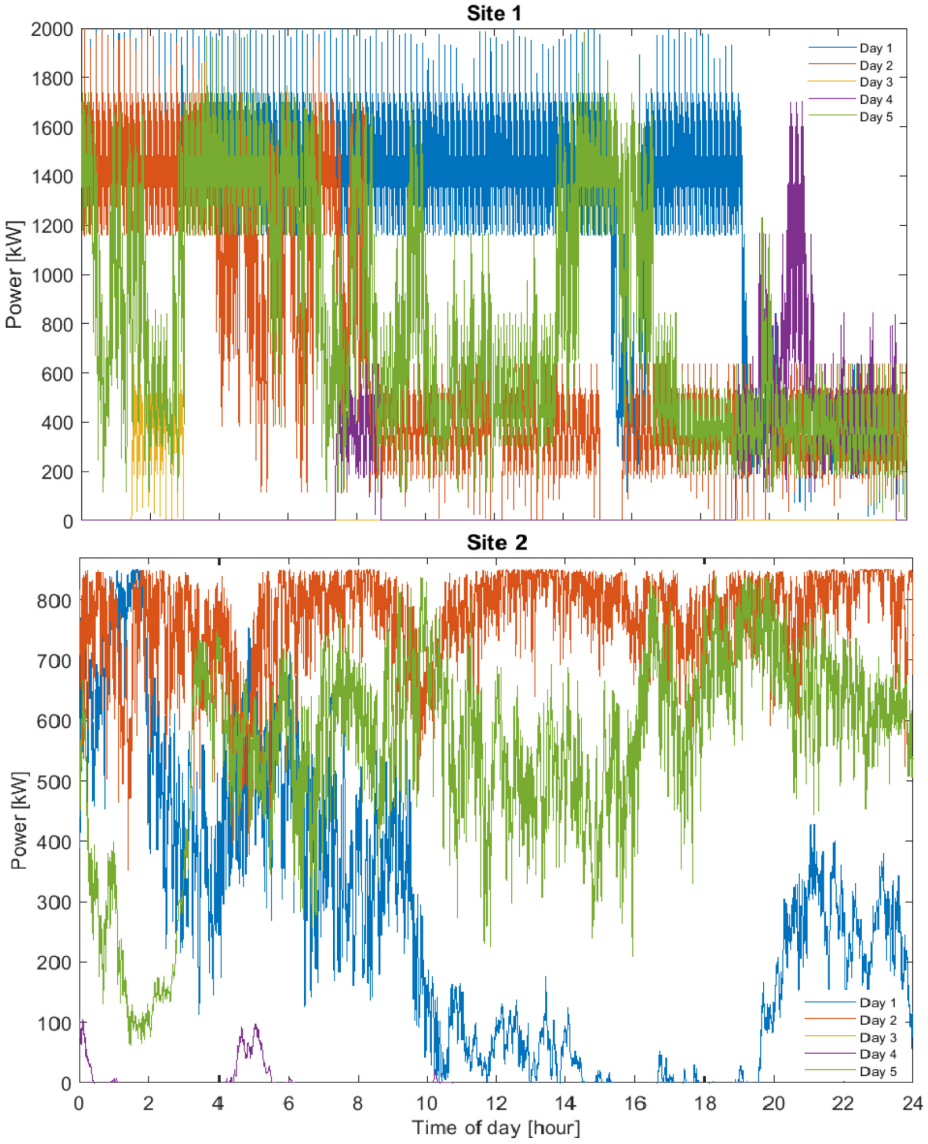

FIGURE 1.2: Wind power profiles for 5 representative days in two sites [8].

Restoration Reserve (FRR).

A short description of each of this service is presented in the following paragraphs.

1.1 *Frequency Containment Reserve*

Primary regulation refers to the active power delivered after a frequency imbalance event in order to stop its deviation from the reference value. The frequency value drops (grows) until the generated power deficit (surplus) is compensated by the collective effort of all the plants participating in the service, incrementing (reducing) the power output, thus delivering the upwards (downwards) FCR.

Primary regulation is the most urgent ancillary service and must be fully activated within seconds from the occurrence of the event. On a state-level, Transmission System Operators (TSOs) define the conditions under which FCR must be provided. From country to country, FCR may be subject to a market-based or a mandatory scheme. With the former, a generator can propose an offer that may result in a bilateral agreement, without being obligated to participate in the service. With the latter, generators connected to the grid are required to reserve a certain amount of generation capacity destined to FCR, for a price determined by the TSO or other agencies (the case for France) or for free (the case for Italy) – or a mixture of the two schemes (the case for Ireland and Nortern Ireland) [14].

FCR is typically delivered with a droop-based control system. Whenever a frequency deviation Δf (Hz) occurs, the target power variation the plant must achieve, ΔP (MW), is calculated with basis on the reference frequency f_{ref} (Hz), the plant rated power P_r (MW), and the permanent droop σ, which is set by the plant owner according to the TSO's regulations:

$$\frac{\Delta P}{P_r} = -\frac{1}{\sigma} \cdot \frac{\Delta f}{f_{ref}}. \tag{1.1}$$

The minus sign implies that for a negative frequency deviation the plants must deliver a positive (upwards) power delivery, and vice-versa.

TSOs define both the magnitude of the permanent droop and the mode of delivery of the FCR. For instance, Terna (the Italian TSO) mandates that each unit participating in the FCR service (which is mandatory for generation units whose rated power is greater or equal than 10 MW_e) must deliver 50 % of the FCR within 15 s from the start of the frequency variation, and 100 % within 30 s [15]. Depending on the type of plant (steam/gas turbine, hydropower, combined-cycle, ...), its rated power, its location (insular or continental Italy), and the magnitude of the frequency error, up to tens of MW may have to be delivered within 15 s to 30 s, with the related consequences in terms of thermo/hydro-mechanical stresses and loss of efficiency.

1.11 *Frequency Restoration Reserve*

Secondary regulation is aimed to restoring the frequency to the rated value after it has been successfully stabilized by the FCR. FRR consists in delivering the necessary energy to make up for the energy deficit/surplus during the time FCR was not fully activated, and as such it is a service that is delivered over a longer time period than FCR.

FRR may be controlled manually (mFRR) or automatically (aFRR). aFRR is controlled by an Automatic Generation Control (AGC), a system that issues a control signal that adjusts the generators' set point in the respective control area [16]. Participation in secondary regulation is market-based in most of Europe [14].

In Italy a plant is qualified to provide FRR if it is able to track a control signal linearly increasing from 0 % (downward FRR fully active) to 100 % (upward FRR fully active) in 200 s (100 s for the islands of Sicily and Sardinia) [15].

1.III Present and future challenges

As outlined in the previous paragraphs, the electric system is currently dealing with conflicting needs. On one hand there is the need to decarbonize the electricity generation, which goes through the installation of new non-programmable RES generators. On the other hand, the need to guarantee the system stability and security, which requires continuous balance between electricity generation and demand.

Until a few years ago, TSOs had to choose between two options to deal with this dilemma. The first option was to guarantee frequency stability thanks to the power modulation of programmable power plants, traditionally fossil-fuel powered plants. The issue with this option is that these plants are designed to operate at maximum efficiency at design conditions: at partial load the process efficiency drops, increasing the burned fuel per unit of electric energy generated. Moreover continuous power adjustments cause thermo-mechanical stress in several parts, increasing the operation and maintenance routines and/or repair and replacement of components. This of course implies additional emissions due to the increased consumption of the parts, besides interfering with the plant uptime period.

The second option was to undercut the excess renewable generation. This is a one-way solution (RES generation can not be incremented on command), that is effective in avoiding thermal plants to provide downward regulation. The issue with this approach is that by doing so, low-carbon renewable energy is wasted and not sold in the electricity market, thus prolonging the investment payback times and reducing the competitiveness of RES installations.

Since the end of XX century, the scientific community and industry stakeholders have begun investigating in a third option for the problem of RES integration: energy storage, whose main technologies and recent developments will be described in the next section.

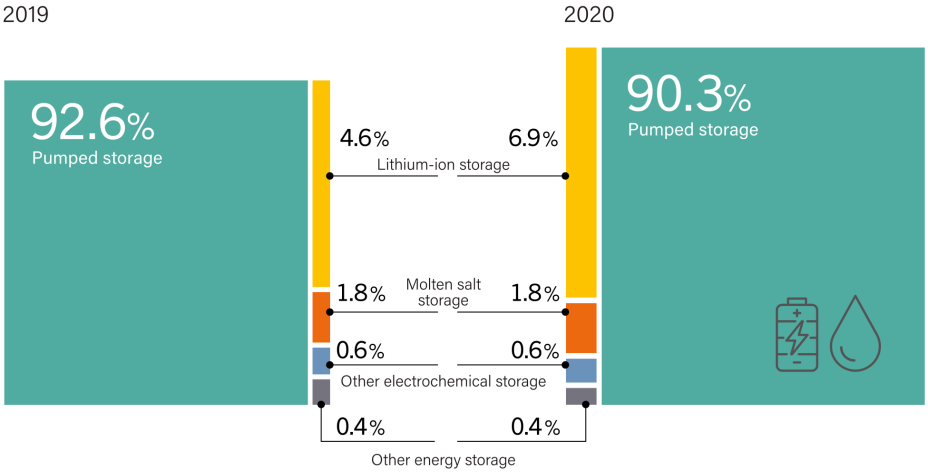

FIGURE 1.3: Global share of electric energy storage capacity [23, 24].

II ENERGY STORAGE TECHNOLOGIES

In this context energy storage technologies refer to a range of Energy Storage Devices (ESDs) that convert electrical energy from the grid into a different form that can be stored (charge process) and, when the time comes, converted back to electricity, delivered to the grid (discharge process).

ESDs work according to different physical principles, and, besides that, each technology presents its own properties in terms of energy and power storage capacity, responsiveness, economic and technological maturity [17–22].

In 2020 the global operational energy storage capacity reached 191.1 GW, growing by 3.4 % from the previous year [23]. Over 90 % of electric energy is stored by Pumped Storage Hydro Power (PSHP), followed by Li-ion batteries (6.9 %) while all the other storage systems combined account for less than 3 % (Figure 1.3). From this data it is clear that Li-ion Battery Energy Storage Systems (BESSs) are experiencing the highest growth in yearly installations, and that PSHP is the leading technology in terms of installed storage capacity.

Among the energy storage technologies, PSHP is the most mature, as the first hydro installations date back more than 100 years. Indeed research is still ongoing on hydropower technology [25–32], especially in relation to the increasing necessity to provide ancillary services [33–37], requiring wider operating ranges and greater flexibility. Hydropower is not a catch-all solution: as any other technology it presents its own advantages and drawbacks [20, 29]. Recently a new approach to the issue of energy storage, renewables integration, and grid stability has emerged: the idea to enhance generation/storage units hybridizing it with one or more ESD of smaller size and effectively coordinate the operation of each unit in order to improve the performance with respect to the units being operated individually.

Among the several types of energy storage technologies, there are four of particular interest for this work: PSHP, BESS, Flywheel Energy Storage System (FESS), and Supercapacitor Energy Storage System (SC). The next paragraphs will present an outline of these energy storage technologies; later on, a state of the art on hybridization solutions taken from the literature will be presented; the chapter will conclude with the presentation of this research motivation and goals followed by a detailed description of the case-study used in the research.

II.1 *Pumped Storage Hydro Powers*

Between 1990 and 2017, the yearly growth in hydropower generation in Organisation for Economic Co-operation and Development (OECD) countries was 0.6 %, whereas for non-OECD was 3.9 % [38]. High investment costs (higher than for wind and solar PV), the scarcity of new suitable places for new installations, together with public opposition due to environmental and social concerns, are the main reasons that slowed down the growth of hydropower generation in the last decades [5, 39].

PSHP stores energy by taking advantage of the geodetic difference between an upper and a lower reservoir, pumping water from the latter

to the former – thus converting electrical energy into potential energy – and, when necessary, discharging the water through a turbine, converting water energy back into electricity [17]. The common elements in all PSHPs are: i) an upper and a lower reservoir (basins) where the water is stored, ii) hydraulic machinery, iii) conduits connecting both reservoirs with the hydraulic machines, iv) electric motors/generators, and in case of a very long water column (conduit) v) one or more surge tanks. In ternary configuration, the hydraulic unit is made of a (typically radial) pump, a turbine (Pelton or Francis), and a synchronous motor/generator. In binary configuration (Figure 1.4), a reversible (Francis) pump-turbine is coupled with a synchronous motor/generator. A PSHP can include one or more hydraulic units. Last, in quaternary configuration, the unit is made of one variable-speed pump and a conventional (most commonly, but not exclusively, a Pelton) turbine, each equipped with their own electrical machine [40, 41]. This configuration offers the highest flexibility – as the variable-speed pump and turbine are operated independently and are installed in hydraulic short-circuit (see page 13) – at high capital investment costs.

PSHPs offer the possibility to store energy at very low cost compared to other technologies [42–44]. Nevertheless, besides the necessity of considerable investments and suitable locations, PSHP suffers from some performance limitations with respect to other ESDs.

The first aspect that deserves consideration is that conventional hydraulic machines (pumps, turbines) are coupled with synchronous motors/generators. On one hand this is an advantage from the TSO's perspective, as the rotating masses of both the electric and hydraulic machines contribute to the grid inertia (damping small frequency oscillations). On the other hand, this is a limiting factor for hydraulic machinery as they must operate at fixed rotational (synchronous) speed. Fixed-speed pumps can not modulate their power input (their working point depends on the pump characteristic curve and the hydraulic circuit resistive curve). Fixed-speed turbines enjoy an additional degree of freedom, since they

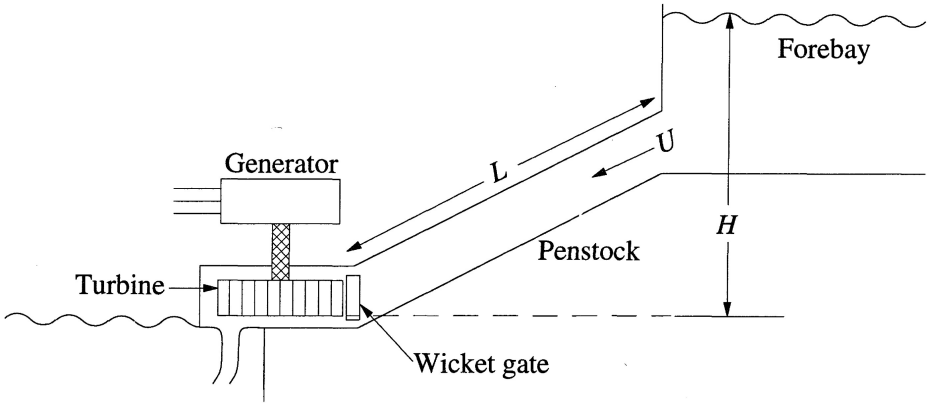

FIGURE 1.4: Simplified scheme of hydropower plant in binary configuration. The upper reservoir is indicated as "Forebay", and the conduit as "penstock". In case of a PSHP, the machine would be a reversible pump-turbine coupled with a motor/generator. Picture taken from Ref. [7].

are equipped with the wicket gate/guide vanes apparatus (needle valves and nozzles in case of Pelton turbines). The Guide Vanes Opening (GVO) controls the inlet flow rate, therefore the electric power output.

Related to this matter, the second key point worth to mention is that hydraulic machines are designed to have the Best Efficiency Point (BEP) at rated hydraulic conditions: fixed values of rotational speed, head, and flow rate [26]. The BEP is unique, therefore when adjusting the turbine power output during the provision of ancillary services, the machine will inevitably shift the working point to a region of lower hydraulic efficiency.

PSHPs operate with a water column of several hundred meters long: sudden shifts in the turbine working point translate into sharp variations in GVO, which cause mechanical solicitations and premature ageing. Frequent and sudden power adjustments cause pressure waves (water hammer), damaging not only the guide vanes and their auxiliaries (blades, pins, ...), but also the conduits in the long run [45]. Moreover, pressure

TABLE 1.1: Reference values of transition times between hydro power plants operational modes in in binary and ternary configuration, adapted from Ref. [47].

Pump Turbine Mode change	Time (s) A	B	C	D	E
Standstill ⟶ Turbine mode	90	75	90	90	65
Standstill ⟶ Pump mode	340	160	230	85	80
Syn. Condenser ⟶ Turbine Mode	70	20	60	40	20
Syn. Condenser ⟶ Pump Mode	70	50	70	30	25
Turbine Mode ⟶ Pump Mode	420		470	45	25
Pump Mode ⟶ Turbine Mode	190	90	280	60	25
Reversible pump-turbine **A** – advanced conventional **B** – extra fast response conventional **C** – variable speed					
Ternary set **D** – with hydraulic converter + hydraulic short circuit, horizontal, Francis Turbine **E** – same as D, vertical with Pelton Turbine					

waves negatively impact in the system's ability to provide ancillary services [46].

The last matter of concern for PSHPs in terms of support for the grid stability is that in binary configuration the hydraulic machine is characterized by unstable operating areas which have to be avoided in order to prevent damages or control issues. The existence of these areas, both in pumping and in generation mode, force the operator to transit from one operating mode to the other in a longer period of time.

In binary configuration the reversible hydraulic machine is very slow in transiting from one operating mode to another (Table 1.1): the transition from standstill mode to "charge" (pump) or "discharge" (turbine) mode requires at least one minute, while shifting from charge mode to discharge mode and vice-versa often takes more than one minute (except for some

very specific configurations, D and E in Table 1.1). Ternary configuration is faster in some cases, but still the process is slow if compared to other types of ESD due to the hydraulic column connected to the machine.

Hydraulic short-circuit can be a way to increase the flexibility of a PSHP. This type of operation makes use of turbine and pump groups working simultaneously, with the former discharging water at the latter's inlet. Hydraulic short-circuit is relatively simple and inexpensive to implement, but comes at the cost of a reduction in hydraulic efficiency. Notable examples of plants with groups operating in hydraulic short-cricuit are Kops II (Austria) and Gorona del Viento in the El Hierro island (Spain).

As pointed out so far, there is a growing necessity for flexibility in hydropower plants, and technological advancements have moved in that direction. The development of the variable-speed technology marked an important milestone in hydropower technology.

Variable-speed hydropower

Variable speed operation means decoupling the rotational speed of the pump/turbine runner from the frequency of the grid, a solution first adopted in Japan [48], and later on in Europe [49]. According to the similarity theory, the characteristic curves of a hydraulic machine are unique for the rotational speed: by its adjustment the machine can operate at the point of maximum efficiency at more than one operational condition [26, 29, 49–54].

In order to decouple the unit's speed from the grid's frequency it's necessary to connect the electrical machine to the grid through power electronics. There exist two options for this purpose. One is using a Doubly Fed Induction Generator (DFIG) whose rotor is connected to the grid through a power converter with a power rating equal to the rotor's one. Another option is using a fully fed synchronous generator with the stator connected to the grid through a power converter of the same power rating as the synchronous machine. Both options allow controlling the

unit's rotational speed. The latter is more flexible specially as regards the unit's start-up in pump mode and the transitions between operation modes, albeit at the expense of higher investment cost. In general this option is adopted when the generation does not exceed 60 MVA [55]. A DFIG is the preferred solution when the generation exceeds 60 MVA: the power electronics' rating is a fraction (typically 10 % to 25 % [56, 57]) of the machine power rating [54, 55], keeping the investment costs low for high generation powers. In fact, with a 60 MVA converter it is possible to feed a DFIG of up to 400 MVA, controlling the rotational speed by $\pm$10 % of the synchronous speed, which is acceptable for most PSHPs applications during normal operation [50, 55, 58].

A disadvantage of the variable-speed technology is that the electrical machine rotor is decoupled from the grid frequency thus not contributing to the system inertia [59]. In this case, the inertial contribution must be provided by other means. This is done with an additional control loop that provides the so-called virtual or synthetic inertia. The recorded frequency error signal (properly filtered) is processed by a proportional-derivative controller issuing the respective power set-point [10, 50, 60, 61].

Variable-speed technology innovation is not only limited to the electric equipment, but also involves innovative design of the runner and stator of the hydraulic machine, to extend the machine operational capabilities over a wider range, taking into account the stability and cavitation limits [26, 29, 62].

Overall, technological advancements make hydropower much more flexible and responsive than in the past. As already stated, hydropower generation and PSHP installations are constrained by the scarcity of suitable locations, whereas their operation is limited by the location hydrological conditions: in 2021 it is estimated that global hydropower generation fell down to 4218 TWh, around 3.5 % [63]. In this sense, it is fundamental to find solutions that do not rely only on freshwater to guarantee stable and continuous energy storage (which would have also the advantage of causing less environmental harm, as freshwater hydropower heavily

FIGURE 1.5: Bird-eye view of the Okinawa sPSHP. The upper reservoir has an octagonal shape, and tetrapods are placed at the outlet of the tailrace for protection against waves [64].

interferes with hydrological basins and the biosphere).

SEAWATER-PUMPED STORAGE HYDRO POWER

Few sites are available for new installations of hydropower systems in Europe and especially in Italy. An alternative approach was first designed and experimented in Japan, with the Okinawa Yanbaru Seawater Pumped Storage Power Station, which entered into service in 1999 (Figure 1.5). The first of this kind, with an available head of 136 m and a maximum power output of 30 MW, the plant functioned as a research facility for 5 years.

The underlying idea of a seawater seawater Pumped Storage Hydro Power (sPSHP) is to use the sea as the lower reservoir, and to realize an artificial upper reservoir on the top of a cliff, taking advantage of the geodetic height difference. At times of low energy price (e.g. at night), the seawater is pumped into the upper reservoir; later on the same water

is discharged through a turbine, recovering part of the electrical energy.

Among the benefits of such a plant there are [65]:

- reduced construction costs: only the upper reservoir needs to be realized, and
- the storage capacity only depends on the upper reservoir (the lower is infinite);
- the pump-turbine design is simpler, as the available head is small;
- the site can be chosen to be closer to the main generation sites than a conventional PSHP, if the orographic conditions allow it.

At the same, such a technology is not exempt from drawbacks:

- seawater favours corrosion of the metallic components;
- marine organisms may stick to the surfaces, causing fouling and increasing the hydraulic losses;
- there exists the risk of seawater infiltration in the environment;
- water intake and outtake may have a negative impact on local currents and biosphere.

Nevertheless, technical and technological solutions were identified for each and every detected issue: these plants can be realized and operated [42, 64, 65], as demonstrated also by the relatively recent interest in such plants [66].

Hydropower technology, and in particular PSHP for energy storage, is playing and will play a crucial role in the decarbonization process that awaits the energy sector.

1.1.1 *Battery Energy Storage Systems*

BESSs are devices that store electricity converting it into chemical energy. A battery is made of one or more electrochemical cells with two liquid,

paste, or solid electrolytes: a positive (anode) and a negative (cathode). Much research was done in the last decades in BESS technology for a variety of purposes, from electrical mobility to stationary applications [17, 20, 42, 67–72], leading to a considerable reduction in capacity costs (a 90 % drop since 2010 [63]) which are expected to further fall in the foreseeable future [43, 44, 72]. BESSs have also been extensively studied for grid storage purposes, meaning their suitability to provide ancillary services, demonstrating their effectiveness in contributing to control frequency excursions [18, 21, 36, 73–82]. As a matter of fact, in Germany the majority of recent BESS large-scale projects are for FCR purposes, and installed BESS capacity increased on a 10 % basis between 2018 and 2019 [78].

In the first place, battery technologies differ as a function of the type of materials and electrolytes used. Several technologies exist (lead acid, flow batteries, lithium-ion, metal air, just to name a few) that differ in terms of energy and mass density, round-trip efficiency, operation temperature, resistance to ageing, technological maturity, costs, etc. [21, 22].

Li-ion BESSs occupy a special place among batteries, as most of the research on batteries has focused on this particular technology due to their versatility and applicability to a wide range of fields: from consumer electronics to electrical mobility, from domestic storage to industrial applications [72, 78]. Li-ion BESSs[2] enjoy high energy density, low self-discharge rates (less than 5 % on a monthly basis), and an acceptable number of charge/discharge cycles before reaching end of life: up to 20 000 [81]. Li-ion BESSs are particularly susceptible to cycle ageing and temperature excursions: to prolong their useful life, their State Of Charge (SOC) is maintained within certain ranges, and during operation they are in general placed in rooms with temperature control [83–86]. It is also worth it to point out that the power rating of a BESS is determined by the inverter coupled to the battery bank, and that, especially for industrial

[2] More than one type of Li-ion batteries exist, such as $LiFePO_4$, Lithium Manganese Oxide, Lithium-titanate. This study does not focus on a specific type of Li-ion batteries, but will deal with it in general terms.

applications, single battery cells are replaced once they reach end of life.

II.III *Flywheel Energy Storage Systems*

A FESS is an ESD that converts electricity into mechanical (kinetic) energy by setting in motion a rotor. In charge mode electrical energy is used to accelerate the rotor, while in discharge mode the rotor rotational energy is converted into electricity, thus causing its deceleration. The flywheel rotor is placed inside a pressurized vessel: a vacuum pump is employed to remove air, hence to minimize drag losses. The vessel is also a protection element in case of malfunction: a solid enclosure guarantees the safety for the personnel and equipment in the surroundings if the rotor disintegrates (due to the high speeds). Key elements of a FESS are the bearings: be either mechanical, magnetic or superconducting, these components undergo extreme stress and must be properly designed to minimize not only friction losses, but also the need for maintenance and replacement [87]. The type of power converter adopted depends on the application; in general terms insulated gate bipolar transistors (IGBTs) are widely employed because of their high switching frequencies and power potentiality [87].

The energy capacity of a FESS depend on the rotor mass and speed limits [17]. The first generation of flywheels reached a maximum speed of about 6000 rpm [17, 88], employing metallic rotors. New composite materials and improvements in the control of magnetic bearings made possible to have high-speed FESS, reaching 50 000 rpm to 60 000 rpm according to some sources [88, 89], and even in order the hundred thousands rpm according to some others [89]. It is common practice to set the usable stored energy to 50 % of the maximum energy, thus fixing the rotor minimum speed [90]. High-power FESS plants employ several flywheel devices in banks [91].

FESSs are known to have a very high power density, high conversion efficiency and their ageing is not dependant on depth of discharge (DOD)

[87] (besides, a FESS appliance can tolerate up to hundreds of thousands charge/discharge cycles [44, 92–94]). On the other hand, FESS traditionally present high self-discharge losses [91, 93, 95], but there is not much available information regarding new generation FESS: these losses may have decreased thanks to new and improved bearings [87]. Moreover FESS energy capacity is very low (with energy-to-power ratios seldom higher than 0.25 h [44]) and ageing has not been studied as thoroughly as in BESSs: only in recent years studies investigating flywheels fatigue have been published [96, 97]. Flywheel applications span a wide range, from large scale systems (e.g. for frequency regulation) to small scale at customer level. They are particularly suited for high-power and low-energy purposes (hundreds of kW, tens of seconds), with frequent charge/discharge cycles involved [87, 91, 93] such as, as already mentioned, grid frequency regulation [92, 98], mobility and aerospace and uninterruptible power supply [87, 91, 96].

II.IV *Supercapacitor Energy Storage Systems*

Supercapacitors (also called ultra-capacitors) store energy in the form of electrostatic field in a dielectric medium that splits two electrodes, to which a DC voltage is applied, without any chemical reaction involved. SCs employ several cells connected in series and in parallel to reach the desired voltage and current rating[3]. With respect to regular power electronics capacitors, this technology differs for employing highly porous electrodes (to increase the surface area), and extremely short gaps (in the order of 1 nm) between the electrodes and the electrolyte [100]. As for BESS and FESS, power electronics play a crucial role in connecting the SC to the grid.

Akin to FESS, supercapacitors are characterized by very high power density and low energy density, high round-trip efficiency and self-discharge

[3] For example, Maxwell Technologies commercializes a 2.7 V × 3000 F cell that can be part of a SC for grid purposes [99].

TABLE 1.2: Synthesis of techno-economic parameters of the ESDs discussed in this document: PSHP, Li-ion BESS, FESS, and SC. If not stated otherwise, data was taken from Ref. [20].

	PSHP	BESS	FESS	SC
Power range (MW)	10 – 5000	0.05 – 100	0.01 – 20[a]	0.01 – 0.3
Energy rating (MWh)	200 – 500	0.25 – 25	0.025 – 5	0.001 – 5
Energy density (Wh/kg)	0.5 – 1.5	120 – 230	5 – 80	0.05 – 15
Discharge time	1 – 24+ h	1 min – 1 h	s – 15 min	ms – min
Response time	1 s – 15 s[b]	ms	ms[c]	ms
Round-trip efficiency (%)	70 – 85	85 – 95	90 – 95	85 – 95
Calendar life (yr)	30 – 60	10 – 20[b,d]	15 – 20+[c]	16[c]
Lifecycles (10^3 cycles)	15[c]	1 – 10	200[c]	1000[c]
Daily self-discharge (%)	–	0.15 – 0.3	1.3 – 100	10 – 40
Total project cost ($/kW)[c]	2638	1876	2880	930
Total project cost ($/kWh)[c]	165	469	11 520	74 480

[a] BEACON POWER [102]
[b] PÉREZ-DÍAZ et al. [32]
[c] MONGIRD et al. [44]
[d] BENINI et al. [103]

rates, and high reliability [20, 93, 101]. Not only: SC degradation is unaffected by DOD and the equipment does not require strict temperature and humidity control (as is the case for BESS), making this solution particularly robust [20]. If there are many similarities between SC and FESS technologies, energy capacity costs are much higher for supercapacitors [21, 44], but it is expected that in the near future SC will experience significant cost reduction, improving its competitiveness [43].

As seen so far, various types of ESDs exist, each with its own properties; a synthesis of the main techno-economic data of each ESD is presented in Table 1.2. Some technologies are more suited to manage extremely frequent power variations as their response time is in the order of milliseconds, power density is very high, and energy capacity very limited: such is the case for FESS and SC; BESS are also quite fast in tracking power

variations, and have a fairly good energy capacity, but are susceptible to cycling degradation; PSHP can store energy at the cheapest price, but it takes seconds in adjusting the power output. New generation variable-speed hydraulic machines can be faster, but at the price of increased wear and tear of the equipment.

As there is no ideal ESD, academia and the industry have been researching on hybrid systems: two or more generators/ESDs that work in synergy, so their contribution is greater than of each device taken singularly.

III Hybrid Energy Storage Systems

Systems of two or more heterogeneous storage technologies with complementary characteristics constitute a Hybrid Energy Storage System (HESS) [20]. A HESS can achieve near optimal operation by synergizing the advantages of each ESD [104]. The main aim of all HESSs is combining high energy density with high power density devices thus achieving an overall high energy and power system with fast response [105]. BESSs, due to their particular nature, fall in between the two aforementioned categories. The response time of BESSs can be comparable to that of SC in light of the requirements of frequency regulation services. Nevertheless having a dedicated device to deal with the high frequency components of the regulation effort, allowing for a smoother BESS operation, contributes to the equipment preservation [106, 107]. The interest in energy storage, hybrid non-programmable and programmable generation plants with ESD, or HESSs raised substantially in recent years [21, 22, 108], expanding to the hybridization of hydropower plants [29]. Hybrid hydro-battery projects are already operational, most involving the installation of BESS storage along a Run-of-river (ROR) plant, but there are also cases of coupling of PSHP and BESS [109]. More projects have been announced, one involving the hybridization of a hydropower plant with SC [110]. Table 1.3 summarizes the known hybrid hydropower projects.

Hybrid systems were first studied as a combination of a non-programmable

TABLE 1.3: Summary of hybrid hydropower projects. Installed power and energy capacity are included when available.

Location	Type	Status	Capacity	Ref.
Pfreimd	137 MW PSHP	Operational	12.5 MW 13 MWh[a]	[109]
Forshuvud	44 MW ROR	Operational	5 MW 6.2 MWh[a]	[111]
Wallsee	210 MW ROR	Operational	8 MW 14.2 MWh[a]	[112]
Vogelgrun	142 MW ROR	Operational	650 kW 300 kWh[a]	[113]
Landafors	11 MW ROR	Operational	1 MW 250 kWh[a]	[114]
Edsele	60 MW ROR	Operational	6 MW [a]	[115, 116]
Lövön	36 MW ROR	Operational	12 MW [a]	[116]
Mankala	37 MW ROR	Planned	[a]	[117, 118]
Kurikaska	27 MW ROR	Planned	SC	[110]
Bodum	12 MW ROR	Planned	[a]	[116]
Fjällsjo	12 MW ROR	Planned	[a]	[116]

[a] Li-ion BESS
[b] Li-ion BESS (second life)

RES generation plant with an ESD in islanded power systems, microgrids, or off-grid contexts [119–126], in some cases employing hydropower to smooth wind power fluctuation [122, 124, 125, 127–131], solar PV generation [119, 121, 132] or both [126, 133, 134].

With advancements in BESS, FESS, and SC technologies and their increasing commercialization, hybridization has been investigated as a way to improve the stability of the grid (power smoothing or frequency control) [21, 32, 36, 37, 61, 80, 82, 90, 106, 135–155], to reduce the PSHP wear and tear [36, 136, 140, 156], or to prolong the BESS lifetime by reducing its cycling [82, 106, 107, 143, 145, 149, 150, 154, 157, 158].

The hybridization of a hydropower plant/PSHP and BESS has been studied by Moghaddam and Chowdhury [148], proposing a method to find the optimal size (for mitigating wind power fluctuations) of a PSHP-BESS plant according to the discrete Fourier transformation of the historical data of the power imbalance caused by Wind Turbine Generators (WTGs): the PSHP is sized according to the low frequency components, whereas the BESS according to the higher [148]. Guezgouz et al. [159] developed an efficient energy management strategy and an algorithm to determine the optimal size of an hybrid battery-PSHP storage system situated in a remote location with only wind and solar power generation. Anindito et al. [160] have assessed the economical benefits of including BESS into a PSHP under different scenarios of RES penetration and ecological constraints. More recently Makinen et al. [36] modelled a combined BESS-hydropower plant participating in the FCR balancing reserve market in the Nordic Power System to assess the plant ability to fulfill its requirements. Valentín et al. [156] studied the benefits of the hybridization of a 35 MW run-of-river Kaplan unit with a small size (650 kW) BESS providing FCR in Germany. The presence of the BESS reduced both the runner and the blade servomotor mileage, which is found to be proportional to the wear and fatigue damage, respectively.

Besides BESS, some works have focussed on hydro-FESS integration: Makarov et al. [98] modelled and simulated a hydro plant hybridized

with FESS. The hybrid configuration proved to be feasible and to provide a robust and accurate frequency regulation service, with the FESS taking the most of the regulation task in terms of variability, thus reducing hydro wearing and tearing problem. Later on, Lu et al. have validated the aforementioned findings via experimental tests [161]. Jin et al. [151] presented a method to coordinate a slow (hydropower/combined cycle) and a fast unit (FESS) implementing a SOC band control algorighm, which proved to provide high quality regulation, minimized generators up and down movements, and effective SOC containment within the desired range. FESS and PSHP integration was studied for the case of the El Hierro island, finding that, although FESS modules installation have proven to reduce the frequency deviations, their optimal amount depends on the adopted control strategy, and a higher number of modules does not guarantee a better system frequency response [147]. For the same case-study, Sarasua et al. [61] proposed a hybrid wind-PSHP-FESS control strategy for enhanced frequency containment in a 100 % renewable energy generation scenario. The control strategy takes into account the provision of synthetic inertial response, the rotational speed of the wind turbine generators, the SOC of the FESS and the primary and secondary frequency regulation actions. The proposed strategy proved to reduce the average frequency deviations to about half the reference case and increase the overall renewable energy utilization. Moreover, the authors found that satisfactory results were achieved with a deadband from 50 mHz to 100 mHz: the higher the value the lower the turbines wear but the higher the frequency deviations, and vice-versa.

As of 2019, the cooperation of fast ESDs (FESS or SC) and hydropower had not been demonstrated in an operational environment [29, 32].

Flywheels, co-operating with BESS, contribute to smooth the power generated by the RESs, help to stabilize microgrids in islanded mode, and lead to an extension of BESS life [107, 120, 139, 147, 152, 162–164].

Karrari et al. [135] applied an improved motif discovery algorithm to identify the most frequent consumption patterns for sizing hybrid

BESS-FESS in a multi-bus system. The optimization procedure aimed at minimizing the energy capacity of the FESS and maximizing the BESS's (vice-versa for the power capacity criterion) and to limit the BESS ramp rate. The sizing is based on the cut-off frequency of a Low-Pass Filter (LPF) for sharing the regulation burden between the two ESDs. It must be pointed out that the case-study is a relatively small power system: the resulting cumulative installed energy capacity and power of both BESS and FESS do not exceed 830 kWh and 150 kW respectively.

Akin to FESSs, SCs have also been studied in hybrid configurations, either with hydropower plants [128, 144, 165] or with BESSs, smoothing the RESs power output [150, 154, 155] or providing frequency regulation services [106, 142, 143, 145, 146, 149, 158, 166], some with experimental validation [82, 157, 167].

Hernández et al. [106] proposed a techno-economic model to find the optimal size and energy management of a BESS-SC HESS for PV household-prosumers. The methodology enhances the self-consumption and self-sufficiency of a household with PV generation, accounting for battery ageing and FCR provision. Different SOC control strategies were proposed, and a long-term economic analysis demonstrated the economic feasibility and attractiveness of the HESS thus found. Mohamed et al. employed the concept of virtual synchronous generator to control a HESS included in a microgrid (with PV and diesel generation). The HESS was made of a 100 Ah Lead-acid BESS coupled with a 108 kW (3.75 F at 240 V) SC. The virtual synchronous generator damping factors have been optimized with Particle Swarm Optimization (PSO), and the system was successfully proven to improve the frequency nadir and Rate Of Change Of post-disturbance Frequency (ROCOF). The improvement in life consumption of the BESS was touched upon, but the main aim of the hybridization was to improve the stability of the frequency in the microgrid. Khan et al. developed a new control strategy based on k-type compensators and nonlinear Proportional Integral (PI) control for a hybrid lead-acid BESS-SC system for voltage control in a microgrid with

solar PV generation and variable loads [169].

Regardless of the employed technology, the hybridization of energy storage devices always implies the coupling of a "slow" unit (intrinsically or artificially slowed down) with a "fast" unit, and a key common element is the control strategy that manages the power flows and the SOC of each unit.

JIN et al. [151, 153] have developed an optimized algorithm to coordinate a "slow" and a "fast" unit, whose purpose is to efficiently distribute in real time the load between the two; another strategy, among the control variables, which considers the SOC of the storage devices has been proposed. Two different control strategies were proposed by LABAN [140] for a hydropower plant coupled with a BESS for the provision of primary frequency control in the Nordic Power System. The comparison between the two was based on the hydro wear and tear and the BESS life consumption due to cycling. Other works have presented different control strategies for either frequency regulation services or RES power smoothing: some based on multiple filtering of the frequency components [170], other based on the droop control method [139, 147], or non-linear proportional scheme [147], or controlling separately the frequency regulation effort and the inertial control, with and without intentional deadband [61]. Most of the studies consider the SOC control [61, 106, 170, 171].

To the author's knowledge, only two research papers exist that focused on a different HESS topology. KHEAWCUM and SANGWONGWANICH [138] have proposed a storage system made of three devices: PSHP, BESS, and FESS. The aim of the HESS was to provide primary frequency control to the electric grid of a small island with high PV penetration, operating in islanded mode. Low-pass filters with different time constants split the regulation effort between the PSHP (the slowest), the BESS, and the FESS (the fastest), but the control strategy does not take the SOC into account. Moreover, the study does not include an analysis on the wear and tear induced by the regulation effort and its possible mitigation due to the hybridization. More recently, JIAO and MÅNSSON [94] performed

a consequential Life Cycle Assessment (LCA) analysis to evaluate the GHG emissions from HESS in different future generation scenarios, all having in common a 100 % RES generation in Sweden. The study took into account several ESDs (among which PSHP, BESS, FESS), finding out that a good chunk of the HESSs cradle-to-gate emissions are due to low utilization rates (in particular for long term ESD such as PSHP) and that the HESS configuration with the lowest GHG emissions in the life cycle is the PSHP-BESS-FESS configuration. The study did not take into account the benefits deriving from the increased flexibility – in terms of the system ability to balance the supply-demand grid ancillary services – offered by HESS, and did not perform any dynamic simulation.

IV Motivation and goals

The studies summarized in the previous Section analyse different ways of enhancing ESDs by combining them into forming a HESS. A common emerging trait is that they are generally composed of two technologies, with the exception of the already mentioned Refs. [94, 138]. These suggest that the three-ESD configuration (PSHP, BESS, FESS) can, in one case, stabilize the frequency of an isolated grid and, in the other, store electrical energy with the least GHG emissions. These two studies do not approach the topic of HESSs made of more than two technologies from other key perspectives: the sizing of each component, the choice and tuning of the energy and power management strategies, the assessment of a different range of techno-economic benefits derived from the hybridization, to name a few. Moreover, researches of this kind involving a PSHP only focus on fixed/variable-speed turbine operation mode, even though variable-speed pumps can adjust their power input and contribute to the grid stability.

From this background, the research activity presented in this thesis aims at filling a gap in the scientific literature and in the industry by evaluating a PSHP hybridized with BESS and FESS to provide ancillary services to the grid. The research activity unrolled in close partnership

with the Italian research institution Ricerca sul Sistema Energetico (RSE), which financed the first two years of research, defined the background and a case study, and developed models. Part of the work presented in this document has been published in RSE's reports [172, 173].

Since 2013 RSE investigated the integration of RES generation by sPSHP in the island of Sardinia, as part of the agreement "for research and development activities of general interest for the national electricity system" with the Italian Ministry of Economic Development [174–176]. The island of Sardinia, in particular, presents a level of criticality in its power system, as it will described more thoroughly in Section 2.1. From the beginning the research focused on a HESS with a variable-speed sPSHP, BESS, and FESS. The purpose of the research path was to preliminary explore the performance of a variable-speed PSHP, with the additional flexibility provided by BESS and FESS. Initially the goal of this first step was to support the TSO: a detailed analysis of the capabilities of a plant with very high flexibility could serve as a first step to design the regulation services of the future, by identifying the response times and costs that can be expected from flexible plants delivering ancillary services. Later on, a different perspective was adopted: given the future trends, a generation/storage plant will most likely be required to fulfil more and more stringent requirements, and from the plant owner's perspective, hybridisation could be an advantageous solution to reduce the wearing of components and associated costs (as touched upon in Section 1.1.III). This perspective was the starting point of the present research whose main objectives were:

i) to provide a detailed yet versatile tool to simulate the dynamic operation of a fixed-speed turbine and variable-speed pump-turbine, each with/out hybridization with fast ESDs;

ii) to compare two different criteria to allocate the power participation of each device making the hybrid plan, also including SOC control;

iii) to consider the variable-speed pump in the analyses, an operation mode which can provide regulation services and was explored in

the literature;

iv) to propose a practical methodology to assess the technical benefits of hybridization to the pump-turbines (in terms of reduction of the wear and tear indicators), and with respect to BESS cycling;

v) to propose a cost function addressing plausible costs related to the wear and tear indicators;

vi) to propose an optimization framework for the design and control of a hybrid plant given one or more frequency events and open-source cost/revenues information;

vii) to introduce the HESS model into the Sardinian power system's, offering an insight on the plant role in the power system;

viii) to improve the modelling of the PSHP with respect to the background literature.

The rest of this thesis is structured as follows: Chapter 2 introduces the case study and details the model equations that have been adopted to represent the ESDs composing the HESS, two different power management strategies based on different principles, as well as their ageing processes; in Chapter 3 includes the results of a series of open-loop simulations of the proposed system by using real historical data of continental Italy, considering the PSHP with and without hybridization and in different operation modes; Chapter 4 presents an optimization procedure to find the optimal hybridization that would guarantee the highest economic revenues over the economic life of the project; last, in Chapter 5, the sPSHP is included into a model of the Sardinian power system and its contribution in containing and restoring the grid frequency after two different tripping events is analysed.

List of symbols

Greek letters		
	Permanent droop (%)	σ
Roman letters		
	Frequency (Hz)	f
	Active power (MW)	P
Subscripts		
	Rated	r
	Reference	ref

2 Dynamic model

The research goal was to develop models and solutions which could be applied to all possible HPs/Pumped Storage Hydro Powers (PSHPs). However, to better highlight their effectiveness peculiarities, a case study was taken as a reference in the Sardinia island.

This chapter is structured as follows: Section 2.I presents the case study from which the modelling choices and assumptions were made; Section 2.II details the top-level model choices as well as the plant relation to the power system; Sections 2.III – 2.V present the model of the PSHP, Battery Energy Storage System (BESS), and Flywheel Energy Storage System (FESS) respectively; eventually, in Section 2.VI, the two strategies developed to control the Hybrid Energy Storage System (HESS) are defined.

I Case study

The Sardinia island is electrically connected to the mainland via two High Voltage Direct Current (HVDC) submarine cables: the SAPEI (500 kV, 1000 MW), and the SACOI (200 kV, 300 MW). As of 2019, the gross electrical energy generation comes from thermo-electric power plants (2386.1 MW_e), hydro (466.4 MW_e), wind turbines generators (1054.9 MW_e), and Photovoltaic (PV) generators (872.6 MW_e) [177].

Ricerca sul Sistema Energetico (RSE) conducted pre-feasibility and feasibility studies for a seawater Pumped Storage Hydro Power (sPSHP) and identified Foxi Murdegu (Figure 2.1) as an appropriate site in which to realize the infrastructure [174–176]. The plant would include one 120 MW

TABLE 2.1: Dimensional characteristics of the Foxi Murdegu project [174].

Upper reservoir volume	1.2×10^6 m^3
Minimum water level	345 m a.s.l.
Maximum water level	367 m a.s.l.
Penstock length	770 m
Penstock diameter	3 m

binary hydro unit consisting of a reversible variable-speed pump-turbine. The plant scheme is shown in Figure 2.1c, whereas the main dimensional parameters are reported in Table 2.1.

In normal operation, during hours of low energy price the plant would pump sea water into the upper reservoir, whereas during high energy price hours it would operate in turbine mode, generating the power committed in the day-ahead market.

Annex A15 of the Italian grid code (*Codice di Rete*, [15]) mandates that every generating unit, Unità di Produzione (UP), whose "efficient power" (*potenza efficiente*) is greater than 10 MW_e must provide primary regulation – Frequency Containment Reserve (FCR). The term "efficient power" is defined as "the maximum active power that the UP can generate in continuity, for thermoelectric power plants, or for a certain amount of hours for hydropower plants". The *efficient power* is among the technical specifications that the plant owner must declare during the (mandatory) registration process in the Generating Units Registry (RUP), and is used to quantify both the FCR and Frequency Restoration Reserve (FRR). In the rest of the document, the term "rated power" will be used in place of "efficient power" to avoid confusion. The provision of secondary regulation – FRR – is not mandatory and, unlike the primary, is remunerated, given that the UP fulfills the requirements. The Foxi Murdegu plant will be expected to participate in both FCR and FRR, and therefore must: a) have a permanent droop set to 0.04; b) commit a minimum FCR of

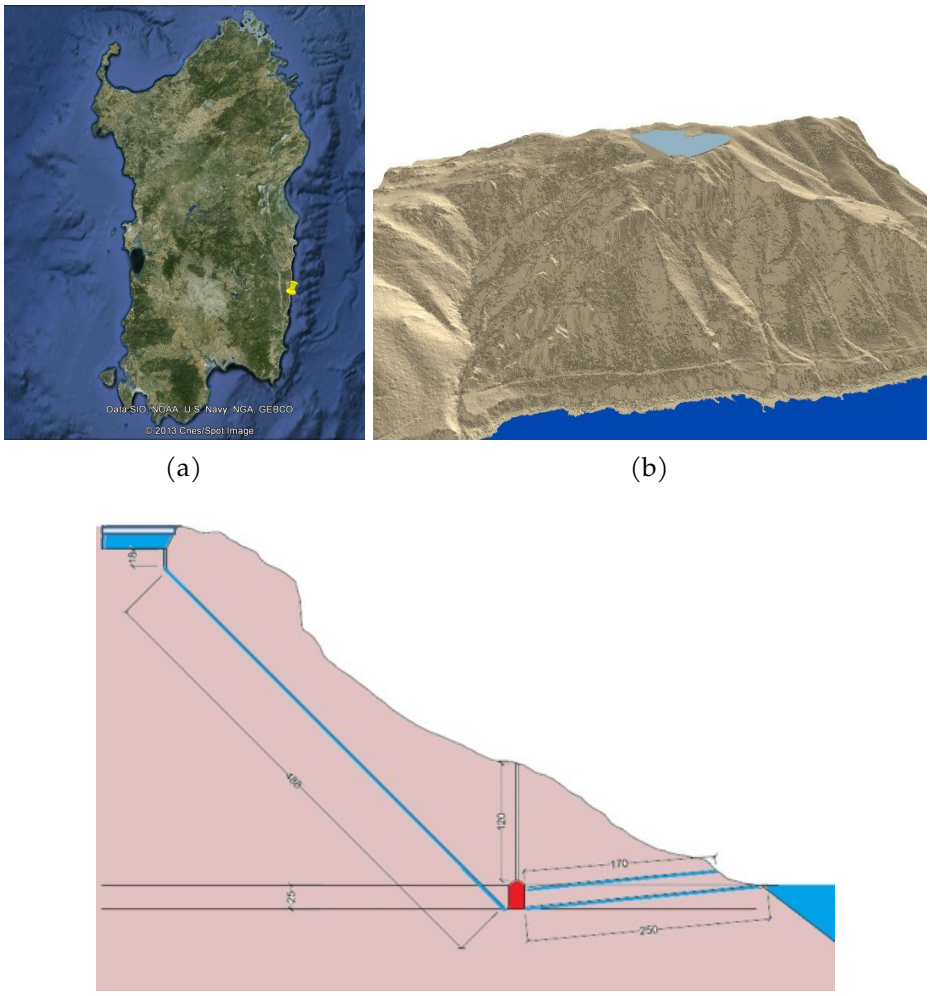

(a) (b)

(c)

FIGURE 2.1: Location of Foxi Murdegu highlighted in the Sardinian satellite view (yellow marker) (a), 3D representation of the upper reservoir, cliff, and sea (b), and plant scheme (c) [174].

10 % of the efficient power (upwards and downwards)[1]; c) deliver at least 50 % of the FCR (with the maximum possible gradient) within 15 s from the beginning of the frequency perturbation (when the frequency deviation exceeds the deadband boundaries), 100 % within 30 s; d) not limit its response unless due to hydraulic conditions, energy availability, and regulation devices intrinsic properties; e) commit a minimum FRR of 15 % of the efficient power (if participating in the service).

It is important to clarify that under the current regulatory framework, the participation of the Foxi Murdegu PSHP, with or without hybridization, would be possible only in turbine mode. Currently in the European Network of Transmission System Operators for Electricity (ENTSO-E) area only Germany, France, Switzerland, Belgium and the Netherlands allow for pumped storage, batteries, demand side response, and distributed generation to take part in FCR and FRR [14]. Moreover, in this work, intentional delays will be introduced as part of the power management strategy of the HESS, which is currently in contrast with the regulations (point d) of the previous list. As pointed out in other works, regulation moves slower than technology [32], and it is also a goal of the research to show the path to regulators and the consequent benefits. So, this research assumes, among the others, that in the future scenario, the regulatory framework will allow the participation of the plant in the provision of ancillary services, with the control settings that will be discussed in the next chapters.

II Hybrid plant

The HESS would be configured in active topology, meaning that hydro, BESS and FESS would be equipped with their own power converter [143].

The model has been developed in Matlab – Simulink environment [178].

[1] This large power allocation is only mandatory for the island of Sardinia, a symptom of the importance and necessity for frequency regulation.

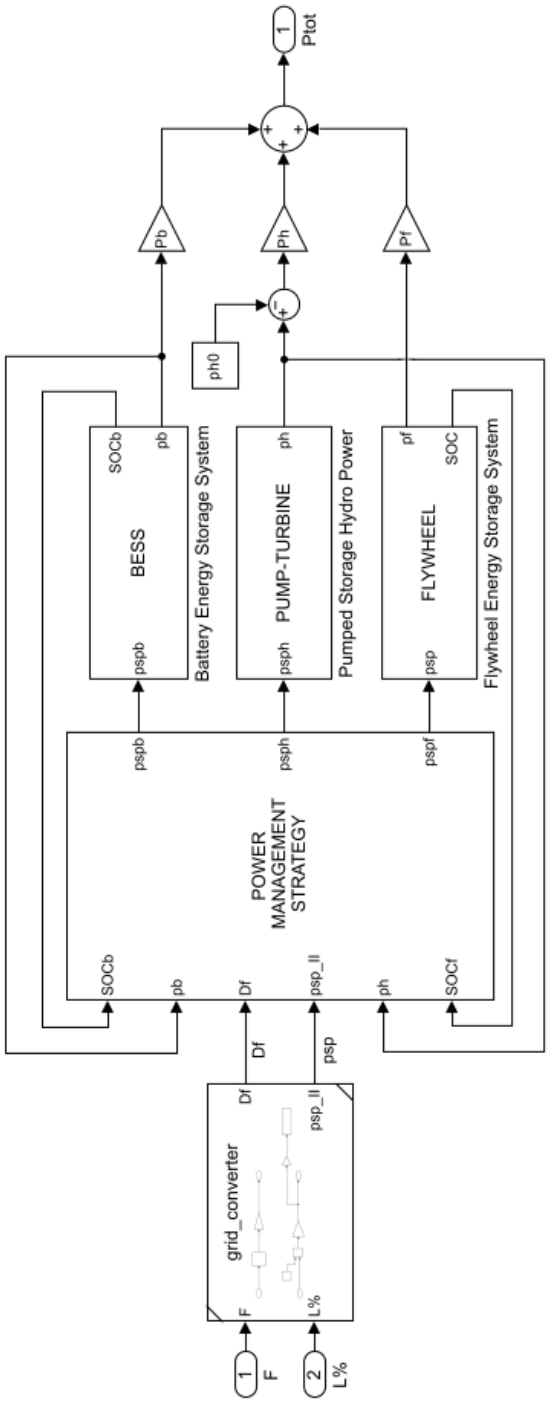

FIGURE 2.2: Block diagram of the HESS (variable-speed turbine). Conceptually, the pump and fixed-speed turbine do not entail any meaningful difference.

When the PSHP is hybridized, the BESS and FESS can be considered as *sections* of the power plant, similarly to the vapour circuit of a combined-cycle power plant. This does not violate the grid code regulations. The hybrid power plant is considered as a hydro power plant whose rated power is defined as the sum of the rated powers of the equipment:

$$\hat{P}_r = \hat{P}_h^b + \hat{P}_b^b + \hat{P}_f^b. \tag{2.1}$$

The subscripts (h, b, f) stand for *hydro*, *battery*, and *flywheel*, respectively; the hat accent ($\hat{}$) indicates that the quantity expressed is in absolute value; the superscript (^{b}) indicates that the quantity expressed is a base for the per-unit notation.

This notation consists in relating each quantity (physical or not) to their own reference value (called *base quantity*), allowing to handle variables with values numerically close to zero. This approach allows to: i) reduce the numerical errors introduced by doing operations with very large and very small numbers, and ii) simplify model equations, as it removes the need to use constants (physical or not). The choice of the base quantity is arbitrary; however the bases need to be consistent with each other to fully ancheve the aforementioned benefits. It is common practice to choose rated values as bases in the per-unit notation.

Throughout the document two base systems will be mentioned: system-base (s.b.) and machine-base (m.b.) respectively. The machine-base system has as base quantities the rated electrical power and energy of the machine (PSHP[2], BESS, FESS), whereas system-base has as base quantity the HESS rated power as expressed in Equation (2.1). The operation to translate a quantity from the i base system to the j base system is:

$$a_j = a_i \cdot \frac{\hat{A}_i^b}{\hat{A}_j^b}, \tag{2.2}$$

[2]There is an exception for hydropower, which will be addressed in Section 2.III.I.

where $\hat{A}$ is a generic quantity, and $a_{i/j}$ is its value in per-unit (pu).

As mentioned in Section 2.1 at page 32, the minimum FCR and FRR must be respectively 10 % and 15 % of the plant rated power, which translates to a reserve of 0.1 pu and 0.15 pu s.b. respectively. Both the FCR and FRR imply a change in output/input power, which is controlled by a power set-point (psp). In particular, each regulation psp can be calculated as:

$$\underline{psp}_I = -\frac{\Delta f}{\sigma}, \tag{2.3}$$

$$\underline{psp}_{II} = 2 \cdot \underline{SB} \cdot \frac{L_{\%} - 50}{100}, \quad L_{\%} \in [0, 100], \tag{2.4}$$

where Δf is the frequency error (pu), σ the permanent droop, $\underline{SB}$ the power reserve for the secondary regulation (pu), and $L_{\%}$ the signal sent by the Automatic Generation Control (AGC) and received by the plant participating in the service (a value of 50 means no FRR, a value of 0/100 means full downwards/upwards FRR activation). The subscripts (I, II) refer to the primary and secondary regulations, respectively, the underline (_) indicates that the quantity is expressed in pu s.b., whereas its absence implies that the same quantity is in pu m.b.. Equation (2.3) is a reformulation of Equation (1.1).

The following sections present the model equations of each element of the system under investigation. Each section will conclude with a paragraph describing the experimental validation (or lack thereof) that has been performed in the course of the research exchanges at Universidad Politecnica de Madrid (UPM) and Centro de Investigaciones Energéticas, Medioambientales y Tecnológicas (CIEMAT). Experimental validation for PSHP was not possible as there are few variable-speed plants currently in operation and it is not an easy task to reach an agreement with a plant owner for sharing technical and/or economic data.

III Pumped-storage hydropower plant

The PSHP is expected to include a single unit with a variable-speed Francis pump-turbine, one Doubly Fed Induction Generator (DFIG), along with the reservoir and penstock whose main design features are presented in Section 2.III.II. As seen in Chapter 1, variable-speed technology provides operation enhancements to the plant, as well as increased costs. The practical approach for the plant owner would be to either decide the purchase and installation of a variable-speed unit (hydro machine, electric motor/generator, power electronics, ...) or the hybridization of an existing fixed-speed unit with BESS and/or FESS.

For these reasons, a dynamic model of the variable-speed pump-turbine was realized, together with a model of the fixed-speed turbine. The fixed-speed pump can not participate in frequency regulation services – only the auxiliaries (BESS, FESS) could modulate their power to participate in such services – and as such has not been considered for the analysis. As will explained later, the hydraulic machine model was obtained from experimental data of a real variable-speed pump-turbine, which has also been utilized for the machine fixed-speed operation.

The PSHP model is made of a total of 5 elements: i) upper and lower reservoirs, ii) penstock, iii) one variable-speed pump-turbine equipped with a iv) speed governor, coupled with v) one DFIG/synchronous machine.

Before diving into the model equations of each element of the PSHP, an explanation on the base system for the PSHP will be offered.

III.1 *Electric and hydraulic base system*

In this work the PSHP is both an electrical and an hydromechanical entity. The provision of ancillary services is regulated according to the plant rated power, which is communicated to the Transmission System Operator (TSO) in the act of registering the plant in the generating units registry (RUP). The actual power that an hydropower plant can generate

depends on the physical state of the equipment: runner speed, Guide Vanes Opening (GVO), gross head, and flow rate. For the PSHP only, the choice has been made to use two machine-base systems: electric and hydraulic.

The electric power base quantity is the rated plant electric power, which is set to be $\hat{P}_h^b = 120\,\text{MW}$. This is the reference value for the minimum FCR and FRR allocation and provision.

The hydraulic base system is defined with respect to a particular steady-state turbine operation point: full reservoir (maximum value of the gross head $\hat{H}_g^{max}$), maximum GVO opening $\hat{\alpha}$, and rated runner speed $\hat{N}$ (525 rpm for variable-speed operation and 500 rpm for fixed-speed operation, see Section 2.III.IV), resulting in the hydraulic base power $\hat{P}^{b,h}$. The other quantities (net head, flow rate, and hydraulic efficiency), were obtained by using energy conservation law (Equation (2.5)) and the dimensional characteristic curves of the turbine (Equations (2.7) – (2.8)):

$$\hat{H}^b = \hat{H}_g^{max} - \hat{K}\hat{Q}^{b^2}, \tag{2.5}$$

$$\hat{K} = \lambda \frac{L_p}{2gD_p \frac{\pi D_p^2}{4}}, \qquad \lambda = \left[-2\log\left(\frac{\epsilon/D_p}{3.7}\right)\right]^{-2}, \tag{2.6}$$

$$\hat{Q}^b = F(\hat{\alpha}, \hat{\psi}^b), \tag{2.7}$$

$$\hat{\eta}^b = G(\hat{\alpha}, \hat{\psi}^b), \tag{2.8}$$

$$\hat{P}^{b,h} = \rho g \hat{H}^b \hat{Q}^b \hat{\eta}^b. \tag{2.9}$$

In Equation (2.5) $\hat{H}^b$ is the base head, $\hat{H}_g^{max}$ the maximum upper reservoir water level, $\hat{K}$ (s^2/m^5) the dimensional hydraulic friction coefficient, and $\hat{Q}^b$ the flow rate. The hydraulic friction losses coefficient is calculated by Equation (2.6), where L_p and D_p are the penstock length and diameter, respectively, g (m/s^2) is the gravitational acceleration, λ the Darcy friction coefficient (fully-developed turbulent flow), and ϵ the roughness coefficient (0.3 mm tar-coated steel pipes, new) [179]). The base flow rate $\hat{Q}^b$ and the base hydraulic efficiency $\hat{\eta}^b$ are functions of the GVO and

TABLE 2.2: Base hydraulic quantities for the variable and fixed speed pump-turbines.

Quantity	Symbol	Var. speed	Fix. speed
Runner speed (rpm)	$\hat{N}_h^b$	525.00	500.00
GVO (°)	$\hat{\alpha}^b$	33.70	33.70
Head (m)	$\hat{H}^b$	355.53	355.33
Flow rate (m^3/s)	$\hat{Q}^b$	49.00	49.42
Efficiency (%)	$\hat{\eta}^b$	79.65	80.66
Power (MW)	$\hat{P}^{b,h}$	139.48	142.38

the non-dimensional pressure number $\hat{\psi}$, (defined in Equation (2.13)); their calculation will be explained later (Section 2.III.III). As the net head is a function of the flow rate, and the flow rate is a function of the net head, the bisection method was used to numerically solve this non-linear set of equations. Eventually, the base hydraulic power is calculated with Equation (2.9). Table 2.2 presents the base quantities for both variable and fixed-speed operation. It was chosen to use two base systems because it is convenient to have the rated runner speed correspond to 1 pu. The conversion from the hydraulic to the electric reference systems and vice-versa is necessary only for the active power and it is done with Equation (2.2).

III.II *Reservoirs and penstock*

The lower reservoir is the sea, whose water capacity is infinite and whose water level is assumed to be constant over time. The upper reservoir, according to the pre-feasibility studies, has a capacity of $1.2 \times 10^6\,m^3$. The water level of the upper reservoir is assumed constant: it has been verified that 3600 s of turbine operation at rated power would decrease the level from 1.0322 pu to 1.0197 pu. Similarly, after one hour of operation in pump mode, the water level would increase to 1.0427 pu. This small change, in the per-unit values of the geodetic water level, justifies the choice to keep the value constant during the simulations, as these do not

last longer than 3600 s.

Mass and momentum conservation laws fully describe the transient flow in the conduit [180]. An elastic water column model was employed, and a lumped parameters approach was used to transform the aforementioned conservation laws into ordinary differential equations [34, 147, 181]. The approach consists in splitting the conduit into consecutive segments and distribute its properties evenly across the segments. After a preliminary sensitivity analysis, $n_{ge} = 3$ segments have been chosen. The flow rate q_i as well as the head h_i at the end of the i-th segment are calculated with:

$$\frac{dq_i}{dt} = \frac{n_{ge}}{T_w}\left(h_{i-1} - h_i - \frac{f_p}{n_{ge}}|q_i|\,q_i\right), \quad T_w = \frac{L}{gA}\frac{\hat{Q}^b}{\hat{H}^b} \tag{2.10}$$

$$f_p = \frac{K\hat{Q}^b}{\hat{H}^b}, \tag{2.11}$$

$$\frac{dh_i}{dt} = \frac{T_w n_{ge}}{\left(L/a_p\right)^2}(q_i - q_{i+1}), \tag{2.12}$$

where T_w (s) is the water starting time, a_p (m/s) the penstock wave speed, and f_p (pu) is the per-unit hydraulic losses coefficient, assumed constant.

III.III *Variable speed pump-turbine*

The analytical representation of a turbine is often done with generic equations, [182–186].

In one of the pre-feasibility studies, the pump-turbine performances were deducted from the characterization of a variable-speed pump-turbine machine made by the University of Padova [175]. In this analysis it was assumed that, according to the similarity theory, the characteristic curves of the machine can describe this pump-turbine operation in Foxi Murdegu.

The experimental points were provided in the non-dimensional coordinate system, pressure number $\hat{\psi}$, flow number $\hat{\phi}$, and efficiency $\hat{\eta}$,

respectively:

$$\hat{\psi} = \frac{g\hat{H}}{\left(\frac{\pi D_1 \hat{N}}{60}\right)^2} \tag{2.13}$$

$$\hat{\phi} = \frac{\hat{Q}}{\pi B_1 D_1 \frac{\pi D_1 \hat{N}}{60}} \tag{2.14}$$

where D_1 (m) is the runner diameter and B_1 (m) the runner inlet width. For turbine mode, the position of the wicket gate blades $\hat{\alpha}$ (deg) was also provided for each sampled point.

Every coordinate is transposed in per-unit notation (with the respective bases $\hat{\alpha}^b, \hat{\psi}^b, \hat{\phi}^b, \hat{\eta}^b$). In most of the literature, hydraulic machines characteristic curves are expressed in the (n_{11}, q_{11}) coordinate system, whereas in this work, the notation (ψ, ϕ) is adopted. Thanks to the per-unit notation, the change of reference system is straightforward, as seen from (2.17) and (2.18).

$$\psi = \frac{h}{n_h^2}, \tag{2.15}$$

$$\phi = \frac{q}{n_h}, \tag{2.16}$$

$$q_{11} = \frac{q}{\sqrt{h}} = \frac{\cancel{n_h}\phi}{\cancel{n_h}\sqrt{\psi}} = \frac{\phi}{\sqrt{\psi}}, \tag{2.17}$$

$$n_{11} = \frac{n_h}{\sqrt{h}} = \frac{\cancel{n_h}}{\cancel{n_h}\sqrt{\psi}} = \frac{1}{\sqrt{\psi}}. \tag{2.18}$$

where n_h (pu) is the machine runner speed. The characteristic curves were expressed by polynomials by interpolating the experimental points to allow their use in the model. It must be pointed out that in turbine mode the fitting coefficients are the result of a constrained linear optimization problem, due to the degree of freedom given by the angles of the guide vanes. The objective function – to minimize – is the sum of squared errors. The variables to be optimized are the polynomial coefficients (c_{ij}, d_{ij}),

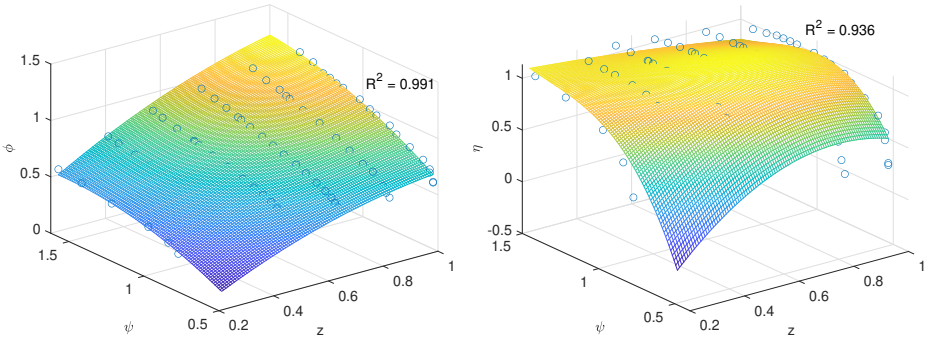

(a) (b)

FIGURE 2.3: Turbine mode: flow number (a) and efficiency (b) characteristic curves. The experimental points are marked with circles. All quantities are in per unit.

subject to a concavity constraint in the dominion: as the real operation of a turbine is a concave phenomenon, such has to be the polynomial representing it. The concavity constraint was not necessary for pump mode. The graphic representation of the characteristic curves for turbine and pump mode, along with the experimental points, are presented in Figures 2.3 and 2.4, and as Equations (2.19) and (2.20):

$$\phi_t = \sum_{i=0}^{2}\sum_{j=0}^{2} c_{ij} \cdot z^i \cdot \psi^j, \qquad \eta_t = \sum_{i=0}^{2}\sum_{j=0}^{3} d_{ij} \cdot z^i \cdot \psi^j, \tag{2.19}$$

$$\psi_p = \sum_{i=0}^{3} e_i \cdot \phi^{3-i}, \qquad \eta_p = \sum_{i=0}^{6} f_i \cdot \phi^{6-i}. \tag{2.20}$$

where η_t and η_p (pu) the hydraulic efficiency respectively in turbine and pump mode, (e_i, f_i) the polynomial coefficients for the characteristic curves in pump mode, and z (pu) the wicket gate position.

Thanks to the per-unit notation, both head and flow rate can be easily converted into pressure and flow numbers and vice/versa, via the runner rotational speed n_h (pu):

$$h = \psi_k \cdot (n_h)^2 \qquad q = \phi_k \cdot n_h, \qquad k \in \{t, p\}. \tag{2.21}$$

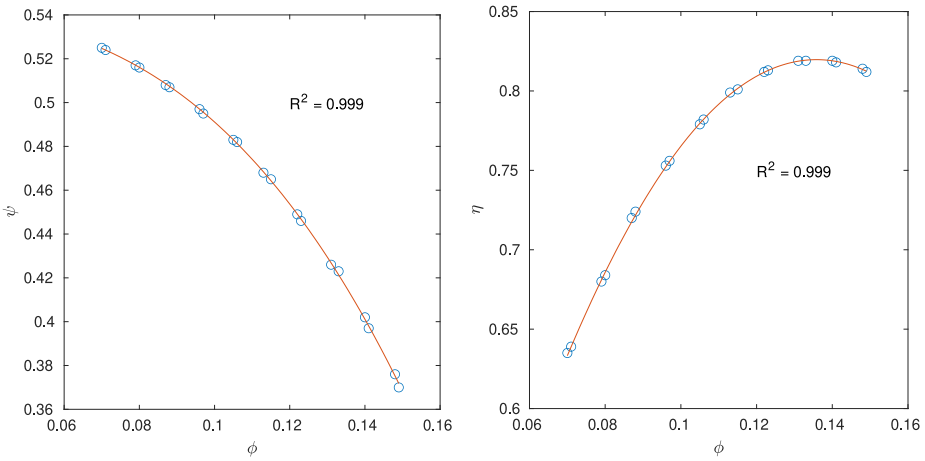

(a) (b)

FIGURE 2.4: Pump mode: pressure number (a) and efficiency (b) characteristic curves. The experimental points are marked with circles. All quantities are in per unit.

The mechanical power at the shaft (hydraulic base), in turbine and pump modes, is calculated as:

$$p_{mech.} = \begin{cases} \eta_t hq, & q > 0 \\ \frac{1}{\eta_p} hq, & q < 0 \end{cases} . \tag{2.22}$$

According to the manufacturer, the variable speed pump-turbine has an operating range of $\pm 10\,\%$ of, with rated speed set at 525 rpm.

III.IV *Synchronous generator*

In the European market, the closest synchronous machine rated speed in that range is 500 rpm. In this work, the same hydraulic machine is assumed to be installed in either the fixed and variable-speed operation.

In fixed-speed operation, a simplified model of the generator was employed, as the goal of this study is to assess the plant ability to deliver

active power [187].

The synchronous generator model is based on the assumption that the mechanical power (p_{mech}) is equal to the electrical power (p_h, with an appropriate base change) (2.23), and that the rotor speed is exactly synchronized to the grid frequency (2.24) [184].

$$p_h = p_{mech} \frac{\hat{P}^{b,h}}{\hat{P}^{b}_{h}}, \tag{2.23}$$

$$\Delta n_h = \Delta f. \tag{2.24}$$

Here, Δf is the frequency error,

III.V *Doubly Fed Induction Generator*

The DFIG interacts mechanically with the pump-turbine and electrically with the grid. These two phenomena are modelled separately. The mechanical interaction between the DFIG and the pump-turbine shaft is represented with Equation (2.25). The base change is omitted for clarity.

$$T_m \frac{dn_h}{dt} = (p_{mech} - p_h) \frac{1}{n_h}, \tag{2.25}$$

where T_m (s) is the generator mechanical starting time (s) and p_h (pu) the electrical power sent to the grid. With regards to the electrical interaction (Figure 2.5), the DFIG absorbs/releases power in accordance to the control signal psp_h received by the Grid Side Converter (GSC), which is assumed to behave as a first order transfer function with time constant T_{cH} (s) [51]. The Rotor Side Converter (RSC) governs the electromagnetic torque c_{em} [188], which is calculated from the input variables (n_h and the psp_h) neglecting the generator losses. The speed deviation from the synchronous speed ($n_{syn} = \pm 1\,pu$), minus the generator slip, is used to calculate the active power at the rotor, p_r, from which the active power p_h is obtained. Both the electromagnetic torque and the power at the rotor are limited by two saturator blocks.

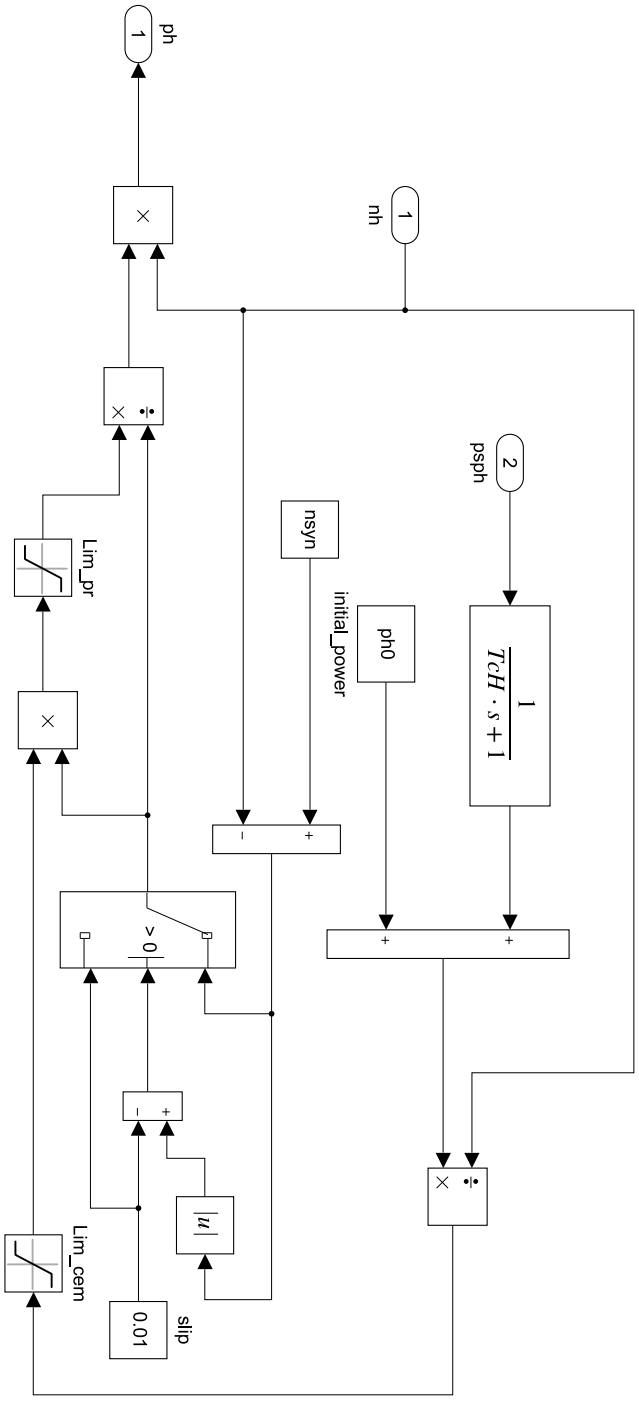

FIGURE 2.5: DFIG block diagram. All quantities are in the proper base system.

III.VI *Speed governor*

The difference between the conventional fixed and variable-speed pump-turbine also reflects on the modelling of the speed governor, whose task is to adapt the wicket gate position to correct a speed error (variable speed) [189] or a power-frequency error (fixed speed) [183].

In pump mode, the wicket gate plays no role in the operation, and no influence on the hydraulic efficiency is assumed. For this reason, the speed governor is modelled only for the turbine mode.

A control signal (CS) is generated by a Proportional Integral (PI) controller and fed to a servomotor, which responds with a first-order lag with a T_s (s) time constant (2.26).

$$\Delta z = \frac{1}{T_s \cdot s + 1} CS_{var/fix}, \tag{2.26}$$

where $CS_{var/fix}$ is the control signal for either variable or fixed-speed operation, defined below. The guide vane servo is assumed to operate a regulating ring, and a backlash Bl proposed by Saarinen et al. is applied [190]. Backlash is a non-linear phenomenon caused by plays between moving mechanical parts that cause an interference between the servomotor position and the controlled parameter. The maximum opening (mxgtor) and closing (mxgctr) rates are imposed to the wicket gate by a rate limiter block, according to Ref. [182].

The text below illustrate how the control signal is calculated in variable and fixed speed operation, respectively.

Variable speed

The control strategy for the turbine power output was taken from [189], having the rotational speed as control variable. A controller with proportional and integral gains, respectively $k_{p,var}$ and $k_{i,var}$, elaborates the

speed error Δn_h and produces a control signal (2.27):

$$CS_{var} = \left(k_{p,var} + \frac{k_{i,var}}{s} \right) \Delta n_h. \tag{2.27}$$

The reference rotational speed can be chosen following different criteria. Being the focus of this study a comparison between different kinds of hybridization of fixed and variable-speed PSHP, this value was set to be the runner rated speed (in variable-speed operation) and kept constant throughout the simulation.

Fixed speed

In fixed-speed operation, the PI controller receives as input a power-frequency error signal, Eq. (2.28), made of the runner speed deviation Δn_h and the power error.

$$CS_{fix} = \left(k_{p,fix} + \frac{k_{i,fix}}{s} \right) \left[\Delta n_h - \sigma_h \left(p_h^0 + p_h^* - p_h \right) \right]. \tag{2.28}$$

A deadband of 10 mHz (0.0002 pu) is applied to the speed error signal, according to [15, 191]. The power error is the sum of the scheduled generated power, p_h^0, the control signal for power generation, p_h^*, and the electrical power currently being generated p_h with negative sign (all quantities in pu). p_h^* is obtained by the power management algorithm, as seen in Section 2.VI, whereas in the non-hybridized case it corresponds to the secondary regulation psp signal, psp_{II}.

To determine the value of the PI gains, $k_{p,fix/var}$, $k_{i,fix/var}$, a 200 mHz frequency error signal was fed, in open-loop, to the non-hybrid fixed and variable-speed models. By observing the mechanical power signal, the gains values were tried until they converged to the pair of values that would result in an overshoot lower than 10 % of the signal steady-state value and a transient duration lower than 30 s. Once found, these values were fixed as parameters for the rest of this work.

One of the advantages of the model presented so far is that it is highly customizable, therefore it can be easily adapted to represent more closely a plant with different delays or different machines.

The complete block diagram of the PSHP model and its component is presented in Figure 2.6, and the complete list of model parameters and their values are presented in Table 2.3.

III.VII *Pump-turbine wear estimation*

As stated in Section 1.IV, the aim of this work is to assess the advantages derived from the hybridization of the PSHP with BESS and FESS in providing ancillary services. One of the advantages can be the hydraulic machine reduced wear and tear.

When studying the hybridization of a PSHP with a "fast" unit, the adopted perspective is often performance-oriented, meaning that the objective is to enhance the quality of the regulation services [36, 128, 148, 153] or the plant profitability [159–161]. Similarly, the adoption of variable-speed pump-turbines is assessed in terms of their ability to provide ancillary services [49, 52, 122], or in the improved performances with respect to their fixed-speed counterparts [54, 192].

On a system-wide perspective, the wicket gate travelled distance (defined as the sum of the displacements) and number of movements (defined as the instant in which the blades' stop either because they have reached the target position or because their movement is inverted) has shown to be good indicators for a turbine performing frequency regulation, hence they have been adopted in this thesis [35, 156, 193].

A variable-speed pump can provide ancillary services (contrary to the fixed-speed counterpart), but to the author's knowledge there are no established methodologies to assess the impacts of the provision of such services. Studies on variable-speed hydraulic machine wear and tear tend to focus on the turbine mode [194, 195]; if not, they employ computational fluid dynamics or finite elements method, looking at the

Table 2.3: Model parameters of the PSHP.

Penstock				Pump Turbine			
$\hat{H}_g^{min}$	345 m	$\hat{H}_g^{max}$	367 m	$\hat{N}^{min}$	472 rpm	$\hat{N}^{max}$	577 rpm
L	770 m	D_p	3 m	$\hat{N}_{r,var}$	525 rpm	$\hat{N}_{r,fix}$	500 rpm
ϵ	0.03 mm	λ	0.0182	D_1	3.2 m	B_1	0.32 m
K	$0.0048\,s^2/m^5$	f_p	0.0323 pu	c_{00}	−0.587 pu	d_{00}	−4.9728 pu
T_w	1.531 s	ρ	$1025\,kg/m^3$	c_{10}	1.2636 pu	d_{10}	6.3459 pu
a_p	$1000\,m/s^2$	g	$9.8066\,m/s^2$	c_{01}	0.9857 pu	d_{01}	10.7409 pu
n_{ge}	3			c_{20}	−0.5758 pu	d_{20}	−3.5486 pu
Governor				c_{11}	0.2401 pu	d_{11}	−4.9975 pu
$k_{p,var}$	1.8	$k_{i,var}$	0.18	c_{02}	−0.3266 pu	d_{02}	−6.9107 pu
$k_{p,fix}$	2	$k_{i,fix}$	4.32			d_{21}	2.2702 pu
T_s	0.5 s	Bl	0.0025 pu			d_{12}	0.4324 pu
mxgctr	−0.1 pu	mxgtor	0.1 pu			d_{03}	1.6401 pu
DFIG				e_3	−0.6440 pu	f_6	−4.6824 pu
p_r^{min}	−0.15 pu	p_r^{max}	0.15 pu	e_2	0.0791 pu	f_5	15.8210 pu
c_{em}^{min}	0 pu	c_{em}^{max}	1.2 pu	e_1	−0.0380 pu	f_4	−21.0811 pu
T_m	6 s	T_{cH}	0.5 s	e_0	1.2095 pu	f_3	13.9513 pu
n_{syn}	1 pu					f_2	−6.3278 pu
						f_1	3.2682 pu
						f_0	−0.0010 pu

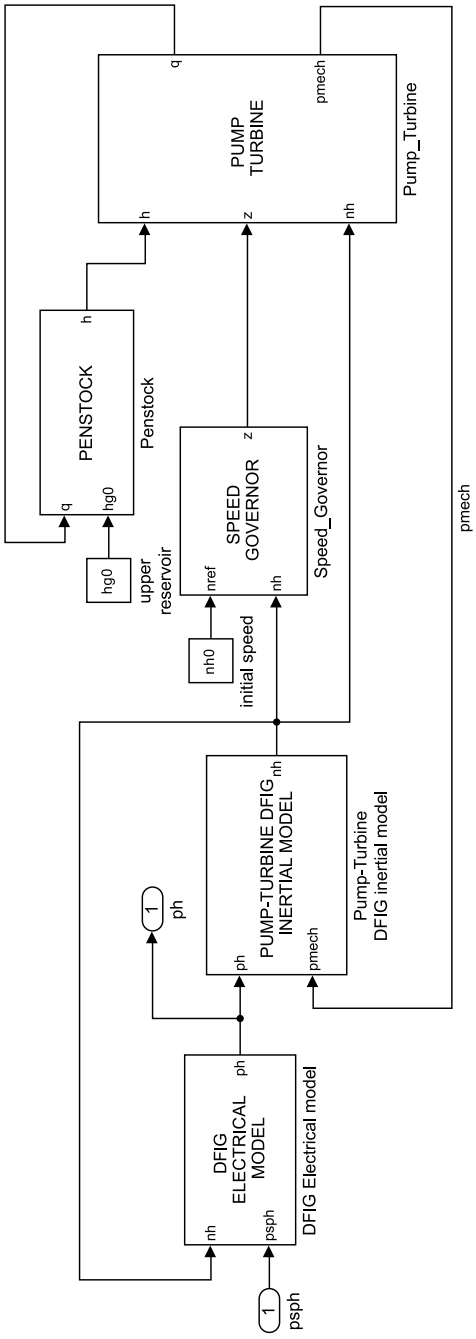

FIGURE 2.6: Block diagram of the PSHP modules and their connections.

phenomena occurring in the machine [28, 62, 196]. All this considered, this study proposes a new method to assess the quality of the operation of the variable-speed pump in providing ancillary services: the assumption is that the fluctuations of the torque at the shaft, $\hat{T}_{mech}\,(N\,m)$, are directly related to the wear and tear of the equipment, of the respective signal:

$$\hat{T}_{mech} = t_{mech} \cdot \frac{\hat{P}^{b,h}}{\hat{\omega}^{b}_{h}} = \frac{p_{mech}}{n_h} \cdot \frac{\hat{P}_{mech}}{\frac{2\pi \hat{N}^{b}_{h}}{60}}. \tag{2.29}$$

Then, this signal was used to compute the Mei-Wang Fluctuation index (MWFi) [131], combining the standard deviation with the rotation angle θ of a signal here defined as a collection of N data points of the type (x, y), x being the time instant and y the recorded value (the mechanical torque in this case):

$$\begin{aligned} MWFi &= \sqrt{\frac{1}{N}\sum_{i=1}^{N}(y(i)-\bar{y})^2} \times \sum_{i=1}^{N}\theta_i \\ \theta_i &= \begin{cases} \arctan|k_i| & i = 1 \text{ or } N \\ |\text{arctank}_i - \text{arctank}_{i-1}| & 2 \le i \le N-1, \text{ and } k_i \times k_{i-1} \ge 0 \\ \arctan|k_i| + \arctan|k_{i-1}| & 2 \le i \le N-1, \text{ and } k_i \times k_{i-1} < 0 \end{cases} \\ k_i &= \begin{cases} \frac{y(i+1)-y(i)}{x(i+1)-x(i)} & 1 \le i \le N-1 \\ \frac{y(N)-y(N-1)}{x(N)-x(N-1)} & i = N \end{cases}, \end{aligned} \tag{2.30}$$

Here, $\bar{y}$ refers to the mean value of the y series. The MWFi was preferred for its ability to detect fluctuations in processes where classical indices fail (zigzag, sine/cosine processes, with different numbers of repetitions) [131].

TABLE 2.4: BESS model parameters.

Parameter	Value
T_{cB}	0.3 s
$T_{del,b}$	0.1 s
$\hat{\eta}_b$	0.9
EP_{ratio}	3600 s

IV BATTERIES

The chemical phenomena are assumed to be at least one order of magnitude faster than the electrical ones [197]. For this reason, and given the time scale of the grid ancillary services considered in this thesis, the chemical phenomena have been neglected. The electrical phenomena mainly correspond to the power converter [140], which has been modelled as a fist order lag combined with a pure delay:

$$p_b = \frac{1}{T_{cB} \cdot s + 1} e^{-sT_{del,b}} psp_b, \tag{2.31}$$

where $T_{del,b}$ represents the time delay of the measurement and control circuits and T_{cB} represents the time necessary for the converter to deliver the active power p_b from the psp signal psp_b. During its operation the BESS State Of Charge (SOC) varies according to the energy stored/released and is calculated by taking into account the round-trip efficiency η_{rt} (assumed constant) of the charge/discharge processes and the device capacity (defined by the energy-to-power ratio, EP_{ratio}):

$$SOC_b = -\frac{1}{EP_{ratio}} \cdot \begin{cases} \hat{\eta}_b^{0.5} \frac{1}{s} p_b, & p_b < 0 \\ \hat{\eta}_b^{-0.5} \frac{1}{s} p_b, & p_b > 0 \end{cases} \quad ; \quad SOC_b \in [0, 1]. \tag{2.32}$$

The list of the BESS parameters, together with their values, is presented in Table 2.4.

IV.1 Experimental validation

Experimental measurements were performed to validate the model, namely the assumption that a Li-ion BESS can be represented by its power converter, as the electrochemical phenomena in the cells occur much faster than those at the power converter.

Field measurements were performed at the CEDER facility (CIEMAT) in Soria (Spain), on Pb-acid and Li-ion battery banks. The aim of the measurements was to determine the delay between the psp fed to the equipment and the active power delivery, and assess if this delay is somehow dependant from the SOC and/or the charge/discharge power demanded.

The issue with the measurement setup was that the power electronics used for the BESS were repurposed PV inverters. The samples were recorded in the control room, without dedicated instrumentation (voltmeters, ammeters). Figure 2.7 shows one example of recorded data. The inverter communication and control system would communicate a value every second. The equipment had one communication channel, used for both sending the psp command and the recorded power values. As was explained by the facility personnel and as can be seen from the Figure 2.7, when the psp varies (from standstill to discharge mode) the inverter is busy in adjusting the power flow and can not effectively communicate the power values: the same measurement is repeated for about 5 s before a new data point is acquired. When steady-state is reached, the inverter manages to record data more frequently, still with low accuracy.

Moreover it looks like the Li-ion BESS requires about 10 s to reach steady-state, which is most likely due to some sort of rate limiter action from the control system, and not due to the BESS own dynamic. No information about intentional delays or rate limiting control schemes were provided by the facility personnel. Pb-acid BESS records were similar to Figure 2.7: they are not displayed as they would not provide any extra meaningful information.

A Li-ion BESS was expected to arrive in early 2022 in the CEDEX

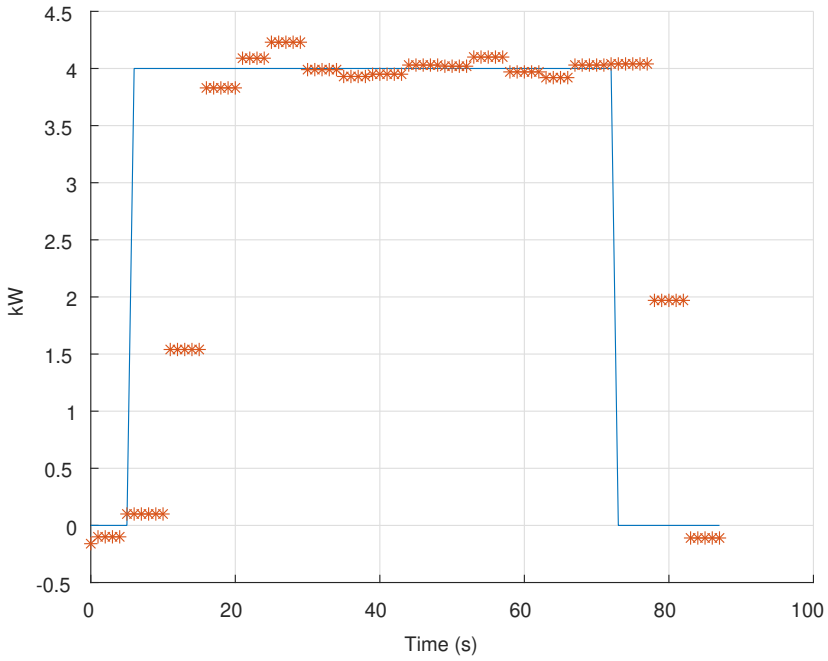

FIGURE 2.7: Experimental measurements on a 20 kW Li-ion battery bank: SOC at 100 % and 4 kW discharge psp. The blue line is the psp, the asterisks the recorded active power output.

(CIEMAT) facility in Madrid, but due to the international logistics crisis in Europe and rest of the world, they arrived at destination too late to allow tests to be done.

For these reasons, experimental validation of the BESS model will be part of future work.

IV.II BESS ageing estimation

Batteries degradation by idling (calendar ageing) is neglected, taking only into account the life consumption due to cycling.

According to Stroe et al. [85], of all the charge/discharge cycles, the j-th cycle generates a corresponding capacity degradation C_{loss_j} which depends on its mean SOC value SOC_{b,avg_j}, the number of the charge/dis-

charge cycles of the same type nc_j, and their depth cd_j. For a Li-ion battery bank operating at 25 °C:

$$C_{loss_j} = 0.021e^{-0.01943SOC_{b,avg_j}} \cdot cd_j^{0.7612} \cdot nc_j^{0.5}. \tag{2.33}$$

The SOC signal outputted from the simulation is processed by the Rainflow algorithm that returns the number, depth, and average SOC of the equivalent cycles [198]. Miner's rule for mechanical fatigue [199] is used for estimating the combined capacity loss for each equivalent cycle the BESS has gone through:

$$LC_b = \sum_j \frac{nc_j}{n_{eol_j}}, \tag{2.34}$$

$$n_{eol_j} = \left[\frac{0.2}{0.021e^{-0.01943SOC^b_{avg_j}} \cdot cd_j^{0.7612}.} \right]^2. \tag{2.35}$$

The number of j-th cycles that lead to the BESS end of life presented in (2.35), n_{eol_j}, are calculated using (2.33) by setting the capacity loss equal to 20 %, the industry standard for BESS end of life. The result is the per-unit life consumption LC that the BESS bears during the simulated period. The base quantity for the BESS cells life has been chosen as the number of hours in 10 years operation, 87.6×10^3 h.

v Flywheel

The model for the FESS was adapted from the "ACEBO" model developed by CIEMAT (Madrid, Spain) [90, 200, 201]. This flywheel has metallic rotor (placed in a vacuum chamber) and is equipped with hybrid angular contact ball rotor bearings with an additional magnetic levitation system. The electrical machine is a 6/4 switched reluctance machine coupled with a three half-bridge insulated gate bipolar transistor (IGBT) converter. The device was designed to have a rated (maximum) power of 25 kW. The

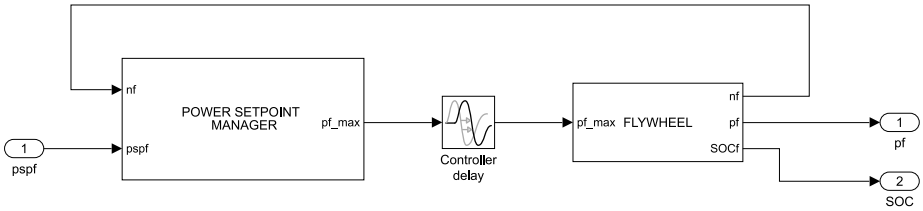

FIGURE 2.8: Block diagram of the FESS

rotor speed range is 6000 rpm to 9000 rpm, guaranteeing that the FESS usable energy is 50 % of the total rotor energy, a common practice in the design of flywheels [90]. The energy capacity is 869.2 Wh, meaning that the energy-to-power ratio is 0.0348 kWh/kW. The block diagram of the FESS is presented in Figure 2.8.

The "Power Set-point Manager" calculates the maximum power p_f^{max} the FESS can deliver according to the rotor rotational speed n_f via Equation (2.36).

$$p_f^{max} = \sum_{i=1}^{4} a_i \cdot n_f^{4-i}, \tag{2.36}$$

The power output p_f is equal to the power set-point psp_f, unless it exceeds the maximum power, in which case the power output is $p_f = p_f^{max}$.

The power converter is modeled as a simple time delay (see "Controller delay" block in Figure 2.8), i.e. the power converter follows the active power set-point calculated in the the "Power Set-point Manager" block with a time delay $T_{del,f}$. The "Flywheel" block calculates the flywheel rotational speed and SOC according to (2.37) and (2.38) respectively. Moreover it contains the logical apparatus that controls the power flows according to the SOC (e.g. if the SOC is 0 the power output can only be negative, meaning only the recharge is possible), and the FESS inertial

model equation.

$$n_f = \frac{1}{s}\frac{\hat{T}^b}{I\hat{\omega}_f^b}\left(-\frac{p_f}{\hat{\eta}_f \cdot n_f} - \frac{\hat{T}_{loss}}{\hat{T}_f^b}\right), \tag{2.37}$$

$$SOC_f = \frac{n_f^2 - n_f^{min\,2}}{n_f^{max\,2} - n_f^{min\,2}}, \tag{2.38}$$

$$\hat{T}_f^b = \frac{\hat{P}_{1f}^b}{\hat{\omega}_f^b}; \quad \hat{\omega}_f^b = \frac{2\pi\hat{N}_f^{max}}{60}.$$

where $\hat{\omega}_f^b$ is the base angular velocity (rad/s), $\hat{P}_{1f}^b$ is the rated power of a single module (25 kW), $\hat{T}_f^b$ is the base torque (N m), I the moment of inertia (kg m^2), $\hat{\eta}_f$ is the round-trip efficiency (assumed constant), $\hat{T}_{loss}$ (N m) represents the self-discharge losses as a resistant torque, n_f^{min} and n_f^{max} (pu) are the rotational speed bounds. The list of the parameters, together with their values, is presented in Table 2.5.

A single FESS module rated power is 25 kW: it is common practice to install several modules so that their cumulative powers achieve the desired power capacity. Model-wise this would be the ideal approach: as seen in (2.36) the model is not completely linear. On the other hand, including hundreds of blocks like the one in Fig. 2.8 raises the computation times to unfeasible levels. For this reason, one upscaled FESS model has been used.

v.1 Experimental validation

Experimental measurements were performed in the CEDEX (CIEMAT) facility in Madrid (Spain), on an "ACEBO" device. During the visiting period, the flywheel device was not fully operational: one of the three phases of the electrical machine was malfunctioning, hence the device was working with two phases only.

It was not possible to perform the measurements in the normal rotational speed range of the FESS, as the technicians reported that the device

TABLE 2.5: FESS model parameters.

Parameter	Value	Unit
a_1	4.0824	pu
a_2	−9.5191	pu
a_3	8.5572	pu
a_4	−2.0744	pu
$\hat{\eta}_f$	0.82	(−)
I	15.5	$N\,m^2$
$\hat{N}_{min}$	6000	rpm
$\hat{N}_{max}$	9000	rpm
$\hat{P}^b_{1f}$	25	kW
$T_{del,f}$	0.1	s
$\hat{T}_{loss}$	0.07	N m

shows a resonance frequency at about 4000 rpm. In normal operation, this rotational speed value is swiftly crossed during startup, but with one phase out of service, the machine could only accelerate at 2/3 of the rated value. For this reason the measurements were performed over a rotational speed range of 500 rpm to 3500 rpm.

The missing phase introduces a signal noise inversely proportional to the rotational speed. In fact, the slower the rotor, the more time a pole of the electrical machine would spend in the area of the malfunctioning phase. Figure 2.9 shows the discharge power of the FESS at an initial rotational speed of 3500 rpm, the maximum speed. The data was sampled at 20 kHz and smoothed with a gaussian-weighted moving-average filter (via MATLAB's `smoothdata` native method), with a 800 data points window.

The conclusion that can be made from the recorded data is that even at very low speeds (< 3500 rpm) and with one malfunctioning phase, the FESS is highly responsive to deliver the required power: as it can be seen from Figure 2.9, (bottom plot), the FESS takes less than 50 ms to reach a steady-state discharge power of 4 kW. It is reasonable to expect that with

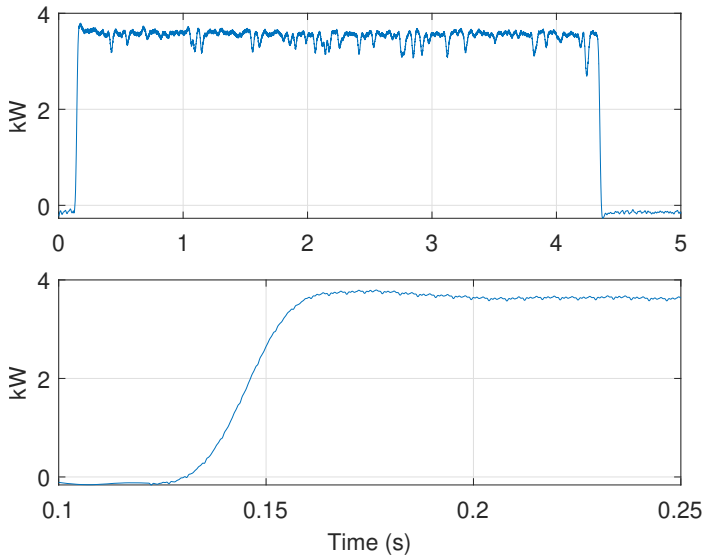

FIGURE 2.9: Discharge power of the "ACEBO" FESS at 3500 rpm initial rotational speed. Top: recorded data (cleaned). Bottom: transient between standstill and discharge mode.

a properly working device at higher speeds, faster response times can be achieved.

The CEDEX facility also hosts a Supercapacitor Energy Storage System (SC) for research purposes. As seen in Section 1.II.IV, supercapacitors have high power density and short response time, as well as low energy density, similarly to FESS. For this reason, data was also recorded for this device.

The SC is composed of 256 2.7 V × 3000 F cells [99] connected in series, for an equivalent capacitance of 11.72 F. The system voltage limits are 340 V and 680 V which have been considered as 0 % and 100 % SOC, respectively. The SC is connected to a three phase bidirectional interleaved DC/DC converter [202].

Each measurement consisted in issuing a charge/discharge psp when the SC was at a given SOC. A voltmeter and an ammeter were placed in the DC bus, between the DC/DC power converter and the SC. The rated

TABLE 2.6: Psps (kW) for the SC experimental measurements. The first row indicates the charge/discharge currents (A), whereas the first column the SC initial voltage (V), corresponding to various SOC levels.

V/A	15.00	30.00	45.00	60.00	120.00
340	5.10	10.20	15.30	20.40	40.80
430.1	6.45	12.90	19.35	25.81	51.61
504.3	7.56	15.13	22.69	30.26	60.52
568.9	8.53	17.07	25.60	34.13	68.27
626.9	9.40	18.81	28.21	37.61	75.23
680	10.20	20.40	30.60	40.80	81.60

power was set to be 40.8 kW ($C_{rate} = 1$), corresponding to a current of 60 A at 680 V. Measurements were done for six SOC values [0, 20, 40, 60, 80, 100]% and five C_{rate}: [0.25, 0.5, 0.75, 1, 2] h^{-1}. The power electronics control was set to be power-based, because in this study the same perspective is applied (as is described in Section 2.VI): the converter would work to maintain a constant power output over time, adjusting the charge/discharge current. Therefore, for each desired voltage-current combination, a psp was calculated and used to control the charge/discharge power of the SC. All the combinations are shown in Table 2.6, and the data from some of them are shown in Figure 2.10. At minimum (maximum) voltage, only the charge (discharge) tests were performed. An oscilloscope with a 20 kHz sampling frequency was used to record the DC voltage and current.

The outcomes of the tests were puzzling. After processing the data with the same method as the FESS recorded data (see page 59) it was clear that the SC did behave in an unpredictable way. Figure 2.10a shows the normalized discharge current of the SC for different initial voltage levels. These correspond to the 120 A column of Table 2.6. It can be seen that there is a relatively slight (at most about 200 ms) increase in the duration of the transient with the decrease of the initial tension (SOC). This behavior is much more visible in Figure 2.10b, which shows the same

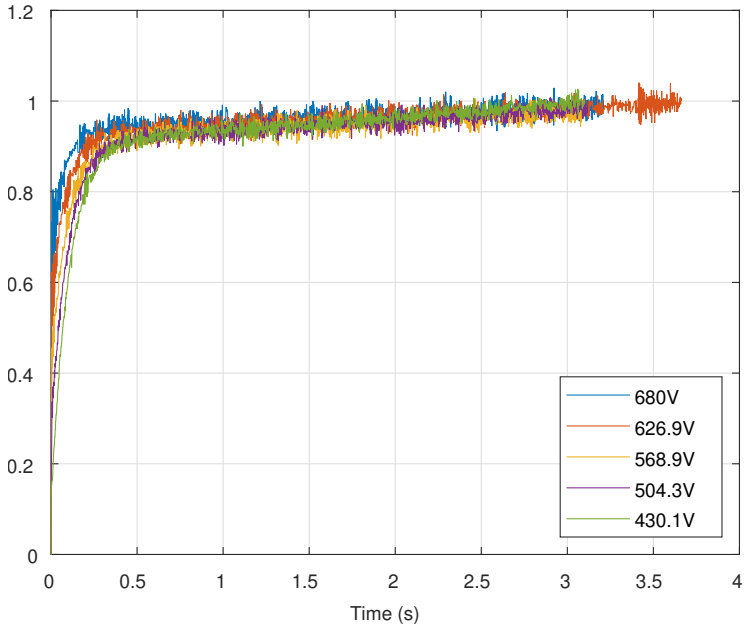

(a) Discharge at different SOCs and 120 A.

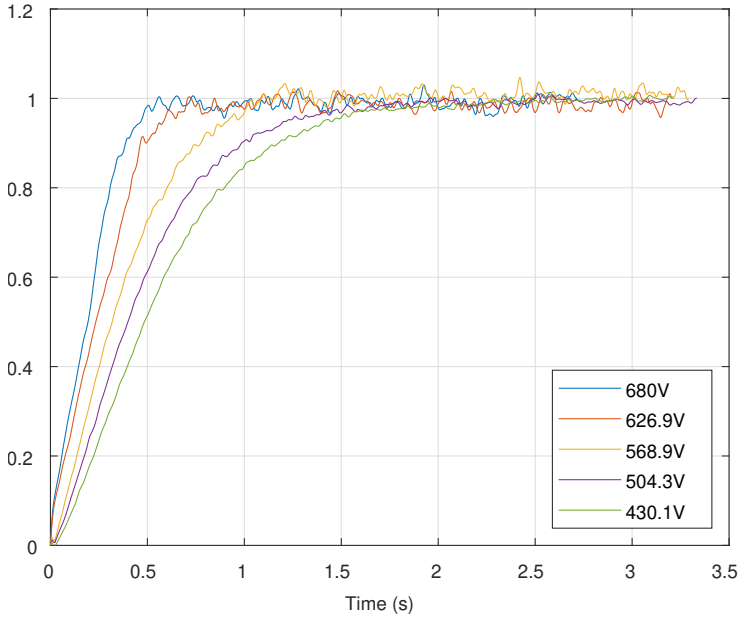

(b) Discharge at different SOCs and 15 A.

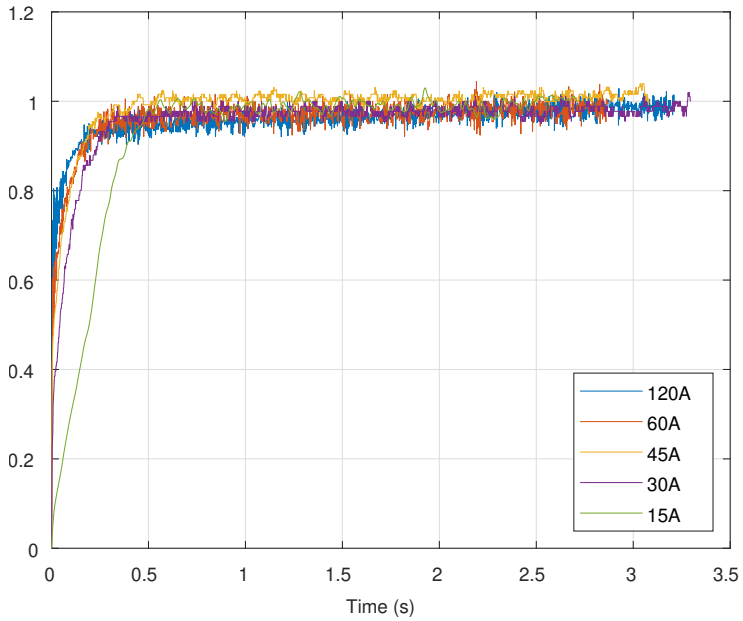

(c) Discharge at maximum SOCs and different currents.

FIGURE 2.10: Normalized discharge currents of the SC.

measurements for a target discharge current of 15 A: here the transient lasts from about 500 ms (680 V curve), up to 1.5 s (430.1 V curve). This behavior appeared both with charge and discharge measurements.

The critical aspects of these measurements can be summarized as follows: i) it appears that the higher is the requested power from the SC, the faster the device is in delivering it; ii) this behavior is more pronounced for lower charge/discharge currents (Figures 2.10a – 2.10b); iii) at constant initial voltage, the same pattern appears: the lower the discharge current the higher the delay (Figure 2.10c); iv) last, in some cases the charge/discharge current would exhibit a linear trend in the first milliseconds after the charge/discharge activation. This is clearly visible from the 680 V curve of Figure 2.10b and 15 A curve of Figure 2.10c.

To find the root cause of this behavior was not an easy task, and it was deeply investigated with the help of the people in CIEMAT (Dr. Gustavo Navarro Soriano in particular) as well as of prof. Manuele Bertoluzzo, senior lecturer of the "Technologies for control of electrical converters and drives" course at the University of Padova, who both confirmed the anomaly in the observations.

Eventually, in early 2023, Dr. Navarro Soriano found the root cause of the SC behavior. The power electronics control software was developed by CIEMAT as a Simulink system, which is later compiled in the C language and loaded into a dSPACE microprocessor[3]. The software normally employs a current-based control loop, as opposed to the power-based logic that was adopted to record the data. Therefore, the control software was modified prior to the measurements, recompiled, and loaded into the microprocessor. The control scheme would convert the reference power signal P_{ref} into a reference current signal I_{ref} by dividing the former by the recorded SC voltage U_{sc}. The reference current signal is later filtered from the noise (with a 100 Hz cutoff frequency low-pass filter), fed into a saturator block (for protection against overcurrents) and a rate limiter block, which is set to limit the current variation to $\pm$1000 A/s. The problem ap-

[3]This software and control logic was not made available to the author.

pears to have occurred during the compilation of the Simulink model: the compiled rate limiter block would be buggy and unnecessarily limit the rate of increase/decrease of the current in some cases. Figure 2.11 shows the current signal recorded from the microprocessor (5 kHz sampling rate), after the filter, and after the rate limiter block.

This experimental work has been useful in showing that SC can behave in an anomalous way due to the power electronics control system. It also showed that power electronics can present extremely fast response times. The BESS sampled data from Section 2.IV.I exhibit an abnormal communication delay in this sense, whereas the non-buggt SC records show that the transient can last for no more than 100 ms, proving that the communication delay may be shorter than the data in the literature suggests. The theory supports the conclusion that the response time of Li-ion cells is short, while these tests do so for the communication delay. Finally, it would be better to investigate the choice to adopt a current-based control loop rather than a power-based one, but unfortunately there was not enough time to delve into the matter.

VI Power management system

The power management system in a HESS determines how the regulation effort of the FCR and FRR is split among the PSHP, BESS, and FESS. One criterion can be to have the fastest devices (FESS and BESS) to take care of the high frequency components while the PSHP deals with the low ones. Another criterion can be to leave the regulation effort to the auxiliaries (BESS, FESS) and make the PSHP adjust its power output only when the required power by the grid exceeds the auxiliaries' power rating. These strategies were respectively called Frequency Split (FS) and Hydro Recharge (HR) by Laban [140], and have inspired this work. While these were originally designed for a two-devices HESS, in this work they have been redesigned for a hybrid system made of three components. In addition to that, both criteria have been adapted and implemented

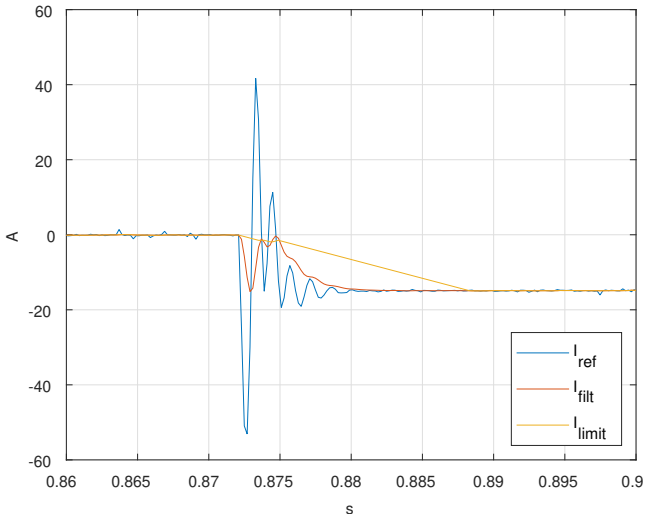

FIGURE 2.11: Sample record of the SC microprocessor, corresponding to the 340 V, 15 A case. I_{ref} is the reference current signal obtained from the measured tension, I_{filt} is the signal's after the filter, and I_{limit} the signal after the rate limiter.

for both the pump-turbine variable-speed and fixed-speed technologies, which are controlled differently, as seen from Equations (2.27) and (2.28).

Given its power and energy availability, the PSHP should have the task to control both the BESS and FESS SOC, by increasing or reducing its power output.

The management system therefore is made of two elements: the SOC control component, and the division of the regulation effort between the different technologies. While in variable-speed operation the PSHP active power generation can be controlled at will, the synchronous motor/generator is strictly coupled to the grid, and the active power control is performed at the speed governor level, by acting on the p_h^* term of Eq. (2.28).

The following paragraphs present the SOC control (which is independent from the criterion upon which the regulation effort is shared between the devices), the Frequency Split, and the Hydro Recharge, respectively.

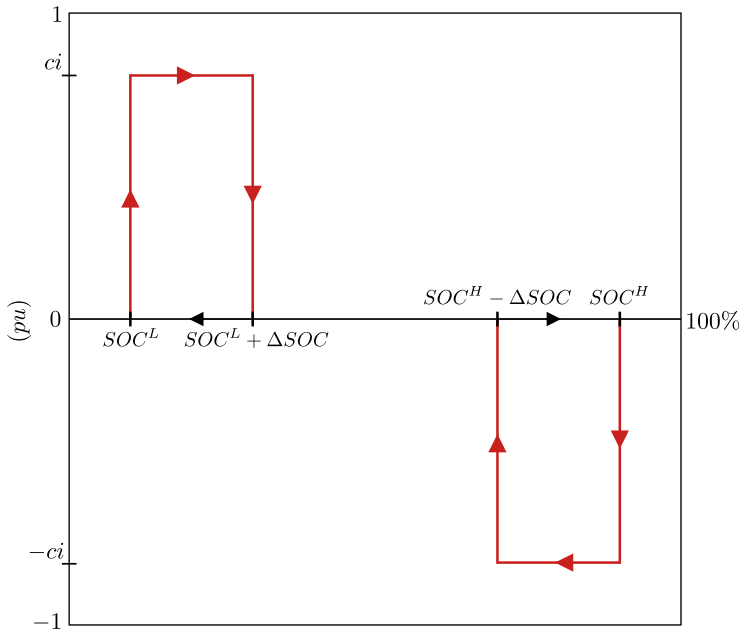

FIGURE 2.12: Graphical representation of the SOC control logic. The red arrows signal when the SOC control is active, the black arrows mean that the control is inactive.

VI.I SOC control

It is important for the PSHP to control the SOC of both BESS and FESS in order to prevent either device to be fully charged (discharged), resulting in the unavailability to provide upwards (downwards) regulation services, and reduce the ageing of the BESS due to cycling.

The SOC control algorithm of either BESS and FESS is the same as in [141], with the difference that the inner bounds are defined as the outer plus/minus a fixed band, ΔSOC. The graphical representation of the SOC control logic is displayed in Figure 2.12.

The PSHP, having the highest energy and power availability, is tasked to perform the necessary upwards/downwards power adjustments to restore the BESS/FESS SOC inside a specific band. This is controlled by means of a dedicated psp: $\text{psp}_{\text{b}}^{\text{SOC}}$ for the BESS SOC, and $\text{psp}_{\text{f}}^{\text{SOC}}$ for

the FESS. If the BESS SOC is inside the low/high bounds, defined by SOC_b^L and SOC_b^H respectively, the SOC control psp is null, as no action is required by the PSHP. As soon as the SOC exceeds one of the bounds, for example $SOC_b < SOC_b^L$, the PSHP receives a psp and increments its power output by a fraction of the BESS rated power, called "charge intensity" ci_b. This charges the BESS, and the procedure deactivates as soon as a certain amount of SOC (defined by the ΔSOC_b) is restored. The same goes for when the SOC exceeds the "high" threshold, SOC_b^H. The same logic applies for the FESS.

The base quantity for $ci_{b/f}$ is the rated power of the respective device, and an appropriate base change is performed before the signal is fed to the PSHP.

VI.II *The Frequency Split power management strategy*

Both the BESS and FESS are equipped with their own power converter, which controls the power output according to the psp that it is fed. In this configuration there are two low-pass filters, for the PSHP and BESS respectively.

$$\underline{psp}_f = \underline{psp}_{tot} - (\underline{p}_h - \underline{p}_h^0) - \underline{p}_b, \tag{2.39}$$

$$\underline{psp}_b = \frac{\underline{psp}_{tot}}{T_{lpf,b}s + 1} - (\underline{p}_h - \underline{p}_h^0) + \frac{1}{T_{lpf,h}s + 1}\underline{psp}_f^{SOC}. \tag{2.40}$$

$$\underline{psp}_{tot} = \underline{psp}_I + \underline{psp}_{II} \tag{2.41}$$

Eq. (2.39) is used to calculate the FESS psp, $\underline{psp}_f$, in system base, as the unfiltered (droop-based) primary and secondary psps, $\underline{psp}_I$ and $\underline{psp}_{II}$ respectively, minus the power that it is currently being delivered by the PSHP and BESS, respectively.

The BESS psp is generated according to eq. (2.40). The primary and secondary required powers are filtered with its low-pass filter with time constant $T_{lpf,b}$ (s), to which the PSHP active power variation is subtracted.

The last term in the equation includes the SOC control psp used for the PSHP to control the FESS SOC, filtered with $T_{lpf,h}$ (s) time constant. This is to make sure that the power meant to control FESS SOC is not absorbed by the BESS.

In variable-speed operation (2.42), the PSHP control signal is generated akin to the BESS and FESS, as it is elaborated by the GSC, whereas in fixed-speed operation (2.43) the signal becomes part of the power-frequency error elaborated by the speed governor PI controller.

$$\underline{psp}_h = \frac{\left(\underline{psp}_{tot} + \underline{psp}_b^{SOC} + \underline{psp}_f^{SOC}\right)}{T_{lpf,h}s + 1} + \frac{T_d s}{T_{fnf}s + 1}\Delta f, \tag{2.42}$$

$$\underline{p}_h^* = \frac{-\underline{psp}_I T_{lpf,h}s + \underline{psp}_{II} + \underline{psp}_b^{SOC} + \underline{psp}_f^{SOC}}{T_{lpf,h}s + 1}. \tag{2.43}$$

As shown in Equation (2.42), the sum of the primary, secondary, and SOC control psps are filtered out from their rapid components. The last term pertains to the synthetic inertia control action, with a $T_d = 0.1\,s$ derivative gain and $T_{fnf} = 2\,s$ time constant for the noise filter [10, 60].

In fixed-speed operation the psp accounts only for the change in the psp due to the secondary regulation and the BESS and FESS SOC control. Such psp is used as input to determine the speed governor power-frequency error (2.28). This is easily seen in (2.43), as the first term in the numerator: the primary regulation psp filtered with a high-pass filter with the same time constant as the low-pass filter of the secondary and SOC control psps.

The appropriate base-changes are actuated to each psp, before they are fed to the corresponding energy storage device.

VI.III The Hydro Recharge power management strategy

The HR power management strategy aims at maintaining as stationary as possible the PSHP operating point. This is achieved until two conditions

are met: there is no need to perform SOC control, and the BESS rated power is enough to provide the necessary regulation. The FESS is meant to absorb high power peaks with low duration and can not sustain a power input/output for long, due to its very low energy density. As such the strategy prioritizes the BESS to perform FCR and FRR, making the PSHP intervene only when the BESS is incapable of providing the regulation services. The FESS can not be considered into this logic, as otherwise its SOC control would activate too often, forcing the PSHP to continuously adjust its power output. The SOC control routine presented in Section 2.VI.I is used in the control.

In either variable-speed or fixed-speed operation, the BESS and FESS psps are obtained by means of Equations (2.40) – (2.39), respectively. The control logic for the variable-speed PSHP is presented in the following equations:

$$\underline{psp}_h = \frac{T_d s}{T_{fnf} s + 1} \Delta f + \frac{\underline{psp}_b^{SOC} + \underline{psp}_f^{SOC}}{T_{lpf,h} s + 1} + \frac{1}{T_{lpf,b} s + 1} \cdot \ldots$$

$$\textbf{if } \underline{psp}_b^{SOC} \neq 0: \quad \frac{\underline{psp}_{tot}}{T_{lpf,h} s + 1}, \tag{2.44}$$

$$\textbf{elseif } \left|\underline{psp}_{tot}\right| > \underline{p}_b: \ \operatorname{sign}\left(\underline{psp}_{tot}\right) \cdot \left(\left|\underline{psp}_{tot}\right| - \underline{p}_b\right) \tag{2.45}$$

$$\textbf{else}: \quad 0. \tag{2.46}$$

The basic components of the psp signal are the synthetic inertia (first term) and the SOC control psps – which are 0 in case there is no SOC control to perform – properly filtered with the PSHP time constant. During normal operation mode nothing is added: Equation (2.46). In case the BESS SOC must be controlled, the PSHP must adjust its power output to charge/discharge the BESS and to replace it in delivering the regulation power, as stated by Equation (2.44). The PSHP action is delayed with a low-pass-filter, akin to the FS strategy, to avoid abrupt power variations. If there is no need for SOC control, it may happen that the BESS power rating is insufficient to deliver the required power to the grid. In this case

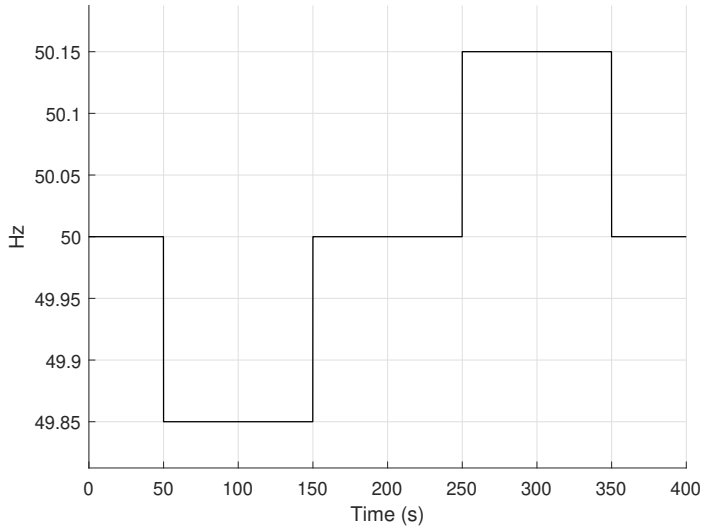

FIGURE 2.13: Test frequency signal.

the missing power is delivered by the PSHP: Equation (2.45). The output of the logical routine is filtered with $T_{lpf,b}$: the SOC control routine is not impacted by this, as the BESS time constant is lower than the the PSHP's; when the BESS power needs to be complemented, the filter makes the PSHP deliver it at the same rate a BESS would.

In fixed-speed operation the same logic applies, with the difference that instead of the synthetic inertia term, the FCR psp is subtracted to the control signal, in order to inhibit the primary regulation.

$$\underline{p}^{*}_{h} = \frac{\underline{psp}^{SOC}_{b} + \underline{psp}^{SOC}_{f}}{T_{lpf,h}s + 1} - \underline{psp}_{I} + \frac{1}{T_{lpf,b}s + 1} \cdot \dots \\ \dots + \text{Equations (2.44)} \div \text{(2.46)}. \tag{2.47}$$

To show the differences between the two strategies, a test round of simulations has been conducted. A 150 mHz step frequency deviation signal (Figure 2.13) was fed into the variable/fixed speed turbine model, with/out hybridization and the simulation results are presented in Fig-

ures 2.14 – 2.15. From top to bottom the plots show: the power plant active power $\hat{P}_{pp}$, the PSHP, BESS and the FESS The power plant power is the active power "visible" by the grid, defined as the sum of the instantaneous PSHP, BESS, and FESS powers:

$$\hat{P}_{pp}(t) = \hat{P}_h(t) + \hat{P}_b(t) + \hat{P}_f(t). \tag{2.48}$$

The plots were obtained with the same parameters in any configuration: 10 MW of installed BESS and FESS, the PSHP and BESS filter time constants set to 30 s and 15 s, and the SOC control bounds equal to 40 % – 60 % for the BESS, and 20 % – 80 % for the FESS, which are found to be wide enough not to trigger the SOC control routine.

When the PSHP is hybridized, its rated power increases, resulting in a proportional increase of the primary and secondary reserves the plant must allocate. This is why the steady-state plant and the PSHP (with the FS strategy) power outputs are higher in hybrid configuration compared to in the non hybrid case.

Both control strategies present two sets of parameters that need to be tuned: the low-pass filter time constants, which determine the plant ability to deliver the FCR in due time, and the SOC control limits and charge intensity, which control BESS and FESS cycling and availability to participate in the regulation. The next chapter will delve into these aspects.

List of symbols

Accents		
	The quantity is in absolute value	$\hat{}$
	The quantity is in per-unit, system base.	$\_$
Greek letters		
	Guide Vanes Opening (°)	α

	Roughness coefficient (mm)	ϵ
	Efficiency	η
	Rotation angle	θ
	Darcy's friction coefficient	λ
	Density (kg/m^3)	ρ
	Permanent droop	σ
	Flow number	ϕ
	Pressure number	ψ
	Angular velocity (rad/s)	ω
Roman letters		
	Polynomial coefficients for the flywheel maximum power (pu)	a_i
	Penstock wave speed (m/s)	a_p
	Runner inlet section (m)	B_1
	Cycle depth	cd
	Polynomial coefficients of the turbine curves (pu)	c_{ij}, d_{ij}
	Charge intensity (pu)	ci
	Capacity lost	C_{loss}
	Control Signal	CS
	Diameter (m)	D
	Polynomial coefficients of the pump curves (pu)	e_i, f_i
	Energy-to-power ratio (h)	EP_{ratio}
	Polynomial functions (dimensional)	F, G
	Hydraulic losses coefficient (pu)	f_p
	Grid frequency	f
	Gravitational acceleration (m/s^2)	g
	Water head (m)	$\hat{H}$
	Hydraulic head (pu)	h
	Flywheel moment of inertia ($kg\,m^2$)	I
	Friction losses coefficient (m)	K

	PI controller integral gain	k_i
	PI controller proportional gain	k_p
	AGC signal (%)	$L_{\%}$
	Penstock length (m)	L_p
	Rotational speed (rpm)	$\hat{N}$
	Number of charge/discharge cycles	nc
	Number of cycles to reach end-of-life	nf
	Penstock segment	n_{ge}
	Active power (MW)	$\hat{P}$
	Active power (pu)	$\hat{p}$
	Flow rate (m^3/s)	$\hat{Q}$
	Flow rate (pu)	q
	Laplacian operator	s
	Allocated FRR (pu)	SB
	Converter time constant of the BESS (s)	T_{cB}
	RSC time constant (s)	T_{cH}
	Servomotor time constant (s)	T_s
	BESS measurement and control circuits delay (s)	$T_{del,b}$
	Generator mechanical starting time (s)	T_m
	Water starting time (s)	T_w
	Mechanical torque (pu)	t_{mech}
	Position of the wicket gate blades (pu)	z
Subscripts		
	Hydraulic machine inlet section	1
	Average	avg
	Battery Energy Storage System	b
	Flywheel Energy Storage System	f
	Fixed	fix
	Gross	g
	Pumped Storage Hydro Power	h
	Primary regulation	I

	Secondary regulation	II
	i-th element	i
	j-th element	j
	k-th element	k
	Lost or related to losses	loss
	Mechanical	mech
	Rotational speed (pu)	n
	Power plant	pp
	Pump	p
	Rated	r
	Reference	ref
	Synchronous	syn
	Total	tot
	Turbine	t
	Variable	var
Superscripts		
	At $t = 0$	0
	Base quantity	b
	Lower bound	L
	Maximum	max
	Minimum	min
	Related to the SOC	SOC
	Upper bound	U

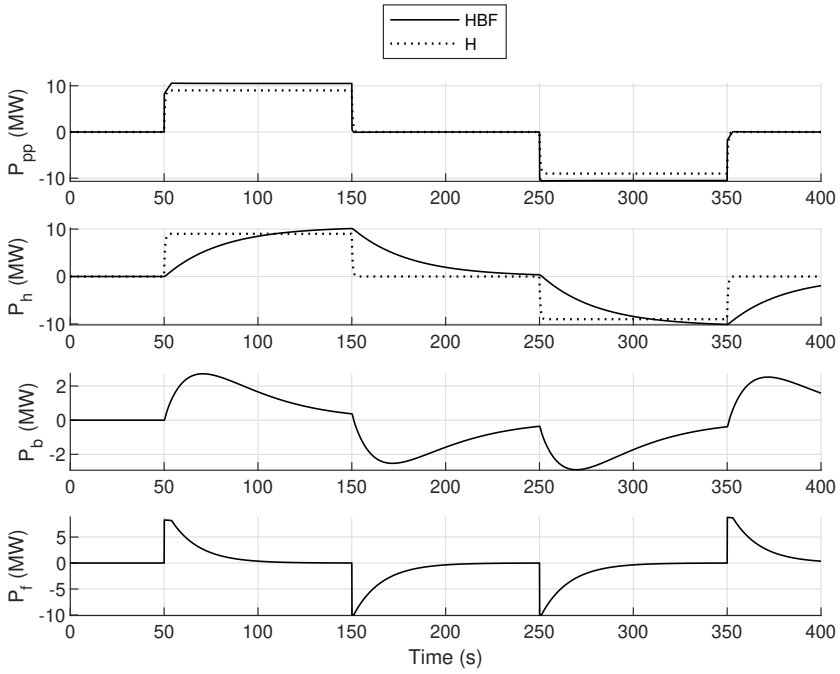

(a)

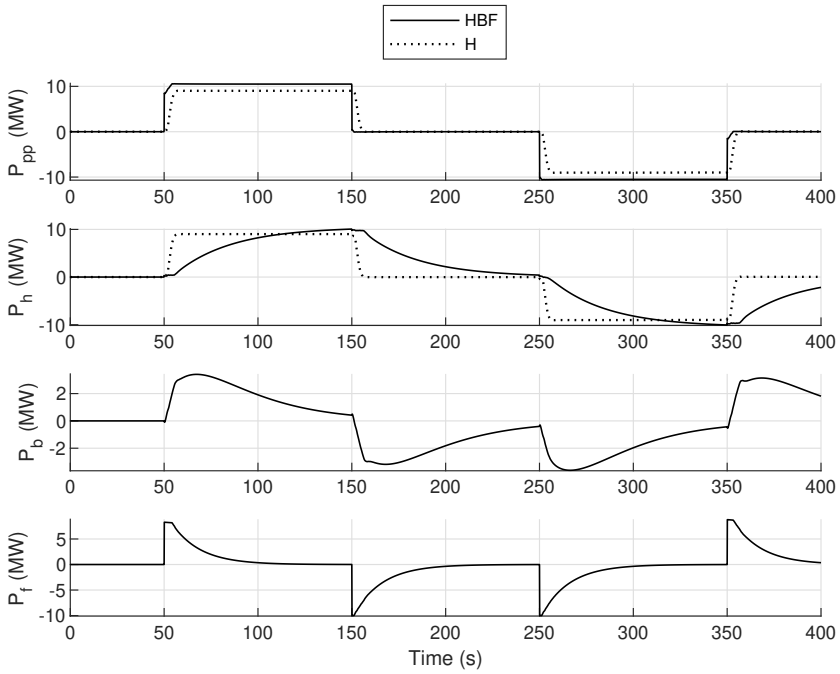

(b)

FIGURE 2.14: Frequency Split control strategy: hybrid (continuous line) and non-hybrid (dotted line) active powers comparison. (a) variable-speed turbine; (b) fixed-speed turbine.

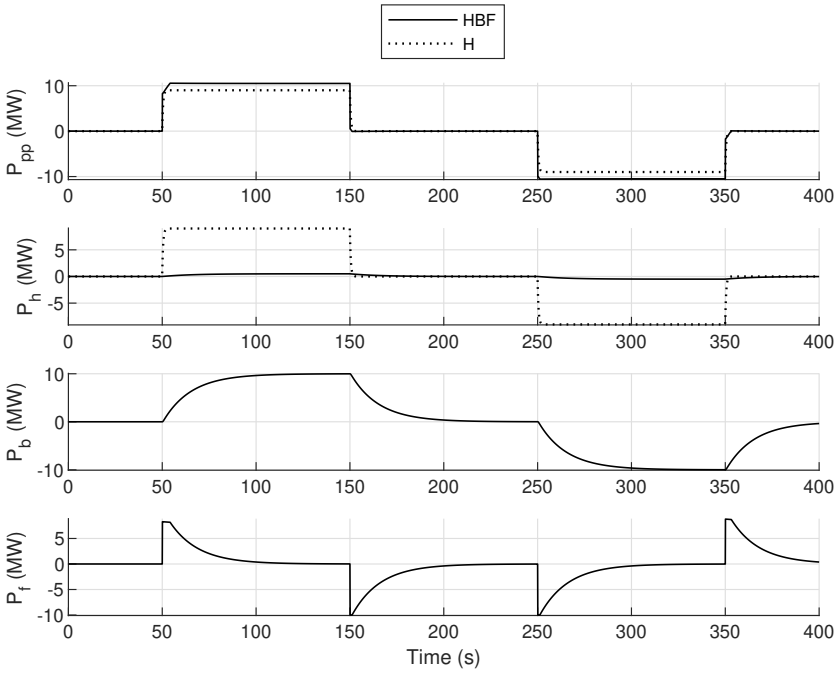

(a)

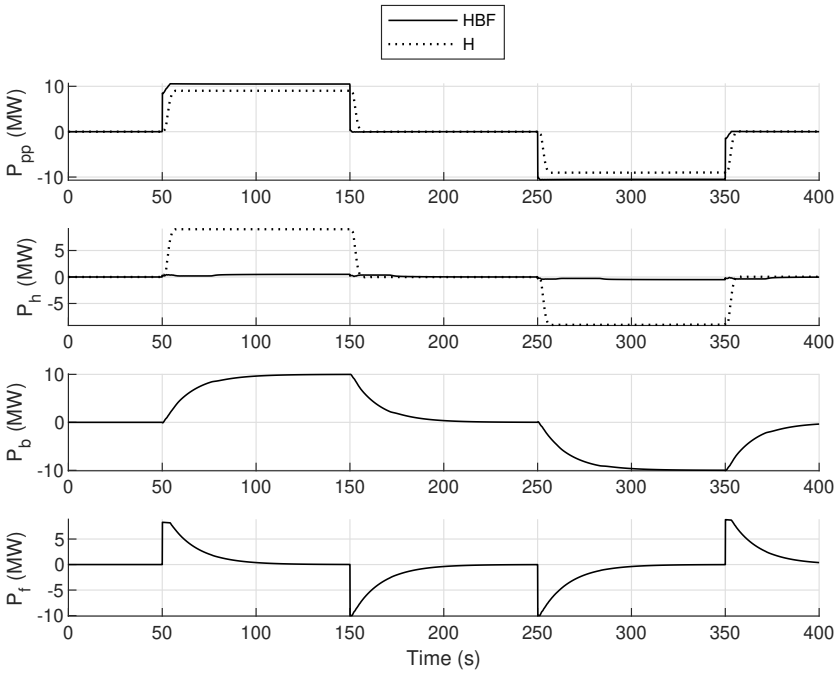

(b)

FIGURE 2.15: Hydro Recharge control strategy: hybrid (continuous line) and non-hybrid (dotted line) active powers comparison. (a) variable-speed turbine; (b) fixed-speed turbine.

3 Open-loop simulations

The hybridization of the Foxi Murdegu Pumped Storage Hydro Power (PSHP) may prove to be beneficial for both the Transmission System Operator (TSO) and the plant owner. This chapter delves into the study of the benefits for the plant owner, estimated as a reduction in the main wear indicators presented in Section 2.III.VII and Section 2.IV.II.

The adopted methodology is to simulate the plant in open-loop under different configurations. This means that the plant's model receives as input the frequency (for Frequency Containment Reserve (FCR)) and the Automatic Generation Control (AGC) (for Frequency Restoration Reserve (FRR)) signals and outputs an active power signal to a sink. The regulating power does not have any effect on the input frequency, hence the simulations allow to assess the readiness of the plant to deliver the output power.

There are many hybridization possibilities, for this reason several combinations of Battery Energy Storage System (BESS) and Flywheel Energy Storage System (FESS) power ratings have been tested. The reference case has been considered the PSHP without hybridization.

This chapter is structured as follows: Section 3.I describes the background common to all the simulated cases; Section 3.II presents the model calibration process that has been used to tune the control parameters; Section 3.III presents the simulation results for the variable-speed turbine and pump with the Frequency Split (FS) (Section 3.III.I) and Hydro Recharge (HR) (Section 3.III.II); last, in Section 3.IV the results are further summarized and commented.

1 Background

The plant is expected to participate in the FCR and FRR services in Sardinia. Real frequency and AGC data for the island of Sardinia were not available, as the TSO deemed them confidential. Instead, 24 h historical frequency and AGC signals from continental Italy were made available (Figure 3.1). It was chosen to simulate 1 h (3600 s) starting from 04:28:17 of 2020-01-21, the recorded hour containing the most intense frequency deviation (over 150 mHz), and beginning at the instant with no frequency error. The frequency's sampling resolution is 20 ms, the AGC signal's is 1 min, linearly interpolated to cover for the missing values.

The variable-speed PSHP is simulated in both turbine and pump mode, whereas the fixed-speed is simulated only in turbine mode, as the pump can not provide FCR nor FRR in the first place.

In every simulation it is assumed that, at $t = 0$, i) the grid's frequency is 50 Hz, the AGC control signal, $L_{\%}$, is 50 (no secondary regulation); ii) the PSHP is in steady state and iii) is consuming/generating the power committed in the day-ahead market, while iv) the BESS and FESS have a null power input/output, and both of their State Of Charge (SOC) is 50 %. The reference rotational speed for the variable-speed hydro machine can be decided at will, and in this work it is set to the rated value (525 rpm), as the same for fixed-speed turbine operation (500 rpm); in variable-speed pump operation the rotational speed depends on the defined power input and the water level at the upper reservoir: the initial power input is chosen so the resulting rotational speed is the rated value, whereas the water level is the same as in turbine mode. The initial quantities of the pump-turbine are presented in Table 3.1. The adoption of numeric tolerances to calculate the initial quantities of the turbine operation lead to minimum discrepancies in the values of $\hat{H}_g^0$.

The PSHP was simulated first without hybridization, and then considering that $\hat{P}_{b/f}$ could assume values in the range of 0.5 MW to 5 MW $\{0.5, 1.5, \dots, 5\}$ MW and testing all the 100 combinations. The search was

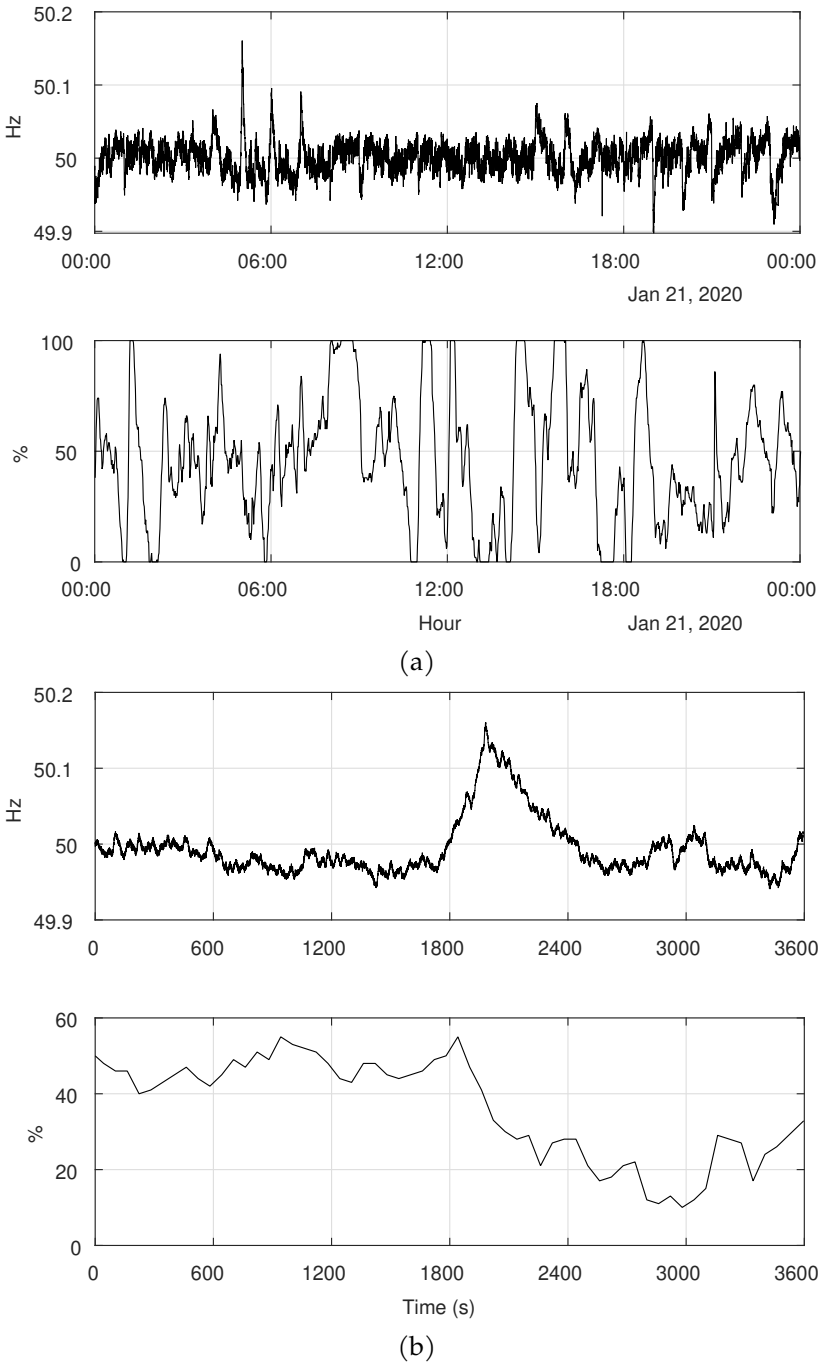

FIGURE 3.1: Continental Italy grid frequency (top) and AGC signals. (a): 24 h data series; (b) selected hour.

TABLE 3.1: Initial conditions of the PSHP, in both turbine (variable and fixed speed) and pump mode. $\hat{H}_g^0$ and $\hat{H}^0$ are in (m), $\hat{Q}^0$ in (m^3/s), $\hat{N}^0$ in (rpm), $\hat{\alpha}^0$ in (°), $\hat{\eta}^0$ in %, and $\hat{P}^0$ in (MW). All the other quantities are in (pu)

	Turbine		Pump		Turbine		Pump
	Variable	Fixed	Variable		Variable	Fixed	Variable
$\hat{H}_g^0$	366.98	366.97	367.00	h_g^0	1.0322	1.0322	1.0322
$\hat{Q}^0$	27.58	26.86	−31.63	q^0	0.5628	0.5482	−0.6456
$\hat{H}^0$	363.34	363.52	371.78	h^0	1.0220	1.0225	1.0457
$\hat{N}^0$	525.00	500.00	−525.20	n^0	1.0000	0.9524	−1.0004
$\hat{\alpha}^0$	12.60	11.80	–	z^0	0.3738	0.3500	–
$\hat{\eta}^0$	79.42	81.50	79.54	η^0	0.9971	1.0232	0.9986
$\hat{P}^0$	80.00	80.00	−94.292	p^0	0.5736	0.5736	−0.6760

limited to the power rating, excluding the energy capacity: the BESS power capacity was fixed as a parameter to 1 MWh/MW, whereas the FESS model used in this study had a fixed speed range (6000 rpm to 9000 rpm).

Obviously the hybrid plant's control depends on the power ratings of both BESS and FESS, therefore the model's control parameters had to be properly calibrated. The next section describes the model calibration process.

II MODEL CALIBRATION

There are two control strategies (FS and HR), each with its set of control parameters: the SOC control's, ($SOC_{b/f}^L$, $SOC_{b/f}^U$, $\Delta SOC_{b/f}$, $ci_{b/f}$), and the low-pas filters' time constants ($T_{lpf,h/b}$).

The SOC control parameters do not directly influence the rapidity of the plant to deliver power. Their values are presented in Table 3.2 and are kept constant in each and every simulation. These were chosen because considered appropriate for both the BESS and the FESS: they prevent

TABLE 3.2: Open-loop simulations SOC control parameters.

	SOC^L (%)	SOC^U (%)	ΔSOC (%)	ci (pu)
BESS	40	60	10	0.8
FESS	20	80	10	0.8

the SOC to reach the extremes (0 or 100 %) and, for the BESS, they are narrow enough to limit the SOC cycling, and wide not to often trigger the SOC control routine. The FESS, having lower energy density, has wider margins as its SOC is more subject to fluctuations than the BESS.

The other set of control parameters, the low-pass filters' time constants, affect the plant's ability to deliver the FCR in due time and their value is a compromise between the plant owner's priority to slow down as much as possible the PSHP and BESS power ramps (to reduce respectively their wear and tear and life consumption), and the TSO's interest in having a fast power delivery to contain the frequency excursions.

The calibration process of these time constants was performed following this procedure. First, all intentional delays ($T_{lpf,h/b}$) were set to zero and the SOC control procedure was suppressed. A −200 mHz[1] step signal was fed to the model, together with a constant AGC signal equal to 50 % (no FRR). The FESS SOC was set to 100 % in order for the device to be able to deliver the maximum power. An interval of possible values of $T_{lpf,h}$ was defined, and the midpoint was used to run a short simulation of the plant. The bisection method was applied to iteratively find the maximum value of $T_{lpf,h}$ that would result in the compliance of the FCR regulations (50 % delivered within 15 s, 100 % within 30 s). A tolerance of 0.05 s between the interval extremes was the stopping criterion of the bisection method. Once the value of $T_{lpf,h}$ was found it was fixed as a parameter, and the same procedure was adopted to find the value of

[1] This value was chosen by rounding up the maximum value of the frequency excursion for the simulated hour.

$T_{lpf,b}$. This process was applied for both the FS and the HR strategies. In the HR strategy the PSHP participates in the FCR when the BESS power is insufficient: this power adjustment is filtered with $T_{lpf,b}$. The $T_{lpf,h}$ constant impacts the SOC control procedure, Equation (2.44), therefore its value does not directly impact the system ability to provide FCR. The procedure, therefore, would converge to the upper bound of the interval. A value of 200 s was set for $T_{lpf,h}$ in the HR strategy.

The graphical representation of the resulting values of the low-pass filters time constants are presented in Figures 3.2 – 3.4.

The first thing to note is that the higher BESS and FESS powers are, the slower the PSHP (under the FS strategy) and BESS (regardless of the strategy) can be operated. The filters time constants are identical for the variable-speed PSHP both in pump and turbine mode, because they are connected to the same electrical machine, which – within certain limits – decouples the electrical and mechanical parts of the PSHP.

Another aspect worth to note is that, while the BESS time constants are almost identical in both operation modes (regardless of the strategy), the values for the PSHP time constants are higher in variable-speed than in fixed-speed (FS strategy). This is expected, as the variable-speed unit is much faster in delivering the active power to the grid, hence it can afford a higher delay without compromising its ability to fulfil the grid obligations. Eventually, $T_{lpf,b}$ shows a slight dependency to the FESS power rating in addition to its own. This is due to the architecture of the control strategies. The rated power of the Hybrid Energy Storage System (HESS) increases with the increase of the FESS installed power, for the same installed BESS. This means that the HESS must deliver more active power for FCR, for the same frequency error. As a result, the BESS must deliver more energy during the transient, and to do so, its low-pass filter time constant must slightly decrease, or the power output would be reduced beforehand. Figure 3.5 shows the plant and BESS active power output after a step underfrequency deviation. The two simulated cases differ only for $T_{lpf,b}$, whose value in Case 2 is higher than in Case 1. It can

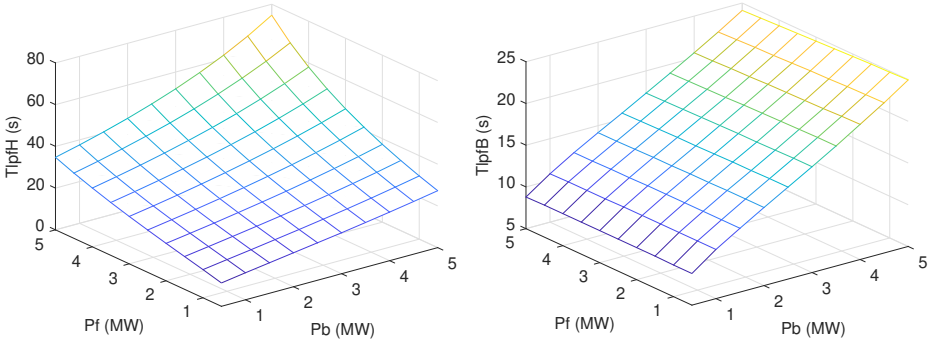

(a) (b)

FIGURE 3.2: Frequency Split: calibrated values of (a) $T_{lpf,h}$ and (b) $T_{lpf,b}$ for the variable-speed PSHP in turbine mode. The values are identical for pump mode.

be seen that, if $T_{lpf,b}$ is too high, the BESS will reduce its power before the plant output value has reached the correct value. The FESS in this case can't supply the additional power as its maximum power depends on its SOC.

III RESULTS

The results presented in this section were obtained with the calibrated values of the Low-Pass Filter (LPF) time constants for each power management strategy separately. Hereafter a "configuration" is a combination of installed BESS and FESS powers, and is indicated as $(\hat{P}_b, \hat{P}_f)$ MW.

III.1 *Operation in Frequency Split*

The simulations results for each operation mode – variable-speed turbine, fixed-speed turbine, and variable-speed pump – are summarized in Figures 3.6 – 3.9. A red circle indicates the global minimum.

In the variable-speed case, the reference case (non hybrid) for the turbine returns a distance travelled by the wicket gate's blades, Lwg, equal

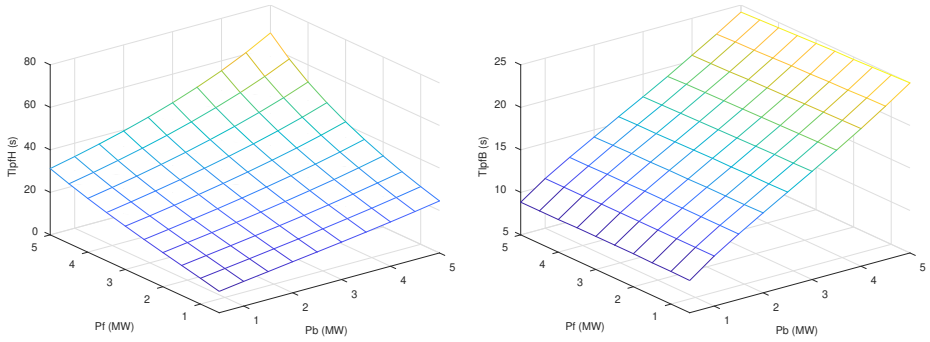

(a) (b)

FIGURE 3.3: Frequency Split: calibrated values of (a) $T_{lpf,h}$ and (b)$T_{lpf,b}$ for the fixed-speed PSHP in turbine mode.

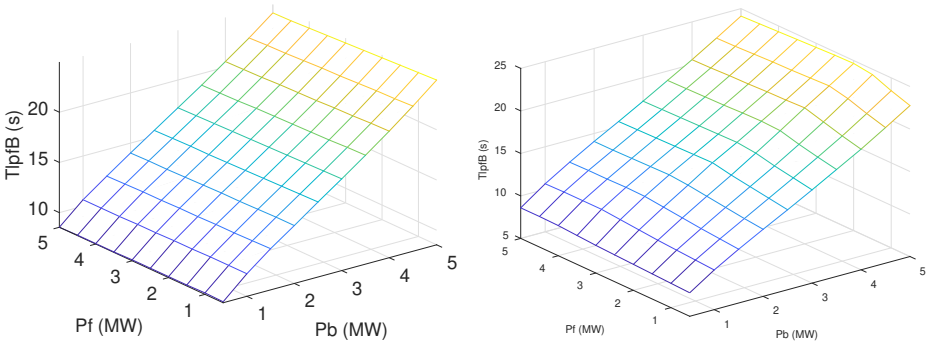

(a) (b)

FIGURE 3.4: Hydro Recharge: calibrated values of $T_{lpf,b}$ for the variable-speed (a) and fixed-speed (b) turbine PSHP.

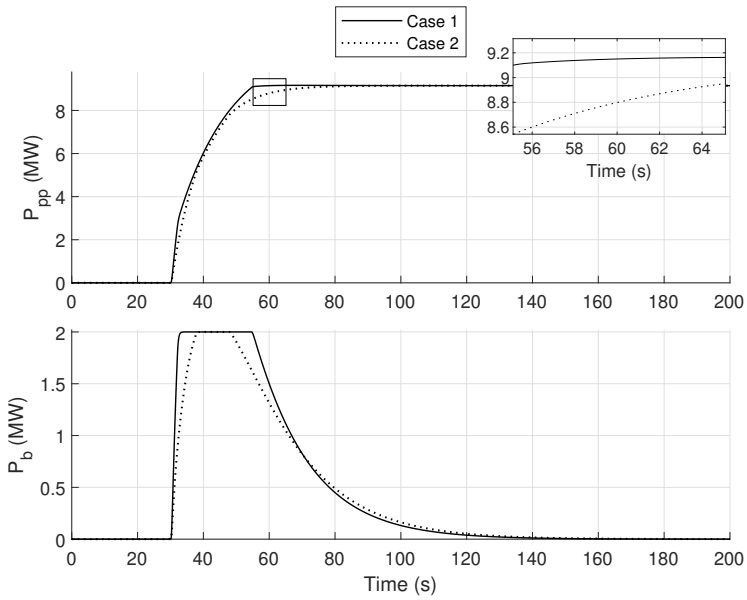

FIGURE 3.5: Active power comparison between two simulations: calibrated and incremented $T_{lpf,b}$ (Case 1 and 2 respectively). Top: plant power. Bottom: BESS power.

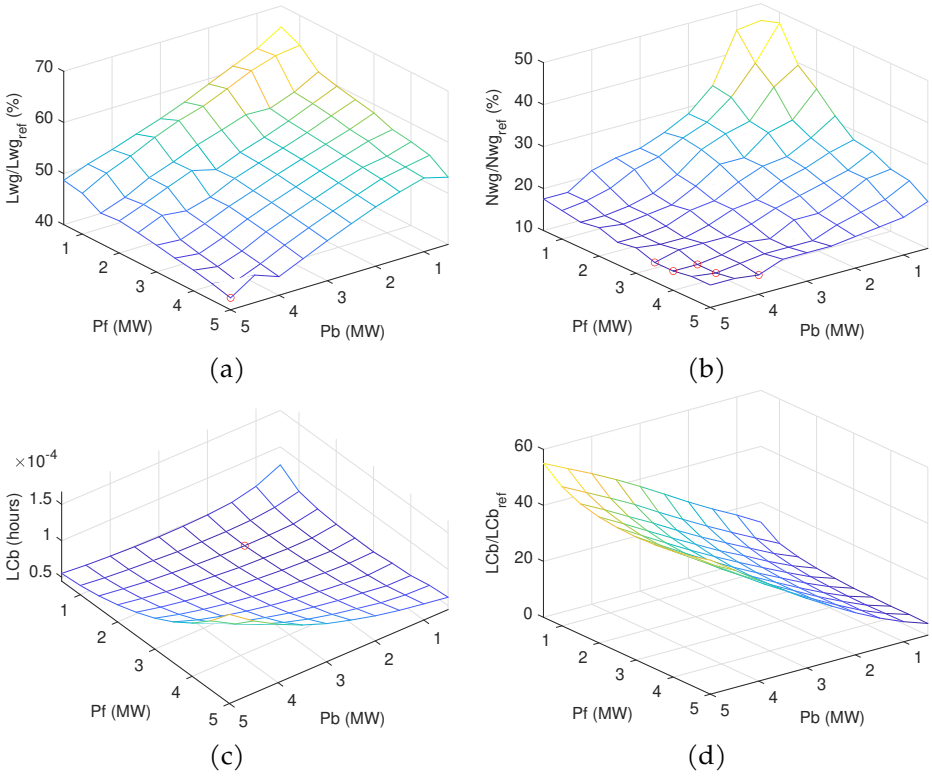

FIGURE 3.6: FS strategy: results for the variable-speed turbine. (a) relative wicket gate's travelled distance and (b) number of movements, (c) BESS absolute and (d) relative life consumption. $\mathrm{Lwg_{ref}} = 0.7564\,\mathrm{pu}$, $\mathrm{Nwg_{ref}} = 137$.

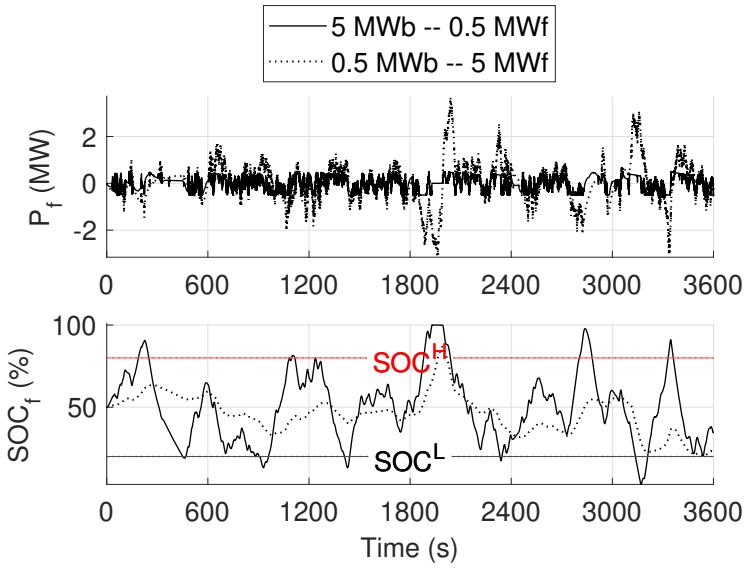

(a)

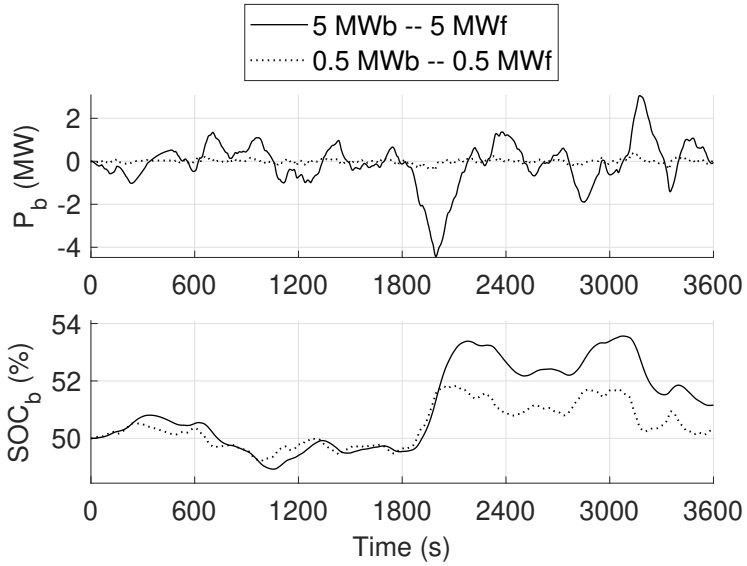

(b)

FIGURE 3.7: FS strategy: comparison between the electric power (top plot) and SOC (bottom plot) of (a) FESS and (b) BESS in two different configurations.

to 0.7564 pu, and a total of 137 movements (Nwg). The configuration (0.5, 0.5) MW is enough to reduce Lwg to 65.86 % (0.4984 pu) w.r.t the reference case and Nwg to 45.99 % (63).

While the maximum hybridizing power corresponds to the minimum Lwg (0.3202 pu, 42.33 %, Figure 3.6a), there are 5 configurations that minimize Nwg, reducing it to 14.60 % (20) of the reference value. The most attractive among these, from the plant owner's point of view, would be the one with the minimal installed power (= minimal capital investment), corresponding to the configuration (4.5, 4) MW, with an associated Lwg of 43.34 % (0.3278 pu); the other configuration, (5, 3.5) MW, has a slightly superior Lwg: 44.55 % (0.3370 pu).

It is worth noting that the BESS and FESS installed powers impact the PSHP performance differently: configuration (5, 0.5) MW is associated with Lwg = 0.3682 pu and Nwg = 24, while configuration (0.5, 5) MW presents Lwg = 0.4021 pu and Nwg = 29. This difference is due to the FESS SOC control process. When the FESS rated power is 0.5 MW, the SOC control routine is triggered several times during one hour of operation (Figure 3.7a), where the PSHP adjusts its power output by 80 % of the FESS rated power: 0.4 MW. When the FESS rated power is maximum (5 MW), only one SOC control event occurs, but this entails a power adjustment by the PSHP of 4 MW (again 80 % of the FESS rated power), resulting in wider movements of the guide vanes.

The BESS life consumption LC_b, does not appear to be correlated with the low-pass filter's time constant $T_{lpf,b}$ (Figure 3.2b), but rather it seems that a low rated power is better from the BESS point of view (Figure 3.6c). In the best case (2, 1.5) MW, 1 h of operation consumes 4.48×10^{-5} h of BESS life, whereas in the worst case (5, 5) MW 1.67×10^{-4} h. The preferred combination for the PSHP, (4.5, 4) MW, has an associated BESS life consumption equal to 1.034×10^{-4} h.

One would expect LC_b and the BESS power rating to be inversely proportional because increasing the rated power means an increase in energy capacity (as the energy to power ratio is fixed), hence the amplitude of the

SOC cycles should be smaller. However what can be seen from Figure 3.6c is that LC_b tends to increase with the BESS power. This behaviour is explained by the low-pass filter's time constant: the higher the power rating the higher the intentional delay (Figure 3.2b). This delay reduces the BESS power fluctuations, but at the same time the power is "slower" in being adjusted, as seen in Figure 3.7b. Given these findings, we ran a set of simulations with $T_{lpf,b} = 0$, to verify that the intentional delay is actually beneficial for the BESS. The LC_b resulting from the simulations with $T_{lpf,b} = 0$ was considered the "reference", and the ratio between the LC_b with and without the delay is shown in Figure 3.6d. It can be seen that at high BESS power rating, its life consumption is about 50 % of the degradation experienced without delay, while at low powers this ratio drops down to less than 10 %. From these findings we can conclude that it is always convenient to have a non-zero low-pass filter's time constant, and the lower the BESS power rating, the more beneficial the delay.

In fixed-speed operation, the non-hybridized turbine's wicket gate covers a distance of 0.6728 pu with a total of 112 movements. With the (0.5, 0.5) MW configuration, Lwg becomes 73.62 % of the reference value (0.4953 pu, the maximum in the hybrid configuration), whereas the minimum value is achieved for the combination (5, 4.5) MW, with a value of 0.3186 pu (45.92 %). The maximum reduction of Nwg (18.75 % of the reference value) is achieved by 2 configurations, the most preferable one (in terms of minimal Lwg) being (5, 4.5) MW.

The fixed-speed results are smaller both in magnitude and in improvement w.r.t. the variable-speed counterpart, as the latter's ability to quickly deliver electrical power generates a rotational speed imbalance that requires a stronger action by the speed governor. Being faster in delivering electrical power, the variable-speed's admissible intentional delay is higher than the fixed-speed's, hence the latter's Lwg and Nwg improvements are inferior, in percentage (Figure 3.8).

Regarding the BESS, the maximum LC_b is experienced with minimal installed powers, (0.5, 0.5) MW: 2.106×10^{-4} h; on the other hand, the

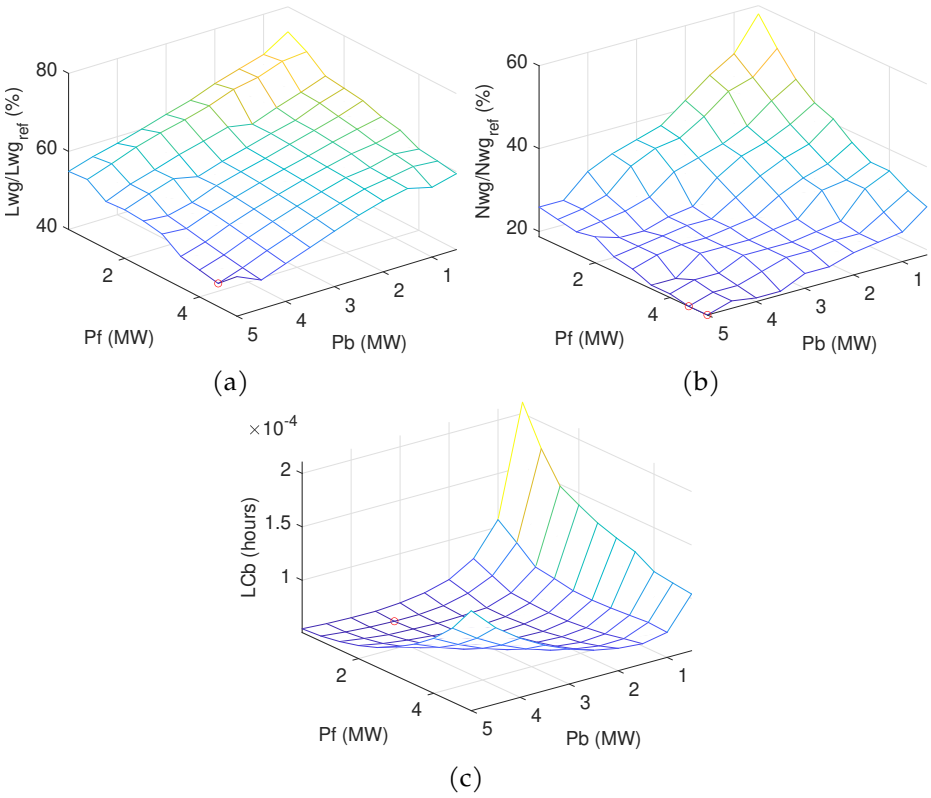

FIGURE 3.8: FS strategy: results for the fixed-speed turbine. In the non-hybridized plant (reference case): $\mathrm{Lwg_{ref}} = 0.6728\,\mathrm{pu}$, $\mathrm{Nwg_{ref}} = 112$.

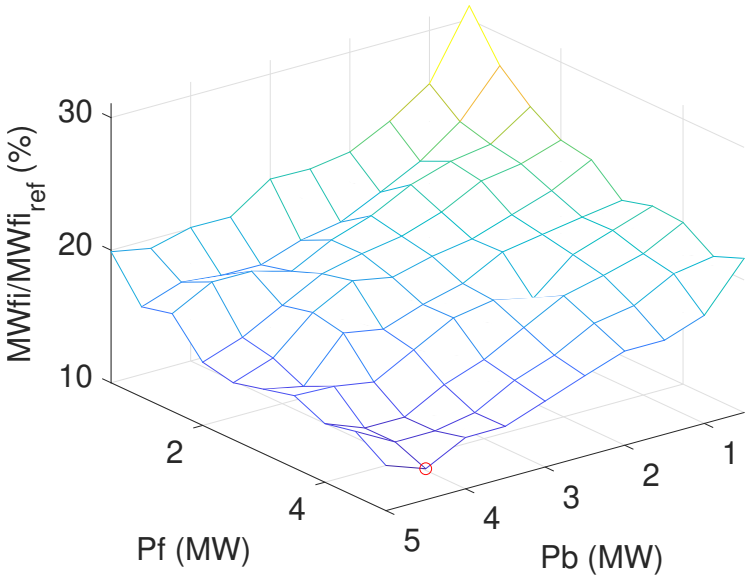

(a)

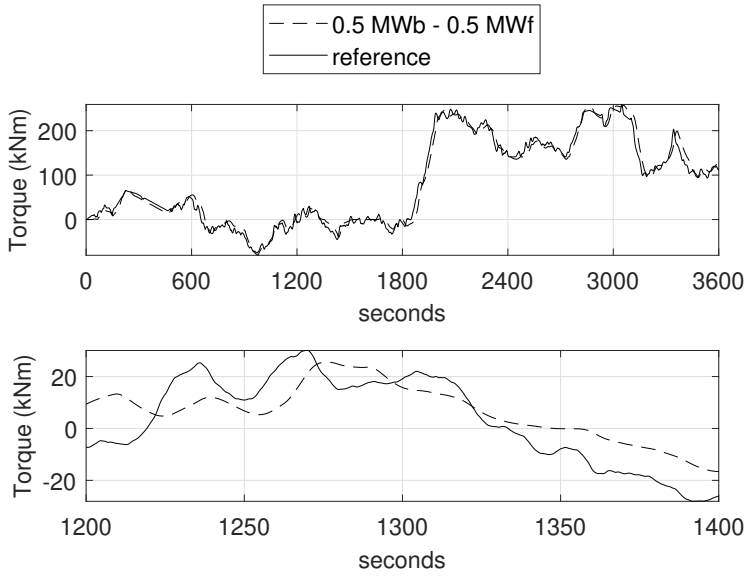

(b)

FIGURE 3.9: FS strategy: results for the variable-speed pump. (a) Mei-Wang fluctuation index of the torque at the shaft (reference case: $MWFi_{ref} = 6.4871 \times 10^9$); (b) comparison of the torque between the (non-hybridized) reference case and the plant hybridized with 5 MW of BESS and FESS (top) and detail (bottom).

minimum life consumption is achieved in the (3.5, 1) MW: 5.107×10^{-5} h. The simulations of the hybrid configurations with $T_{lpf,b} = 0$ confirm that the intentional delay reduces the life consumption of the device. The plot has been omitted as it does not provide additional information w.r.t. Figure 3.6d.

In pump mode, the torque's Mei-Wang Fluctuation index (MWFi) decreases at least by about two thirds w.r.t. the non-hybridized case (Figure 3.9a). The fluctuation index was applied to the dimensional torque (kNm), sampled every 1 s, to avoid the numerical fluctuations due to the small simulation step size affecting the outcome. The dimensional torque was employed as the MWFi calculation is non-linear, hence the per-unit notation would be inadequate to describe the phenomenon. The index reduction is mostly caused by the rotation angle component θ_i of (2.30): the ratio between the standard deviations (first term of the product) between the configuration (0.5, 0.5) MW and the reference case is 0.9934, whereas the ratio of the sum of the rotation angles is 0.1386. This can also be seen graphically from Figure 3.9b and more clearly in the detail: the two plots have similar standard deviations but different rotation angles over time. The MWFi ranges from 12.34 % (4.5, 5) MW of the reference value to 31.05 % (0.5 MW BESS – 0.5 MW FESS).

III.II *Operation in Hydro Recharge mode*

The results offered by the HR power management strategy present visible differences compared to the FS strategy. The graphical representations of the results are presented in Figures 3.10, 3.12 and 3.13.

The minimum achieved wicket gate travelled distance for the variable-speed pump-turbine Lwg is obtained with the (3.5,0.5) MW configuration: 38.08 % (0.2880 pu), Figure 3.10a. This indicator is always inferior than the reference case, and in most of the cases it is inferior compared to the results of the FS strategy . In this configuration the values of Nwg and LC_b are respectively 16.06 % (22) and 3.32×10^{-3} h. There are 4 configurations that

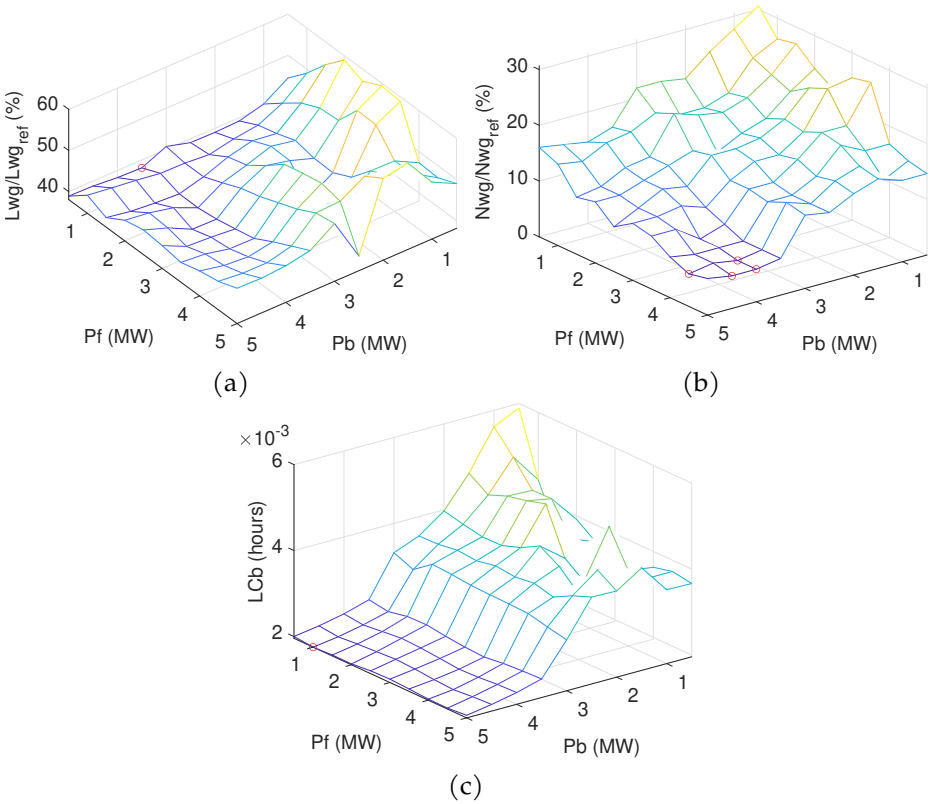

FIGURE 3.10: HR strategy: results for the variable-speed turbine operation mode. (a) relative wicket gate's travelled distance and (b) number of movements, (c) BESS. $\text{Lwg}_{\text{ref}} = 0.7564\,\text{pu}$, $\text{Nwg}_{\text{ref}} = 137$.

minimize Nwg (Figure 3.10b), the most attractive among them being the (4,4.5) MW, the one with minimum installed power among them. With the HR strategy there is a sharper reduction in wicket gate movements: in fact if with the FS strategy the best solution would lead to a total of 20 movements, with the current strategy the number drops to 8 (5.84 %), with a corresponding travelled distance of 0.3356 pu (44.37 %).

The main difference between the FS and the HR strategy is, as expected, related to the BESS life consumption: in the best case, configuration (5, 1) MW LC_b is 1.96×10^{-3} h, two order of magnitude greater than in the FS case (in which the minimum value was 4.48×10^{-5} h). This is expected, as the BESS has to deal with a wider range of frequency components of the regulation effort than in the previous case. From Figure 3.10c it is clear that for values of BESS rated power greater than 2.5 MW the lost life due to cycling sharply decreases. Figure 3.11a shows the active powers (plant's, PSHP, BESS, and FESS respectively). It can be seen that, overall, the plant can properly provide the grid's frequency (top plot), and that the power rating of the BESS becomes insufficient in providing the regulation at about 2000 s from the start of the simulation. Moreover, the SOC control routine has a deep impact in the plant behavior: this procedure is active for more than 10 min (from second 2300 to over 3000). At the end of the simulation, there is a time window in which the BESS power is saturated, but thanks to the FESS power availability and the PSHP action, the plant can still accurately track the grid's frequency. Figure 3.11b presents a comparison between the configuration (5, 1) MW (continuous line) and the one with maximum installed powers – (5, 5) MW, dotted line. In the first case, the PSHP performs more low-amplitude movements (Lwg = 0.3214 pu, Nwg = 20), whereas in the second case the opposite occurs (Lwg = 0.3530 pu, Nwg = 9). The BESS life consumption is 2.95 % smaller in the (5, 1) MW with respect to the (5, 5) MW.

The results for the fixed-speed turbine are in line with what seen so far for its variable-speed counterpart (Figure 3.12). The minimum Lwg is had for the same configuration as in variable-speed operation: (3.5, 0.5) MW,

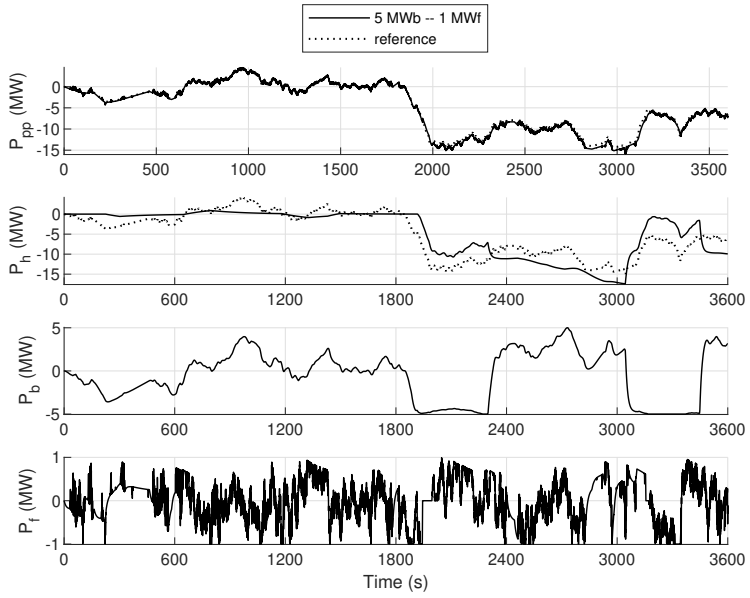

(a)

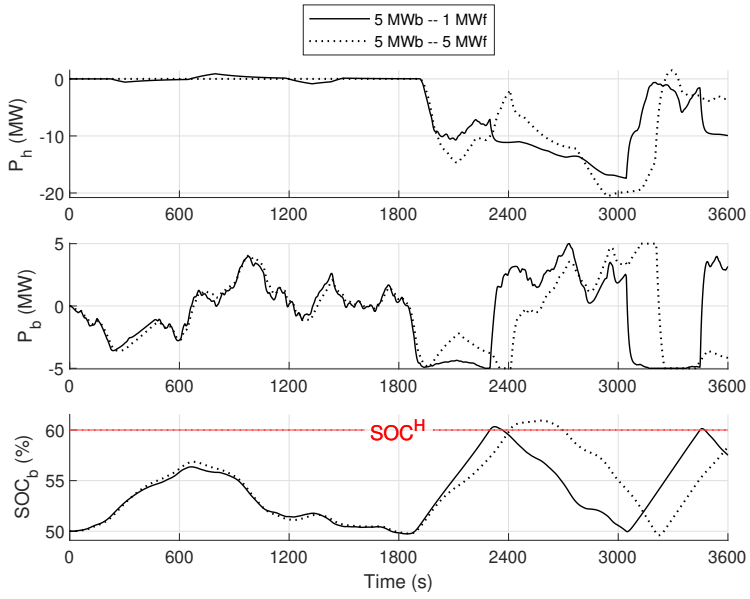

(b)

FIGURE 3.11: HR strategy: variable-speed turbine operation. (a) comparison between active powers: best configuration w.r.t. LC_b vs the reference case; (b) comparison between PSHP and BESS powers, and the latter's SOC for two hybrid configurations.

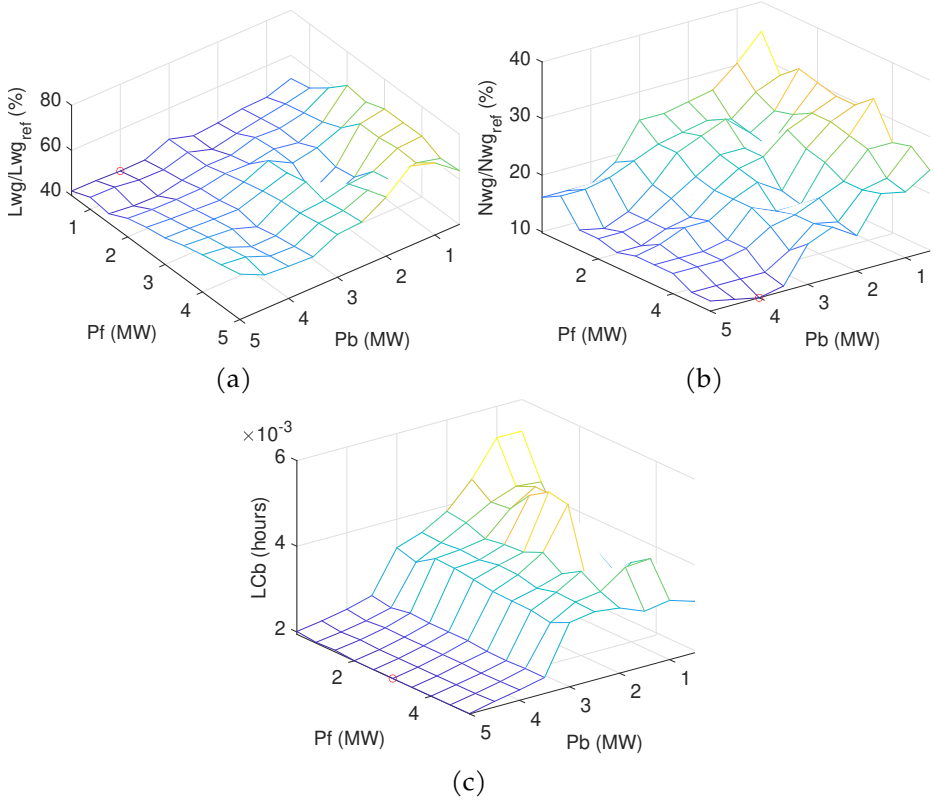

FIGURE 3.12: HR strategy: results for the fixed-speed turbine operation. (a) relative wicket gate's travelled distance and (b) number of movements, (c) BESS absolute. $\mathrm{Lwg_{ref}} = 0.6728\,\mathrm{pu}$, $\mathrm{Nwg_{ref}} = 112$.

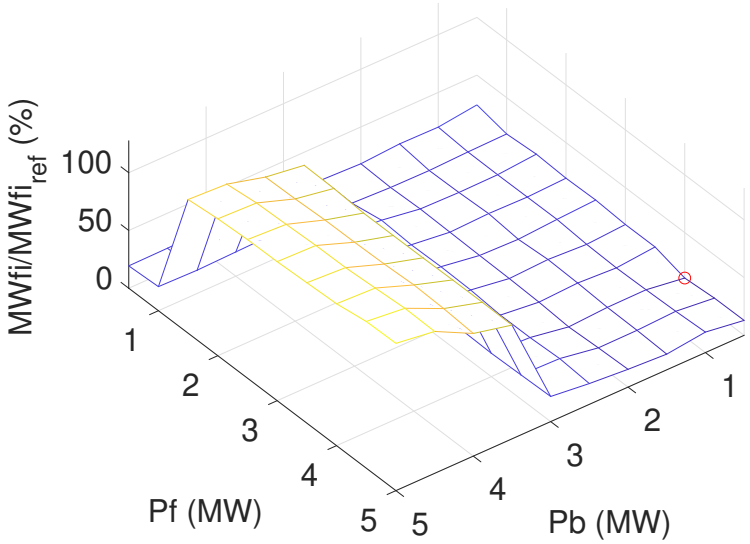

FIGURE 3.13: HR strategy: Mei-Wang fluctuation index of the torque at the shaft (reference case: $MWFi_{ref} = 6.4871 \times 10^9$) for the variable-speed pump.

with a value of 0.2790 pu (41.46 %). There is only one configuration that minimizes Nwg to 10 movements (16.07 %), and the BESS life consumption follows a very similar pattern, with a minimum life consumption equal to 1.97×10^{-3} pu.

The results for the variable-speed pump greatly differ between the two strategies. As seen in Figure 3.13, the MWFi tends to sharply increase for BESS powers greater than 3 MW and FESS powers greater than 0.5 MW, reaching values as high as 120 % than the reference value. It appears that the fluctuation index is very sensitive to high gradients, occurring when the SOC control routine is triggered or when the hydraulic machine has to intervene when the BESS can not provide the regulation by itself. In Figure 3.14a the variable-speed pump-turbine operates in pump mode stationarily for more than half of the simulation, and adapts its power output as soon as the frequency imbalance worsens (around t = 2000 s). The main cause of the increase of fluctuation index is the SOC control

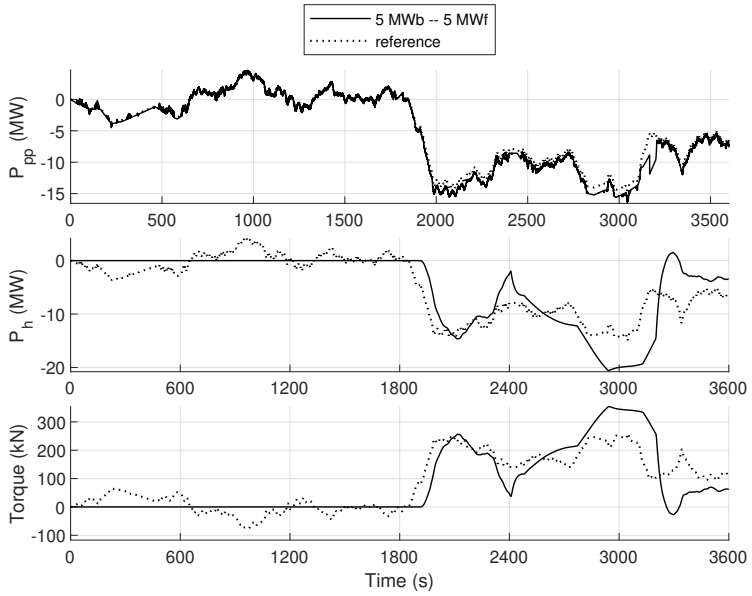

(a)

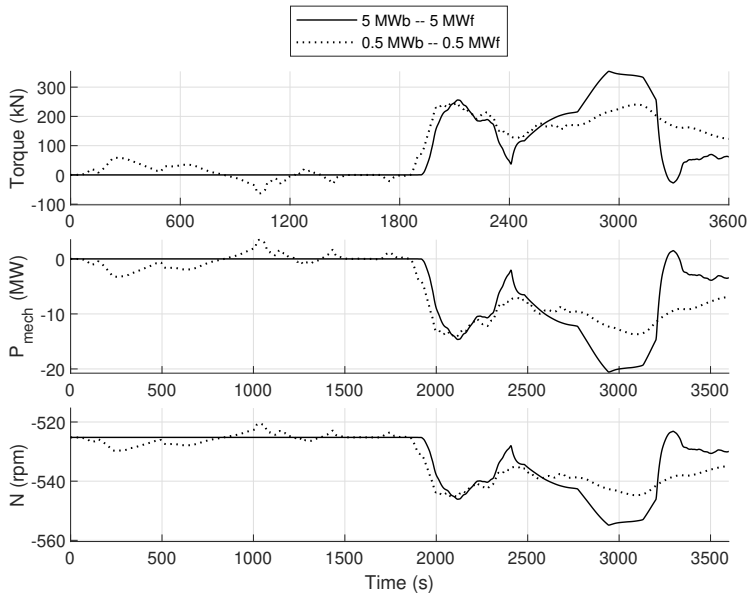

(b)

FIGURE 3.14: HR strategy: powers and torque comparisons between (a) hybrid and non-hybrid pump, and (b) minimum (continuous line) and maximum (dotted lines) installed powers.

routine, introducing three PSHP power (and torque, contextually) spikes after t = 2300 s (Figure 3.14a). With more installed power, the SOC control procedure implies wider power adjustments, therefore the BESS and FESS power is installed, the more the torque fluctuates (Figure 3.14). This comes at the cost of very wide torque fluctuations. The best configuration in this regard, (0.5, 4) MW has a small BESS rated power as well as low-pass filter time constant: this makes the pump operate in a similar way as in the FS strategy, and this can be clearly seen from Figure 3.14b, in which the dotted lines of configuration (0.5, 0.5) MW are never stationary.

IV Discussion of the results

In this chapter the Foxi Murdegu PSHP has been simulated in open-loop, taking as input real frequency and AGC signal recorded data from Italy's continental grid, and in different scenarios. The plant was simulated assuming it was equipped with a variable-speed pump-turbine or a fixed-speed and one with/without hybridization.

The adopted perspective was the plant owner's: to assess if the hybridization would improve the plant operation by means of decreasing the wear indicators presented in Chapter 2. A total of 100 combinations of installed BESS and FESS powers have been selected: from 0.5 MW to 5 MW for each Energy Storage Device (ESD), with a step of 0.5 MW. The hybrid plant was simulated under two control strategies, the FS and the HR, to assess how the plant would respond under the different logics.

While the SOC control parameters have been kept invariant across all simulations (as well as the initial conditions), the intentional delays (PSHP and BESS low-pass filter time constants $T_{lpf,h}$ and $T_{lpf,b}$ respectively) have been calibrated by finding their maximum allowable values that still fulfil the TSO regulations, in particular to deliver 100 % FCR within 30 s from the beginning of the frequency imbalance.

The variable-speed pump-turbine always shows an enhanced operation in turbine mode when hybridized, in terms of reduction of the wicket gate

travelled distance and number of movements, Lwg and Nwg respectively, regardless of the adopted strategy or the installed powers (Figures 3.6 and 3.10). With the FS strategy, the higher the installed BESS and FESS powers the greater the benefit: Lwg can drop up to 42.33 % (0.3202 pu) of the reference value and Nwg up to 14.60 % (20). The best hybridization to minimize the PSHP wear indicators does not coincide with that minimizing the BESS lost life due to cycling, LC_b, which is found for 2 MW BESS and 1.5 MW FESS (1.034 h). The BESS tends to cycle more at high powers because $T_{lpf,b}$ tends to increase, making the BESS deal with lower frequency components, associated with a smoother power flow, but increased energy flow, causing deeper SOC cycles (Figure 3.7b). The HR strategy changes the system behavior, resulting in a more pronounced PSHP wear indicators decrease (Figure 3.10), with Lwg dropping as low as 0.2880 pu (38.08 %), and Nwg as 8 (5.84 %). The main differences are that i) these minima are had for different power combinations as in the FS (especially for Lwg), and ii) the life consumption due to cycling experienced by the BESS is greater by at least two orders of magnitude with the HR strategy (Figure 3.10c). This is to be expected as the HR strategy prioritizes the BESS to deliver the FCR, and makes the PSHP intervene only when necessary (to perform SOC control or to deliver the power the BESS can not provide).

The fixed-speed turbine is less flexible than its variable-speed counterpart, and therefore the wicket gate blades perform less movements in the first place. With the FS strategy (Figure 3.8), Lwg and Nwg can decrease down to 0.3186 pu (45.92 %) and 21 (18.75 %), whereas with the HR (Figure 3.12) down to 0.2790 pu (41.46 %) and 10 (16.07 %) respectively. Again the BESS is penalized by this operation mode, consuming 2.106×10^{-4} h with the FS, and 1.97×10^{-3} h with the HR (best case for both).

The variable-speed pump-turbine operating in pump mode appears to benefit much more from the FS operation at high installed BESS and FESS powers (Figure 3.9a), and with the HR strategy at low installed

powers(Figure 3.13). It is too early to say that the MWFi reduction (down to 12.34 % with the FS, 10.65 % with the HR) corresponds to a decrease of a physical phenomenon of the same intensity, or if the fluctuation index that has been used is adequate in estimating the wear of a pump while continuously adjusting its power output. Nevertheless, there is no established methodology in this regards the author is aware of, and further research could be made in the future to validate or invalidate this methodology.

Overall, for the case-study under analysis, and for the range of installed BESS/FESS powers considered, the FS strategy looks more promising, as it offers a good compromise in terms of benefits for installed powers, especially for the duration of the BESS. The HR could prove to be better suited at higher BESS installed powers, but the author thinks that it is more interesting to search for the highest benefits with the least hybridizing power installation, from both an economic point of view (capital investments and relative costs are reduced) as well as from a resource-wise point of view (the less equipment is installed, the less resources are utilized with the respective greenhouse gas emissions).

List of symbols

Accents		
	The quantity is in absolute value	$\hat{}$
Greek letters		
	Guide Vanes Opening (°)	α
	Efficiency	η
Roman letters		
	Charge intensity (pu)	ci
	Water head (m)	$\hat{H}$
	Hydraulic head (pu)	h

	AGC signal (%)	$L_{\%}$
	Life Consumption	LC
	Distance travelled by the wicket gate (pu)	Lwg
	Rotational speed (rpm)	$\hat{N}$
	Number of wicket gate movements	Nwg
	Active power (MW)	$\hat{P}$
	Active power (pu)	$\hat{p}$
	Flow rate (m^3/s)	$\hat{Q}$
	Flow rate (pu)	q
	Time (s)	T
	Position of the wicket gate blades (pu)	z
Subscripts		
	Battery Energy Storage System	b
	Flywheel Energy Storage System	f
	Pumped Storage Hydro Power	h
	Low-pass filter	lpf
Superscripts		
	At $t = 0$	0
	Lower bound	L
	Upper bound	U

4 Optimization procedure

The hybridization of a Pumped Storage Hydro Power (PSHP) can be performed in many different ways, and for every combination of installed Battery Energy Storage System (BESS) and Flywheel Energy Storage System (FESS) powers theoretically exist infinite control possibilities that profoundly influence the plant behaviour, even under the same simulation inputs (initial conditions and frequency and Automatic Generation Control (AGC) signals).

So far, the Hybrid Energy Storage System (HESS) has been studied by considering a limited amount of installed BESS and FESS powers (from 0.5 MW to 5 MW each), one particular hour of operation (based on real recorded data) and by tuning part of the parameters (the low-pass filter time constants) that manage the active powers of each device.

A procedure to find the "optimal hybridization" of a PSHP was developed as part of the collaboration with Ricerca sul Sistema Energetico (RSE), which financed part of this research programme, and during the 2021 exchange period at Universidad Politecnica de Madrid (UPM) (Madrid). The aim of this project was to find the optimal BESS and FESS installed powers and the optimal power management strategy that would guarantee the maximum return of investment during the estimated project life. To do so, three elements were necessary: i) the formulation of an optimization problem, meaning defining the objective function, variables, and constraints; ii) the data to correlate the output quantities from a model simulation with the cost and revenue components of the objective function; iii) the data to characterize a period of time of plant operation, or – in short terms – a representative year to simulate the HESS.

As part of the agreement with RSE, the focus was placed on finding an hybridization solution that would be valid for both pump and turbine mode. For this reason the work presented in this chapter only considers the variable-speed operation of the hydraulic machine. Parts of this work were published as Ref. [173].

This chapter is structured as follows: Section 4.I outlines the optimization problem and how the different objectives in the objective function were modeled; Section 4.II provides an insight over the custom algorithm that was employed for the search; the results from the optimization process are presented in Section 4.III , and further discussed in Section 4.IV.

I Optimization problem definition

The problem of the optimal hybridization of a PSHP consists in two subproblems: optimal design and optimal control of the HESS. "Optimal design" here means the optimal amount of installed power and energy capacity of BESS and/or FESS, while "optimal control" refers to the optimal values of the control parameters that manage the power flows between the devices making up the HESS and which of the two power management strategies to adopt. In the early stages of project development it was opted to follow a simplified approach, consisting in finding the optimal control for a set of candidate configurations: a limited number of P_b and P_f pairs were given as input to the optimizer, the algorithm would find the optimal control for each of the candidate configurations, and subsequently perform a comparative analysis to detect the configuration associated with the best value of the objective function. Later on, the approach has evolved into a proper optimization problem, in which the optimal design and control are found contextually.

An optimization problem generically consists in the search for the values of a finite set of decision variables $\mathbf{x}$ that minimize an objective function $f(\mathbf{x})$, the goal of the optimization procedure. The solution found is valid

only if it respects a number of constraints. In mathematical terms:

$$\begin{aligned} \min \quad & f(\mathbf{x}) \qquad \mathbf{x} = [x_1, x_2, \dots, x_n]^T \\ \text{subject to} \quad & A\mathbf{x} \leq b \\ & C\mathbf{x} = d \\ & \mathbf{x} \geq lb \\ & \mathbf{x} \leq ub, \end{aligned} \tag{4.1}$$

where n is the number of decision variables, A and b are respectively the matrix and array of the inequality constraints, C and d the matrix and array of the equality constraints, and lb and ub the lower and upper bound arrays.

In the next paragraphs, each element making up the optimization problem is defined and presented.

1.1 Objective Function

In this problem the goal of the optimization procedure was to maximize the economic feasibility of the project. This is assessed with the Net Present Value (NPV) method, the sum of the discounted costs and revenues during the useful economic life of the project. As it is convention to find the minimum value of an Objective Function (OF), this has been defined as the NPV with negative sign:

$$OF = -NPV = C_{inv} + \sum_{k=0}^{N_y} \frac{C_{fix} + C_{var} - R_{fix} - R_{var} + \mathbb{P}}{(1+r)^k}, \tag{4.2}$$

where C_{inv} is the capital investment of the installation of BESS/FESS (€), N_y the expected lifetime of the investment (years), $C_{fix/var}$ and $R_{fix/var}$ are the yearly fixed and variable costs and revenues respectively (€), r is the discount rate (%), and $\mathbb{P}$ (€) a penalty factor (described at page 118).

The optimization problem focuses on the hybridization of the PSHP, meaning that it is assumed that the hydropower plant is realized regard-

less of the choice of hybridizing the plant or not. For this reason, the capital investment and the fixed Operation and Maintenance (O&M) costs are considered only for the BESS and/or FESS. Moreover, the revenues from the sale of energy in the day-ahead market, as well as the costs to operate the pump, are not considered as it is assumed the schedule would be the same with or without hybridization.

The fixed costs are those that only depend on the installed power/energy capacity of the equipment and do not depend on the energy usage. On the other hand, variable costs depend on how the equipment is used along the examined period, and as such are derived from the output data of the simulations. More details on the fixed and variable costs are provided at page 110.

The model, presented in Chapter 2, is not suited to run simulations longer than one hour, as many phenomena spanning multiple hours have not been modeled, e.g. the variation of the water level in the upper reservoir, the transition from one operating mode to the other or the startup/shutdown processes.The plant owner's operation schedule determines the generated power and its change over time. This not only depends on the energy availability of the PSHP, but also on the result of the day-ahead market bids. Due to the lack of available information and the different scope of this research, this aspect has not been modeled.

However, since the economic analysis imposes to consider one year of operation, a set of representative hours N^h has been used. Each hour is defined by the conditions of the plant at $t = 0$, frequency and AGC input signals, and an associated probability of occurrence of that hour during the year, $p(i)$ (%). The yearly variable costs and revenues are calculated with the following equation:

$$C_{var} = \sum_{i=1}^{N^h} C_{var,i} p(i) Y, \tag{4.3}$$

$$R_{var} = \sum_{i=1}^{N^h} R_{var,i} p(i) Y. \tag{4.4}$$

In the equations, Y is the number of hours of the year the plant is expected to operate. This value is either 7760 h or 8760 h, depending on the type of hybridization (see Page 114). More details on the representative hours are presented in Section 4.I.IV.

Data about equipment costs and ageing processes can be hard to gather, depending on the technology under assessment. Li-ion batteries are one of the most studied energy storage technologies, with high volume production of devices, as already presented in Chapter 1. Regarding PSHP and FESS there is not as much available data as for BESS.

Economic information was found in some references [43, 44, 101]. After consulting with people expert in the subject, it was chosen to use cost data from Mongird et al. [44], as the values were deemed closer to their experience, especially regarding the FESS technology. Unless stated otherwise, the cost elements and prices presented in the next paragraphs are taken from this reference. The reference presents the costs in $, and a conversion rate of 0.84 €/$ was used, a reasonable rate at the time this work was developed.

The next paragraphs describe in detail how the costs and revenues are calculated.

Capital investment

For Li-ion BESS, the specific capital investment, $c_{inv,b}$ is expressed in $/kWh. The EP_{ratio} for the BESS is fixed as a parameter and set to 1 kWh/kW, therefore this cost element is expressed as a function of the installed BESS power. The value of 362 $/kWh, the predicted price for 2025, was used.

The FESS technology is not as established as the BESS. This also reflects on the limited available information in the literature about performances and costs. A correlation proposed by Mongird et al. [44] was used to estimate the unit installation cost of a FESS:

$$c_{inv,f} = 6873.3EP_{ratio,f} + 692.96, \tag{4.5}$$

where $c_{inv,f}$ ($/kW) corresponds to the specific capital investment for FESS, and $EP_{ratio,f}$ to the FESS energy-to-power ratio (kWh/kW). In this case $EP_{ratio,f}$ is 0.0348 kWh/kW, resulting in a specific installation cost $c_{inv,f}$ of 932.15 $/kW.

The hybridization capital investment is therefore calculated as:

$$C_{inv} = c_{inv,b} P_b EP_{ratio} + c_{inv,f} P_f. \tag{4.6}$$

Fixed O&M

The fixed O&M include all costs necessary to keep the storage system operational throughout the duration of its economic life that do not depend on the energy usage. The calendar ageing of BESS and FESS has not been modelled in this work.

PSHP fixed costs have been excluded from the analysis for the same reason as its capital investment: these cost elements would exist regardless of the hybridization, as they are a function of the installed power, which is set as a parameter.

For BESS and FESS, they are proportional on the installed power, and are calculated with the following equation:

$$C_{fix} = c_{fix,b} P_b + c_{fix,f} P_f, \tag{4.7}$$

with values of the specific fixed costs for BESS and FESS, $c_{fix,b/f}$, equal to 8 $/(kW/yr) and 5.6 $/(kW/yr) respectively.

Variable O&M and replacement costs

Variable costs, C_{var}, depend on the performances of the plant during the examined working period, therefore they depend on the simulation outcomes. They are grouped into two categories: variable O&M costs experienced by each device, $C_{om,h/b/f}$ and the costs related to the useful life of the device, $C_{LC,h/b/f}$. According to Ref. [44], "variable O&M ac-

count for all costs necessary to operate the storage system throughout the duration of its economic life and are normalized with respect to the annual discharge throughput", including the wear and tear and lost efficiency of the device. Acknowledging the scarcity of data in the literature, the authors of [44] declared that a catch-all value for BESS and FESS is 0.03 cents/kWh, whereas for PSHP 2.5×10^{-4} cents/kWh. As this analysis focuses on the primary and secondary frequency regulation services, it is the energy moved to provide such services that generates these costs:

$$C_{var,om_i} = En_{h_i} c_{var,h} + En_{b_i} c_{var,b} + En_{f_i} c_{om,f}, \quad i = \{1, \dots, N^h\}, \quad (4.8)$$

where $En_{h/b/f}$ is the energy moved by each Energy Storage Device (ESD) for the primary/secondary regulation, and $c_{var,h/b/f}$ the respective unit cost factor.

Regarding the costs related to the loss of useful life, it was decided to consider the costs due to the wear and tear of the equipment in providing frequency regulation services, as the variable O&M were not estimated specifically for such services (which entail frequent and repeated power adjustments).

The problem to correctly estimate the life consumption of each ESD corresponds to the problem of relating the appropriate simulation outputs to costs. This was relatively easy for the BESS, as there are plenty of information in the literature, being one of the most studied and applied ESD, especially Li-ion batteries. The methodology described in Section 2.IV.II is employed to calculate the life consumed during the simulated period, LC_b. It is assumed that, when this value reaches 1, the BESS cells must be replaced and hence the replacement cost, $c_{repl,b}$, must be sustained. This cost was assumed equal to the 2025 Capital Cost of Li-ion batteries, (189 \$/kWh) of Ref. [44], assuming that the other cost voices (power conversion systems, balance of plant, construction and commissioning) are not related with the replacement of the damaged parts.

As there is no established methodology for the FESS, a similar approach

as for the BESS has been adopted: it is assumed that the FESS degrades due to cycling. The Rainflow counting algorithm is applied to the the flywheel State Of Charge (SOC), and the number of cycles is obtained. As there is a consensus that the FESS degradation is independent from the charge/discharge cycle depth and amplitude, the numbers of each cycle type are summed. Cycles whose amplitude is lower than 2.67×10^{-3} pu, corresponding to a variation in rotational speed lower than 10 rpm, are filtered out (the operating range of the device is 6000 rpm to 9000 rpm). The amount of charge/discharge cycles that lead to the end of life is set to 4×10^6 [203]. The replacement cost is assumed to be 600 \$/kW, that is the minimum FESS Capital Cost in [44].

To the author's knowledge, almost no data are available for correlating the PSHP wear and tear indicators to a cost element. First: such plants have a fairly long lifetime, therefore it is not easy to estimate the impact of ancillary services provision, among other operating conditions, to the equipment useful life. Second: the increase in the penetration of variable renewable generation is causing an increase in the provision of ancillary services by hydropower plants, and this situation is relatively recent. Third: plant owners do not easily share techno-economic data about their plants.

Some technical reports published in the late '90s were consulted: these present a thorough study and propose a protocol to estimate the cost of providing ancillary services [204–207]. These reports were meant for plant owners and the personnel working in the facility as a way to gather the relevant data, but do not include any data at all.

In Section 2.III.VII the wear and tear of a turbine was estimated via two quantities: the distance travelled by the wicket gate and the number of movements. These indicators can be useful for a qualitative analysis, i.e. to identify an improvement in the system design and operation that results in a decrease in these indicators, but are inadequate for the optimization approach, as their values that lead to the equipment replacement are unknown. In short: with the available information it is impossible to ad-

dress a cost to one movement of the wicket gate blades and the respective travelled distance. For variable-speed pump operation, there is a lack of information not only about the cost of providing ancillary services, but also about the methodologies to identify the wear and tear caused to the equipment providing such services.

A practical approach was therefore chosen: to address a cost for each PSHP power ramp. This approach has the advantage not to require extra data besides the simulation outputs, and it is applicable to either turbine or pump operation. A power ramp is defined as a power increment/decrement at the shaft divided by the time it took to perform it. This approach was proposed in a technical report by Hamal and Sharma [208], quantifying the cost of power ramps for coal-fired power plants and hydro power plants in Ontario. For the i-th simulated hour:

$$C_{LC,h/b/f_i} = c_{ramp,h} \cdot Ramp_i + c_{repl,b} LC_{b_i} + \\ + c_{repl,f} LC_{f_i} \qquad i \in \{1, \dots, N^h\}. \quad (4.9)$$

In the equation presented above, $c_{ramp,h}$ is the cost of a ramp, here assumed to be $6\,€/(MW/s)$ and equal for both turbine and pump mode operation, $Ramp_i$ is the sum of all the power ramps detected for the PSHP in the i-th simulated hour, $c_{repl,b/f}$ is the replacement cost for the BESS/FESS when they reach the end of life, and LC_{b/f_i} are the per-unit life lost due to SOC cycling for BESS and FESS respectively. A PSHP performs power adjustments both when providing frequency regulation services and by participating in the day-ahead market, incrementing or reducing the power output according to the quota the plant was awarded. As data about the schedule of operation of a PSHP were not made available, it was assumed that the power committed to the day-ahead market was fixed as a parameter and constant over time. Moreover, it was assumed that the plant is already in steady-state at the beginning of the simulated hour, meaning that the transient to reach the target power output (input) ended before the start of the simulated hour by the plant operating in turbine

(pump) mode.

The procedure to identify each ramp is the following: the first data point of the series (corresponding to $P(t = 0)$ becomes the "reference point" and the algorithm neatly reviews each other data point, which is discarded if it is not a local minimum or maximum (peak). When a peak is found, the absolute value of the difference between the reference point and the peak associated powers is calculated: if it is lower than a tolerance (1 MW), the peak is discarded and the search continues, if not, the peak becomes the "reference point" and the search goes on. When all data has been evaluated, the sum of the ramps is calculated as follows:

$$\text{Ramps} = \sum_{i=1}^{N-1} \frac{|P_{mech}(i+1) - P_{mech}(i)|}{t(i+1) - t(i)}, \tag{4.10}$$

where i is the i-th peak identified by the algorithm.

Fixed revenues

Similarly to the fixed costs, fixed revenues, R_{fix}, are those that only depend on the installed BESS/FESS power. In this work, they correspond to a particular type of pilot service defined by the Transmission System Operator (TSO), which is assumed to become established in the future scenario considered in this study. In the framework of increasing non-programmable Renewable Energy Source (RES) penetration, the TSO developed the pilot project named Fast Reserve (FR), a new regulation service that is aimed at coping with these future challenges [209]. In short, the FR is a Frequency Containment Reserve (FCR) with more stringent requisites. A plant participating in the service must provide upwards/downwards regulation proportionally to the frequency error. The FR must be activated within 300 ms from the start of the frequency imbalance, be fully activated within 1 s, and be delivered for at least 30 s, before being linearly deactivated over 300 s. Participation in this service is remunerated proportionally to the power committed to such

a service, which must not be less than 5 MW and not superior to 25 MW [210]. Each contracted Fast Reserve Unit must guarantee 1000 hours/year of FR operation per year. During the hours of availability, the contracted capacity shall be exclusively subservient to the FR service.

Given these conditions, the following assumptions have been made: i) the power the plant owner bids for the FR service, corresponds to the sum of the installed BESS and FESS powers; ii) all the power is accepted for the service and, in case, is capped to 25 MW; iii) during the participation to the FR, the plant control settings are tuned for that particular service, removing every intentional delay; iv) the amount of time, represented by the typical hours, amounts to the remaining hours of the year, meaning that the product of the hourly variable costs for the probability of occurrence of said hour in Equation (4.3) is multiplied by 7760 hours/year. The revenues from FR provision are therefore calculated as:

$$R_{fix} = p_{FR} \left(P_b + P_f \right). \tag{4.11}$$

where p_{FR} is the price per megawatt the TSO rewards for the participation in the service (€/(MW/year)). The last bid for the island of Sardinia resulted in a mean weighted price of 61 016 MW/yr, which was used in this work [211].

Variable revenues

The revenues derived from the sales in the day-ahead market are not considered, as it is assumed that they would exist with or without the hybridization and because the scheduled power was assumed constant over the simulated hours. Variable revenues are those derived by the provision of the regulation services. Currently, in Italy, FCR is mandatory and not remunerated; on the contrary, participation in the Frequency Restoration Reserve (FRR) is voluntary, and a remuneration scheme based on the energy delivered for that purpose is in force. In this study the future scenario with a remunerated FCR is considered and the following

remuneration scheme was provided by RSE:

$$R_{var,i} = R_{I_i} + R_{II_i}, \qquad i \in \{1, \dots, N^h\} \tag{4.12}$$

$$R_{I_i} = \left|En_{Iup_i}\right| p_{Iup_i} - \left|En_{Idown_i}\right| p_{Idown_i}, \tag{4.13}$$

$$R_{II_i} = \left|En_{IIup_i}\right| p_{IIup_i} - \left|En_{IIdown_i}\right| p_{IIdown_i}. \tag{4.14}$$

where R_{I_i} and R_{II_i} are the revenues due to the provision of FCR and FRR respectively. 'En' means the energy delivered for the primary or secondary regulation, either upwards or downwards (subscript 'up' and 'down' respectively). In other terms, the revenues from the primary and secondary regulations derive from the difference between the products of the delivered energies (MWh) and the respective price (€/MWh) (different between the upwards and downwards regulations).

The prices for the FCR were calculated from the energy price in the *Mercato del Giorno Prima*, day-ahead market (MGP) p_{mgp} according to Refs. [212–214]:

$$p_{Iup_i} = p_{mgp_i} + \left(K_{II,up} - K_{mgp,up}\right)/2 \tag{4.15}$$

$$p_{Idown_i} = p_{mgp_i} - \left(K_{mgp,down} - K_{II,down}\right)/2 \tag{4.16}$$

where $K_{II,up}$, $K_{II,down}$ and $K_{mgp,up}$, $K_{mgp,down}$ are yearly constants determined by Terna (the TSO), defined respectively as the weighted average price of the accepted bids for upwards and downwards secondary regulation on the market for the dispatch service (*Mercato per il Servizio di Dispacciamento*, MSD), and the weighted average of the zonal prices of the recorded sales on the MGP, weighted by the quantities accepted for the upwards/downwards RS in the relevant zones; the MGP prices for the year of interest and the trading prices on the MSD/MB for FRR are used in the calculation realized in the previous year (e.g., in applying the optimization procedure, the values of the constants for the year 2019 will be calculated with data from the year 2018).

As for the FRR prices, on the other hand, the prices for the accepted bids

TABLE 4.1: Techno-economic data used in the optimization process. A conversion factor of 0.84 €/$ has been used to translate all the prices in euro.

Category	Symbol	Unit	Value
Fixed costs	$c_{inv,b}$	(€/kWh)	304.08
	$c_{inv,f}$	(€/kW)	783.01
	$c_{fix,b}$	(€/kW)	6.88
	$c_{fix,f}$	(€/kW)	4.82
Variable costs	$c_{var,h}$	(10^{-6} €/kWh)	2.15
	$c_{var,b}$	(10^{-4} €/kWh)	2.58
	$c_{var,f}$	(10^{-4} €/kWh)	2.58
	$c_{ramp,h}$	(€/(MW/s))	6.00
	$c_{repl,b}$[a]	(€/kWh)	325.08
	$c_{repl,f}$	(€/kW)	504.00
Fixed revenues	p_{FR}	(k€/MW)	61.016
Variable revenues	$K_{I,up}$	(€/MWh)	109.01
	$K_{I,down}$	(€/MWh)	26.34
	$K_{mgp,up}$	(€/MWh)	61.83
	$K_{mgp,down}$	(€/MWh)	62.69
Discount rate	r	(%)	8.00
Investment life	N_y	(years)	20

[a]: as the project estimated life is 20 years and a BESS life is 10 years according to [44], the replacement cost has been doubled.

by the plant for that service are considered. It should be noted that the individual plant offers hourly prices on the MSD for the service, and that acceptance on the MB is done on a quarter-hourly basis with a pay-as-bid mechanism [215].

All the values of the aforementioned parameters are presented in Table 4.1, with the exception of the unitary prices for the secondary regulation that are presented in Table 4.4.

Penalties

The optimization approach is based on the simulation of the HESS under a set of scenarios. Since some technical requirements can not be expressed in terms of linear or non-linear constraints, their violations are accounted as penalties. For example, one may want the SOC of either the BESS or the FESS to never saturate to 0 % or 100 %, as the device would not be able to perform downwards/upwards regulation respectively.

As the goal of the optimization problem is to find the global minimum, introducing a penalty to the objective function increases its value, making the candidate solution more likely to be overtaken by another that does not include any violation generating a penalty.

Of the two types of penalties that are considered, the first is related to the plant ability to fulfil the FCR obligations towards the grid presented in Section 3.1.

In particular, a 100 k€ penalty is administered to the configuration if the plant, can not deliver the FCR associated to a step-like frequency error of 200 mHz amplitude in due time. The compliance to this requirement is calculated separately, as a short (35 s long) simulation for each candidate solution, at each iteration (see Section 4.11).

A penalty factor is also introduced when the SOC of either BESS or FESS reaches 0 % or 100 %, to avoid the devices to be unable to provide downwards and upwards regulation respectively. In this case, the administered penalty for each violation is 1 k€ (a violation in this sense is less serious than the other case). Moreover, while the previous penalty is unique (the candidate solution either passes the test or fails it), the SOC-related penalties are hour-based, meaning that up to 34 of these penalties can be administered for a single solution, if the SOC saturates once or more every hour.

No penalty has been assumed for the FRR violations, because such a service is delivered at a higher time scale than the FCR[1], and it was

[1] Annex A15 of the Grid Code describes the test for the FRR qualification: a test AGC

assumed the plant would be able to deliver the respective power.

Regarding the FR service, no test is done to assess the plant capability to deliver the service. This is to keep low the computational cost of the optimization procedure (see Section 4.II). The FR service is delivered during a specific time window (agreed with the TSO beforehand), and with a dedicated control setting. Testing for the compliance of the FR service would have required to run a sub-optimization problem, determining another set of control parameters for the hybridization design of the candidate solution. This aspect may be explored in future works.

The magnitude of the penalties was determined after several trial-and-errors and were chosen as they ensured the exclusion of inadequate solutions, without restricting excessively the problem.

Summed together, all the penalties make up for the penalty factor $\mathbb{P}$ of Equation (4.2).

I.II *Decision variables*

The optimal solution of the objective function is given by the optimal value of the decision variables.

There are a total of 13 decision variables in this problem, 12 continuous and one binary. Two decision variables are related to the size of the HESS: P_b and P_f. All the others refer to the control of the plant: $T_{lpf,h/b}$, $SOC_{b/f}^{L/U}$, $\Delta SOC_{b/f}$, and $ci_{b/f}$. The last variable is a binary variable that determines which of the two power management strategies (Frequency Split (FS) or Hydro Recharge (HR)) is adopted, and has been named HR_{on}. If 0, the FS strategy is adopted, if 1 the HR. The array of the decision variables is

signal is sent to the plant, going from 50 i to 100 in 100 s, with a maximum gradient of 0.5 %/s [15].

TABLE 4.2: Decision variables, lower and upper bounds.

Symbol	Unit	lb	ub
P_b	(MW)	1	25
P_f	(MW)	1	25
$T_{lpf,h}$	(s)	0.001	300
$T_{lpf,b}$	(s)	0.001	300
$SOC^L_{b/f}$	(%)	5	60
$SOC^H_{b/f}$	(%)	40	95
$\Delta SOC_{b/f}$	(%)	5	50
ci_b/f	(pu)	0.05	1
HR_{on}	–	0	1

presented in the following equation:

$$\begin{aligned} \mathbf{x} = \Big[& P_b, P_f, \quad T_{lpf,h}, \quad T_{lpf,b}, \dots \\ & \dots SOC^L_b, \quad SOC^H_b, \quad \Delta SOC_b, \quad ci_b, \quad \dots \\ & \dots SOC^L_f, \quad SOC^H_f, \quad \Delta SOC_f, \quad ci_f, \quad HR_{on} \Big]^T. \end{aligned} \tag{4.17}$$

1.III Bounds and constraints

The decision variables are all bounded, meaning that the admissible values they can assume for the solution, to be valid, must lie between the upper and lower bounds. All the variables and bounds are displayed in Table 4.2.

There are in total four linear constraints and no equality constraint:

$$P_b + P_f \leq 30\,\text{MW}, \tag{4.18}$$

$$T_{lpf,b} \leq T_{lpf,h}, \tag{4.19}$$

$$SOC^L_b + \Delta SOC_b + 1\,\% \leq SOC^H_b - \Delta SOC_b, \tag{4.20}$$

$$SOC^L_f + \Delta SOC_f + 1\,\% \leq SOC^H_f - \Delta SOC_f. \tag{4.21}$$

The first linear constraint, Equation (4.18), sets to 30 MW the limit of the installed hybrid power. The second constraint, (4.19) imposes a hierarchy

in the intentional delays: the installation of the BESS is aimed at smoothing the PSHP operation and not vice-versa. The last two constraints, Equations (4.20) and (4.21), impose that the SOC control procedures do not overlap, avoiding that the charge and discharge processes activate at the same time.

In matricial form, the linear constraints are expressed as follows:

$$A = \begin{bmatrix} 1 & 1 & 0 & 0 & 0 & 0 & 0 & 0 & 0 & 0 & 0 & 0 & 0 \\ 0 & 0 & -1 & 1 & 0 & 0 & 0 & 0 & 0 & 0 & 0 & 0 & 0 \\ 0 & 0 & 0 & 0 & 1 & -1 & 2 & 0 & 0 & 0 & 0 & 0 & 0 \\ 0 & 0 & 0 & 0 & 0 & 0 & 0 & 0 & 1 & -1 & 2 & 0 & 0 \end{bmatrix} \tag{4.22}$$

$$b = \begin{pmatrix} 30 \\ 0 \\ -1 \\ -1 \\ -10 \\ -10 \end{pmatrix} \tag{4.23}$$

1.IV *Definition of the future scenarios*

As mentioned in the previous paragraphs, the analysis is aimed at finding the optimal design and control of the HESS during one year of operation in a future scenario. In this scenario the plant can contribute to the provision of various services to support the stability and security of the power system, namely FCR, FRR and FR.

It was assumed that the plant would confront with a limited series of events sufficiently representative of the possible frequency perturbations of the network. RSE defined a total of 17 hours, representative of the possible frequency events during one year in Sardinia. Table 4.3 displays the peak frequency deviation Δf^{max}, the value of the AGC signal at the end of the simulation $L_{\%}$, and the probability for the event to occur in one year, $p(i)$. The frequency and AGC signals in every hour share the same

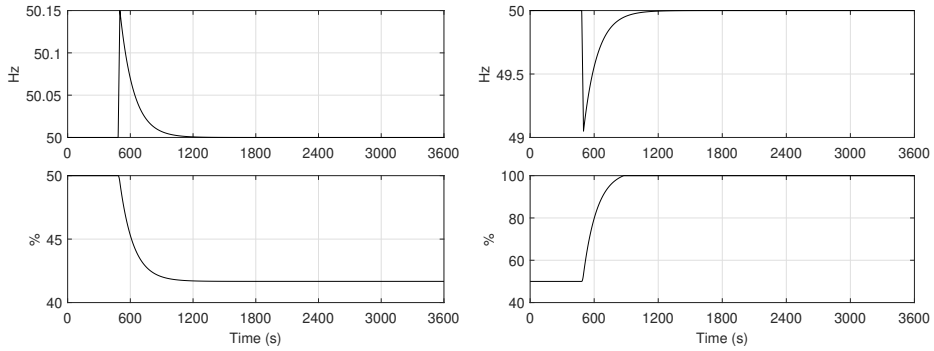

(a) (b)

FIGURE 4.1: Frequency and AGC signal of representative hour (a) number 2, and (b) number 17.

TABLE 4.3: Characterization of the representative hours: maximum frequency deviation Δf^{max}, final value of the AGC signal $L_{\%}$, and probability of occurrence of the hour over the year, $p(i)$. The other quantities, which are fixed among the hours, are reported in Table 4.4.

Hour number	Δf^{max} (mHz)	$L_{\%}$ (%)	$p(i)$ (%)
1	50	47.22	0.721
2	150	41.67	23.142
3	250	36.12	18.509
4	350	30.57	5.474
5	450	25.01	1.655
6	550	19.46	0.403
7	650	13.91	0.085
8	850	2.80	0.007
9	−50	52.78	0.898
10	−150	58.33	21.982
11	−250	63.88	17.915
12	−350	69.43	6.585
13	−450	74.99	1.910
14	−550	80.54	0.601
15	−650	86.09	0.085
16	−750	86.09	0.014
17	−950	100.00	0.014

TABLE 4.4: Characteristic hours: input parameters that are common for each hour

Quantity	Symbol	Value
Secondary reserve	SB (pu)	0.15
PSHP power output (turbine)	P_h^0 (MW)	70
PSHP power input (pump)	P_h^0 (MW)	110
Water level	H_g^0 (m)	367
Rotational speed (turbine)	N^0 (rpm)	525
Rotational speed (pump)	N^0 (rpm)	547.6
State Of Charge	SOC_b^0 (%)	50
	SOC_f^0 (%)	50
Day-ahead market price	p_{mgp} (€/MWh)	51.8
Upwards FRR price	p_{2up} (€/MWh)	87.25
Downwards FRR price	p_{2down} (€/MWh)	59.34

trend as seen in Figure 4.1. Hours numer 1 to 8 consist of overfrequency events, whereas hours from 9 to 17 underfrequency events. The most likely frequency deviations are found for hours number 2 and 10, with a frequency deviation of ± 150 mHz and a probability of occurrence of 23.142 % and 21.982 % respectively. It is more likely that the mild frequency deviations (150 mHz to 250 mHz) are overfrequency, while more serious events (≥ 350 mHz) are more likely to be underfrequencies.

The operation during one of the hours is not characterized only by the input frequency and AGC signals, but also by the initial conditions, the secondary regulation reserve, the day-ahead market price and so on. RSE proposed values for these quantities and decided to keep them constant over the different years. They are reported in Table 4.4. Moreover, RSE highlighted the importance of finding a solution that would reflect both pump and turbine mode operation. As such, the 17 hours presented above doubled, hence considering that the year is represented by 34 hours: the plant operates in turbine mode for 17 hours, and in pump mode for the other 17. The probability of each hour was halved between pump and turbine mode.

As in the open-loop simulations, at $t = 0$ the plant is supposed to be in steady-state, no regulation is provided (meaning that the power outputs of BESS and FESS is null), and the PSHP is generating/consuming the power committed in the day-ahead market. In pump mode, the initial rotational speed is calculated from the defined power input for that hour (547.6 rpm for the conditions presented in Table 4.4).

II Solver

There are many possible approaches to search for the optimum in an optimization problem. A solver is usually selected depending on the nature of the problem to face.

In this case, a modified Particle Swarm Optimization (PSO) algorithm has been selected. PSO is a meta-heuristic algorithm, a general method (not developed specifically for a particular problem) that requires little assumptions about the problem it has to solve. On one side this is an advantage in terms of versatility, on the other the method does not offer the mathematical certainty that the solution is the global optimum of the objective function.

The PSO is an iterative algorithm and draws inspiration from the motion of bird flocks, in which each individual moves autonomously, but to some extent its motion is related to the positions and velocities of the other individuals for a common goal (e.g., finding food).

In a swarm of N particles, each individual represents a possible solution x in a D-dimensional search space (with D being the number of the variables). The position x_i^j and the respective velocity v_i^j of the $i-th$ particle ($i = 1, \dots, N$) in its j-th dimension ($j = 1, \dots, D$) are adjusted at

each time step (iteration) according to the following equations [216]:

$$\begin{aligned} v_i^j(t+1) &= I \cdot v_i^j(t) + c_1 \cdot rand_{1_i}^j \cdot (pbest_i^j(t) - x_i^j(t)) + \\ &\quad + c_2 \cdot rand_{2_i}^j \cdot (gbest^j(t) - x_i^j(t)), \end{aligned} \tag{4.24}$$

$$x_i^j(t+1) = x_i^j(t) + v_i^j(t+1), \tag{4.25}$$

where t is the current iteration, $rand_{1_i}^j$ and $rand_{2_i}^j$ are two random numbers generated uniformly in the interval $[0, 1]$, $pbest_i^j(t)$ and $gbest^j(t)$ are, respectively, the best position[2] found during the current iteration and the best position ever found, I is the inertia weight, and c_1 and c_2 are two coefficients balancing the relative importance of the stochastic acceleration terms.

The individual, moving through the search space with a certain speed, updates its position and velocity in the search domain at each iteration: thus, a new solution and a new value of the objective function, are found. The speed at which the individual moves to update its position, is not random but depends on three factors: i) the direction of movement of the previous iteration (related to I); ii) the historical memory of the individual (the best position found in the past, related to pbest); iii) the historical memory of the whole swarm (the best position found by the whole swarm in previous iterations, related to gbest). Given enough iterations, the flock converges to the optimal solution.

PSO has been widely used for the optimal design/control of energy systems [134, 168, 217–220].

The PSO algorithm employed in this work was taken from the work of Ardizzon et al. [216], in which the stochastic acceleration coefficients, as well as the inertia weights, are dynamically updated at each iteration based on the distance between each particle from the best position (*gbest*). In addition to that, the algorithm was further modified to make it compatible with the linear constraints and binary variables. At each iteration,

[2] The position associated to the lowest value of the OF.

as soon as the positions are updated, a check if there is any constraint violation is made. The residuals (line 4 of the following pseudocode) are calculated and used to correct the velocity matrix, which instantly updates the position matrix, until no violation is detected anymore. The 0.4 scaling factor for the velocity has been selected because it proved to rapidly correct the violations without falling into an infinite loop.

```
1: violation = A * x^T − b;
2: residual = violation(violation > 0)
3: while violation≠0 do
4:     correction = −A^T * residual;
5:     v=v+correction*0.4;
6:     x(correction)=x(correction)+v(correction);
7:     violation = A * x^T − b;
```

Regarding the binary variables, a practical approach has been followed: the solver algorithm consider them as continuous variables, bounded to the interval $[0, 1]$. The variable is then rounded to the closest integer value.

Genetic Algorithm (GA) is an optimization algorithm that is natively capable to handle properly both constraints and non-continuous variables, but the PSO algorithm has been preferred because it showed to be faster in converging to a solution. Moreover,after several trials, the PSO solution would always be better than the GA one and hence the method presented above has been chosen.

The PSO solver function takes the following inputs: i) the objective function $f(\mathbf{x})$ (already defined); ii) the number of individuals making the swarm, n_p; iii) the linear constraints matrices, A, b, and the bound matrices lb, ub (already defined); iv) the maximum amount of stall iterations, Nit, and v) the function tolerance for the search end, 'tol'.

The population was chosen to be made of 20 individuals, as it proved to be a good compromise between the search effectiveness and the computational time. In fact, at each iteration the objective function is calculated

for each particle, meaning that each representative hour is simulated for each particle (34 simulations per particle per iteration). The number of stall iterations Nit, and search tolerance 'tol' are stopping criteria. The algorithm stops whether after Nit stall iterations, meant as the number of consecutive iterations of unsuccessful search, or if the difference between the new best solution and the predecessor is inferior to ftol. The maximum number of stall iterations was set to 20, and the function tolerance to 1 k€.

III Results

The optimal solution returned by the optimizer is presented below:

$$
\begin{aligned}
P_b &= 22.803\,\text{MW} & P_f &= 2.022\,\text{MW} \\
T_{lpf,h} &= 276.57\,\text{s} & T_{lpf,b} &= 9.45\,\text{s} \\
SOC_b^L &= 39.53\,\% & SOC_f^L &= 36.49\,\% \\
SOC_b^H &= 91.85\,\% & SOC_f^H &= 61.38\,\% \\
\Delta SOC_b &= 5.18\,\% & \Delta SOC_f &= 5.11\,\% \\
ci_b &= 0.8118\,\text{pu} & ci_f &= 0.9450\,\text{pu} \\
HR_{on} &= 0.
\end{aligned}
$$

The optimal hybridization is based on almost 23 MW of installed BESS versus about 2 MW of installed FESS. The optimal power management strategy is the FS, with very high PSHP intentional delay (its low-pass filter time constant is set to about 276.6 s) and a very small BESS delay (about 9.5 s). The BESS SOC control boundaries are quite wide (39.53 % to 91.85 %) whereas the FESS ones are quite narrow (36.49 % to 61.38 %). The SOC control band ΔSOC is similar for both technologies, about 5 %, and the charge intensity parameters are close to 0.9 pu. Such an hybridization leads to a NPV of 10 478 k€ in 20 years of operation.

The objective function was calculated for two more cases: the case for

TABLE 4.5: Breakdown of the objective function cost/revenues voices for three cases: non-hybrid case, optimal hybridization (FS strategy), HR strategy. All values are in (k€).

Voice	Non-hybrid	Optimal (FS)	Sub-optimal (HR)
C_{inv}	0	8516.732	8516.732
$C_{inv,b}$	0	6933.793	6933.793
$C_{inv,f}$	0	1582.938	1582.938
C_{fix}	0	166.617	166.617
$C_{fix,b}$	0	156.881	156.881
$C_{fix,f}$	0	9.736	9.736
$C_{var,om}$	0.079	1.677	11.448
C_{ramp}	39.569	1.147	19.352
$C_{LC,b}$	0	0.015	1.051
$C_{LC,f}$	0	14.205	14.958
R_{fix}	0	1514.670	1514.670
R_{I}	93.810	94.284	94.674
R_{II}	487.677	521.374	521.374
$\mathbb{P}$	0	12.000	6.000
NPV	5319.855	10 478.115	10 248.616

the HR strategy, by simulating the plant (over the 34 hours) with the optimal value of the decision variables (except for the HR_{on}, set to 1), and the reference case, by performing the same simulations for the non-hybrid plant (in either turbine and pump mode). Table 4.5 presents the cost/revenues breakdown of the objective function for each of the three cases.

The hybridization introduces more fixed and variable yearly costs (less than 200 k€/year), increasing at the same time the revenues from FCR and FRR. The main difference in terms of revenues between the hybridized and non-hybridized case, though, is the revenue stream given by the FR service: 1514.67 k€/year, making the hybridization investment very attractive. Moreover, by incrementing the rated power of the plant and fixing the per-unit primary and secondary reserves, more energy is delivered for the FCR and FRR services, hence more profit is made.

Comparing the results of the simulations between the two power management strategies, the difference in NPV is about 200 k€, mostly due to the increased costs for the PSHP ramps and the variable O&M costs, related to the energy moved by the devices.

Looking at the penalties, the plant passes the FCR test (described in page 118) in both the hybrid and non-hybrid cases. Nevertheless, the FS causes double the violation of the non-saturation SOC criterion with the FS strategy, w.r.t. the HR. In particular, the FS causes a violation at hours 6, 7 and 15 (in both turbine and pump operation), when the HR does not. Both strategies receive a penalty at hours 8, 16, and 17. Figure 4.2 shows the comparison of the BESS and FESS powers and SOCs, together with the HESS total output power for hour number 15.

The installed BESS and FESS powers in the hybrid case are high enough to guarantee that the plant is capable to deliver the FCR in due time with a 200 mHz step signal. The penalties in this case are given for representative hour number 8, with an associated overfrequency of 850 mHz peak. In that hour, in both turbine and in pump operation modes, the FESS SOC briefly saturates to 100 %.

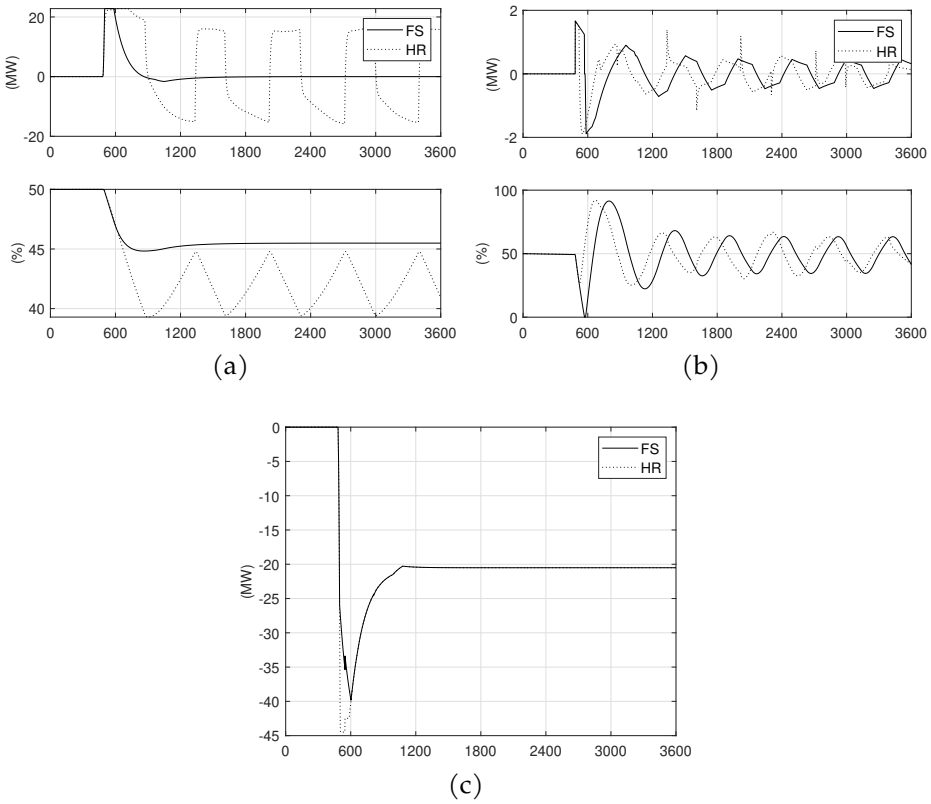

FIGURE 4.2: Comparison of the power (top) and SOC (bottom) of (a) BESS, (b) FESS, and (c) the plant power between the FS (continuous line) and the HR (dotted line). The hour simulated is number 15.

The BESS is also much more used with the HR strategy ($C_{LC,b}$ = 1.051 k€/year) than under the FS ($C_{LC,b}$ = 0.015 k€/year), as seen in Figure 4.2a. Having to deal also with the FRR regulation, the BESS cycles continuously. Even the FESS experiences repeated cycles, due to the narrow SOC control bounds and the high PSHP filter time constant Figure 4.2b. The FESS cycling is similar between the two strategies (the replacement cost is about 14.5 k€/year in both cases). The costs associated to FESS cycling are much higher than the those of the BESS. On one hand this can be justified by the fact that the FESS technology is not as established as the BESS,and as such does not benefit from the scale economies, on the other this could indicate that the methodology employed overestimates the FESS degradation due to cycling.

The last observation that can be done is that the HR strategy is better at tracking the frequency error Figure 4.2c, as the frequency imbalance requires an amount of FCR higher than the BESS rated power, therefore the PSHP delivers the extra power required,at the same speed (with the same Low-Pass Filter (LPF) time constant) as the BESS.

IV Discussion of the results

This chapter presents an optimization framework to find the optimal size of installed BESS and FESS and optimal control, to hybridize a PSHP operating in a future scenario in Sardinia. A modified PSO algorithm performs an iterative search to find the hybridization that offers to the plant owner the maximum NPV over the investment economic life, assumed to be 20 years. Costs were roughly estimated from the little information available in the literature, whereas revenues were estimated according to information provided by RSE.

The case-study for the optimization was one year operation in Sardinia, characterized by 17 representative hours, during which the plant is being operated in either turbine or pump mode (for a total of 34 hours), each with an associated frequency and AGC signal and a probability of

occurrence.

The results show that about 23 MW of BESS and 2 MW of FESS result in a NPV of 10 364 k€, compared to the value of 3598 k€ for the non-hybridized case. By adopting the HR strategy instead of the FS one in the optimal configuration, the NPV decreases to about 10 249 k€. The principal reason for the economic attractiveness of the hybridization is the cash flow deriving from the plant participation in the FR service. The last bid for the island of Sardinia resulted in a mean price for the FR of 61.016 k€/MW/year, leading to an income of 1514.67 k€/year. The requirements for participating in such a services are so stringent that the plant without hybridization would not manage to fulfill them.

The optimal solution (hybrid plant with the FS strategy) earns a total of 94.284 k€ and 521.374 k€ from the provision of primary and secondary frequency regulation services respectively. On the other hand, the sub-optimal solution (HR strategy) leads to an income of 94.674 k€ (0.4 %) for the FCR and 521.374 k€ for the FRR, the same as the optimal solution. Last, the non-hybrid plant earns 93.810 k€ (−0.5 %) and 487.677 k€ (−6.4 %) for the FRR. The hybrid plant, having its rated power increased by 24.825 MW (20.69 %) must commit more energy for the FCR and FRR services, thus achieving higher revenues streams.

The proposed optimal hybridization was open-loop simulated with the same frequency and AGC input signals as in Chapter 3. The wicket gate traveled distance w.r.t the reference drops down to 22.429 % (0.1696 pu) and the number of movements down to 9.4891 % (13). The BESS experiences a life consumption equal to 1.4556×10^{-4} h. Figure 4.3 presents the comparison between selected signals of the three cases (optimal, sub-optimal, and non-hybrid variable-speed turbine operation). These signals are the HESS and PSHP active power output Figures 4.3a and 4.3b, and the BESS and its SOC (Figure 4.3c). The BESS is oversized for this scenario, as its power peaks to −12.58 MW in the optimal case. The FESS signals have been omitted because they coincide in the two hybrid configurations.

The HESS power accurately tracks the frequency variation and, from

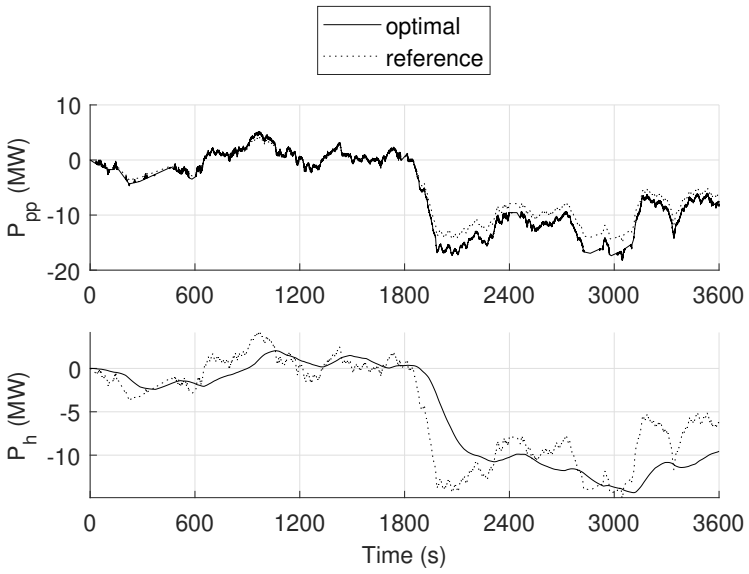
optimal
reference
10
0
-10
-20
P_{pp} (MW)
0
600
1200
1800
2400
3000
3600
0
-5
-10
P_h (MW)
Time (s)

(a)

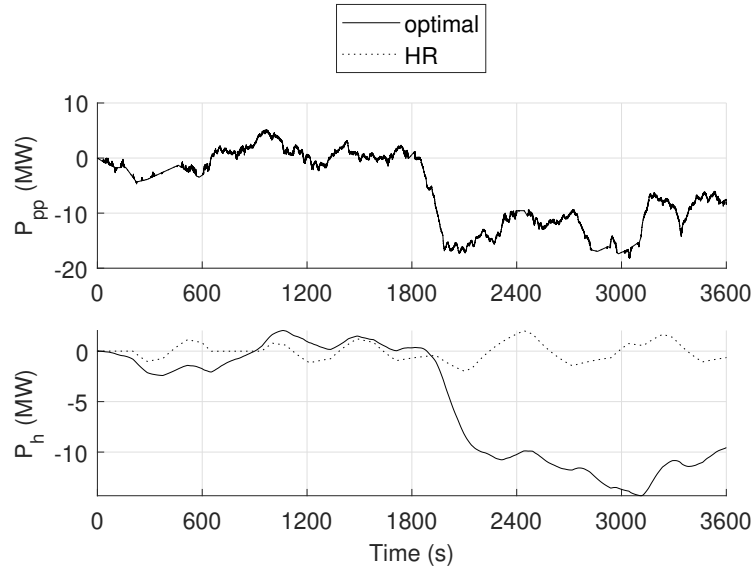
optimal
HR
10
0
-10
-20
P_{pp} (MW)
0
600
1200
1800
2400
3000
3600
0
-5
-10
P_h (MW)
Time (s)

(b)

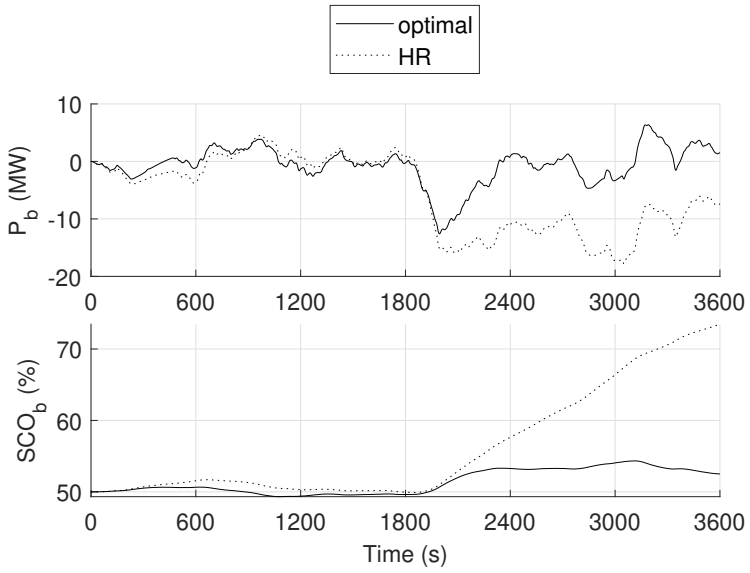

(c)

FIGURE 4.3: Open-loop simulations with historical frequency data: comparison between optimal, reference, and HR (sub-optimal) configurations for variable-speed turbine operation. (a, b) HESS power (top) and PSHP power (bottom) outputs; (c) BESS power (top) and the respectiveSOC power (bottom) outputs.

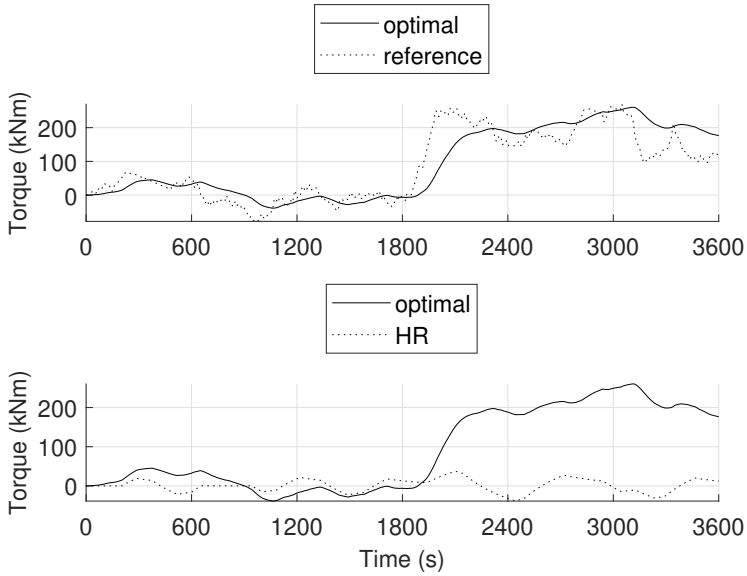

FIGURE 4.4: Torque comparison of the variable-speed pump operation in open-loop simulation.

the grid perspective, there is no difference between the FS and the HR strategies (Figure 4.3b). On the other hand the HR strategy entails a slight increase in movements of the wicket gate blades, due to the SOC control of the FESS: the traveled distance drops to 17.5656 % (0.1328 pu) while the number of movements is the same as the FS (13). In pump mode operation, the Mei-Wang Fluctuation index (MWFi) drops to 3.39 % of the reference value for the optimal solution, and to 2.76 % for the case with the HR strategy. Figure 4.4 shows the comparison of the torque signals between the optimal and non-hybrid solution (top) and the optimal and sub-optimal (HR) solutions (bottom).

These findings confirm that the more historic or synthetic frequency events scenarios must be obtained to fully explore the potential of the hybridization, from both the plant owner's perspective and the TSO's. As the historic frequency signals for Sardinia are confidential information, open-access power system models and data will allow more detailed and

more complete analysis on the hybridization of ESDs.

While these results are encouraging in terms of assessing the economic benefit of hybridizing a PSHP, they are preliminary, in terms that further research should be done in this regard. These results are highly dependent on several assumptions. The first aspect that should be addressed in future works is the lack of established methodologies to relate physical quantities to cost voices. Wear and tear may be estimated in some cases, but especially for PSHPs and FESSs there is not enough publicly available data to relate the wear indicators to costs. The results are also strictly dependent from the input data, especially the typical hours. The frequency signals result from tripping events, using other types of input signals, better representing the randomness and unpredictability of the RES generators, would surely be an added value. One may argue that a plant owner, confronting with a power system that exhibit this behavior, may opt for a completely different solution than hybridization.

List of symbols

Roman letters

Cost (€)	C
Unit cost	c
Charge intensity (pu)	ci
Energy (MWh)	En
Life consumption	LC
Power ramp (MW/s)	Ramp
Grid frequency (Hz)	f
Water head (m)	$\hat{H}$
Friction losses coefficient (m)	K
AGC signal (%)	$L_{\%}$
Lower bounds array	lb

	Rotational speed (rpm)	N
	Number of years	N_y
	Unit price	p
	Penalty factor (€)	$\mathbb{P}$
	Active power (MW)	P
	Probability (%)	p
	Revenue (€)	R
	Discount rate (%)	r
	Allocated FRR (pu)	SB
	Time (s)	T
	Upper bounds array	ub
	Array of the decision variables	$\mathbf{x}$
	Number of hours in the year	Y
Subscripts		
	Battery Energy Storage System	b
	Downwards	down
	Flywheel Energy Storage System	f
	Fixed	fix
	Gross	g
	Fast Reserve	FR
	PSHP	h
	Life consumed	LC
	Primary regulation	I
	Secondary regulation	II
	i-th element	i
	Investment	inv
	k-th element	k
	Mechanical	mech
	Day-ahead market	mgp
	n-th element	n
	Operation and Maintenance	om
	Ramp	ramp

	Replacement	repl
	Upwards	up
	Variable	var
Superscripts		
	At $t = 0$	0
	Hour	h
	Lower bound	L
	Maximum	max
	Transposed	T
	Upper bound	U

5 Closed-loop simulations

In the previous chapters, open-loop simulations have been performed to model the behavior of the seawater Pumped Storage Hydro Power (sPSHP) in Foxi Murdegu, Sardinia. These show how the plant adjusts its power output given an input frequency and Automatic Generation Control (AGC) signal pair. In open-loop the change in power output does not affect the frequency error, and the achieved results reflect the plant owner's point of view, meaning the search for an optimal Hybrid Energy Storage System (HESS) that reduces wear and tear indicators (Chapter 3), or maximize the economic benefit (Chapter 4).

In this chapter the Transmission System Operator (TSO) perspective is adopted: the Foxi Murdegu sPSHP performance is evaluated in terms of its contribution to contain the frequency error after a tripping event. For this purpose, closed-loop simulations are performed

This chapter is structured as follows: Section 5.I describes how the Sardinian power system is modeled; Section 5.II presents the 2030 scenario the model is set in, outlining the generators and load types, as well as the prescriptions the plants must follow in providing frequency regulation services; in Section 5.III two simulation scenarios are presented, and the results are shown in Section 5.IV. The chapter ends with the discussion of the results in Section 5.V.

I Power system model description

The Sardinian power system model was provided by Ricerca sul Sistema Energetico (RSE), in which the model presented in Chapter 2 was inte-

grated. The power system model is composed of two different elements: the electric system and the totality of the plants that are qualified to provide frequency regulation services.

1.1 Electric system model

The Sardinian grid is represented with a single-busbar equivalent system. The linearized swing equation for synchronous machines is used to calculate the frequency variation (Δf) resulting from an electrical power imbalance:

$$\Delta f = \frac{f_n}{T_a P_r} \int (\Delta P_m - \Delta P_e)\, dt, \tag{5.1}$$

where f_n is the nominal grid frequency (50 Hz), T_a (s) is the equivalent grid starting time, P_r (MW) is the maximum rated power of the generators contributing to the rotating inertia of the system, ΔP_m and ΔP_e are respectively the variation of the mechanical (generation) and electrical (load) power.

The equivalent grid starting time T_a is calculated as the average of each connected generator starting time, weighted by its apparent power (calculated by assuming a power factor of 0.9, excepted for synchronous compensators):

$$A_{r,i} = \frac{P_{r,i}}{0.9}, \tag{5.2}$$

$$T_{ag} = \frac{\sum_i A_{r,i} T_{a,i}}{\sum_i A_{r,i}}, \tag{5.3}$$

where $A_{r,i}$ (MVA) and $T_{a,i}$ (s) are the i-th plant apparent power and starting time respectively.

The generator starting time is defined as the time required for the alternator to reach the rated speed from standstill, at no-load, neglecting the mechanical losses, and by constantly applying the rated torque over time [7, 221]. In other terms, the generator starting time can be expressed

as twice its constant of inertia H (s), defined by the following equation:

$$H = \frac{E_k}{P_r} = \frac{\frac{1}{2}J\omega_m^2}{P_r} = \frac{T_a}{2} \tag{5.4}$$

where E_k (J) is the kinetic energy of the rotating mass, ω_m (rad/s) the angular velocity, J ($kg\,s^2$) the moment of inertia.

1.11 *Model of the qualified plants*

In Sardinia, besides the conventional generation plants (thermoelectric, hydropower, wind generators, and Photovoltaic (PV) plants) that are qualified to perform frequency regulation, two High Voltage Direct Current (HVDC) connections (see Section 2.1), can also participate in the service. Generic model equations have been used to describe each of the aforementioned systems (with the exception of the Foxi Murdegu Pumped Storage Hydro Power (PSHP), for which the detailed model presented in Chapter 2 was used). The block diagram shown in Figure 5.1 shows the model of a plant. In the figure, three groups are highlighted, corresponding to the models of the primary regulation – Frequency Containment Reserve (FCR), the secondary regulation – Frequency Restoration Reserve (FRR), and the plant itself.

Being a conventional generation unit or a HVDC cable, the system is modeled as a zero-pole, τ (s) and T (s) being the respective time constants, transfer function. Information exchanges with RSE lead to assume the value of eyese constants equal to 3.3 s and 10 s, respectively. A pure delay is included in the plant model, which assumes the value of 0.5 s for gas turbine power plants only, whereas for the other plants its value is set to 0. A power gradient limiter ("Gradient limiter" block, (MW/min)) accounts for the possible limitations intrinsic to plant type, and a saturation block ("Power limiter" block) bounds the active power to the plant minimum and maximum admissible variations.

The primary regulation, taking as input the frequency error, is modeled

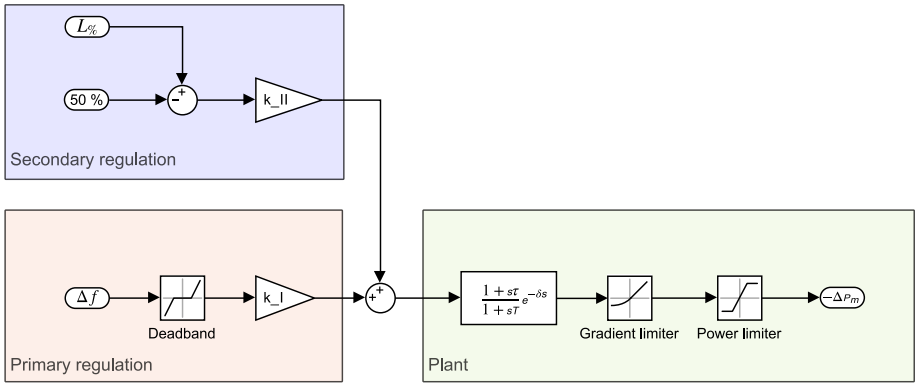

FIGURE 5.1: Model of a generic plant (including the HVDC connections) qualified to perform primary and secondary regulation services.

including a 10 mHz deadband that prevents its activation when the error is too small [15], and a constant k_I (MW/Hz), equal to the so-called "regulating energy". This is a parameter that is derived from the dimensional calculation of the power set-point (psp) (see Equation (2.3)):

$$\Delta P = k_I \Delta f, \tag{5.5}$$

$$k_I = \frac{P_r}{\sigma f_n} \tag{5.6}$$

where σ is the plant permanent droop, Δf (Hz) is the frequency error, and ΔP (MW) the primary regulation power set-point.

The secondary regulation takes as input the AGC signal $L_{\%}$, and the dimensional psp is obtained with the k_{II} constant (see Equation (2.4)):

$$k_{II} = \frac{2SB}{100} \tag{5.7}$$

where SB(MW) corresponds to the plant available FRR allocated power which – according to [15], is equal to: i) the highest value between 10 MW and 6 % of the maximum plant power, for thermoelectric plants; ii) 15 % of the maximum plant power for hydroelectric plants.

The AGC signal is calculated with the following equation:

$$L_{\%} = -\frac{100}{BR} \cdot \frac{k_{rs}}{T} \int \Delta f + 50, \tag{5.8}$$

$$BR = 2 \sum_{i} SB_i, \tag{5.9}$$

$$k_{rs} = \sum_{i} k_{I_i} \tag{5.10}$$

where BR(MW) corresponds to the total secondary regulation band in the system (incorporating the upwards and downwards allocated FRR power), T is the integrator time constant, considered equal to 1/0.015 s in order to decouple the primary and secondary regulations, and k_{rs}(MJ/Hz) is the integrator gain which, according to the equivalent areas criterion, is equal to the global regulating energy [7, 221].

A deadband has been included to the AGC signal calculation, to neglect frequency errors lower than 10 mHz, and the signal gradient is limited to $\frac{100\,\%}{100\,s}$ by a rate limiter block.

I.III Wind generators upwards regulation

Wind generators have been assumed to be able to provide upwards frequency regulation by taking advantage of the blade inertia [222]. The following control law is adopted:

$$\Delta P_w = -\frac{\alpha s}{1 + 10s + 20s^2} \Delta f, \tag{5.11}$$

where α is a parameter chosen as to obtain the wind generators to deliver 6 % of the available power, the default value set in the Grid Code [223].

I.IV RES downwards regulation

Since 2012 the Grid Code establishes the duty for non-programmable Renewable Energy Sources (RESs) to provide downwards regulation in case of overfrequency. This model considers the contribution of:

I. the wind generators, who intervene when the frequency gets higher than 50.2 Hz [223], considering a maximum power gradient that results in the complete delivery of the downwards regulation power within 10 s[1];

II. the PV generation, considering the contribution of the High Voltage (HV) plants, intervenes when the frequency exceeds 50.2 Hz [224], and of the Medium Voltage (MV) plants, intervening when the frequency exceeds 50.3 Hz [225]. Regarding the power gradients, their intervention must be five time faster[2] than wind generators (here the reserve full activation time is assumed to be 2 s). For MV PV generators, an activation delay has been set to 0.1 s [225].

The downwards RES regulation is proportional to the (positive) frequency error for frequency values between 50.2 Hz and 51.5 Hz, with a permanent droop between 2 % and 5 %. Common values are 2.6 % or 2.4 % [225], which are set for frequency excursions of 200 mHz and 300 mHz respectively.

Without any further indication in the Grid Code, the model considers the power restoration for wind and PV (both in HV and MV) as described in Annex A.68: a maximum allowable gradient of 20 % of the power the plant can generate per minute [224].

II Reference scenario

The Sardinian power system scenario is shaped around the 2017 National Energy Strategy (*Strategia Energetica Nazionale*), outlining a complete phase-out of coal-fired power plants to the 2030 time horizon [226,

[1] The referenced Grid Code Annex defines an exception: if the wind generators confront with a step-like frequency deviation, corresponding to a power ramp of more than 50 % its available power, the time limit for full FCR activation is 30 s. For simplicity, an a-priori maximum gradient is assumed.

[2] Akin for wind generators, for simplicity an a-priori maximum gradient is assumed.

TABLE 5.1: Generation and load types for the 2030 National Energy Strategy.

Generators	Share (%)	Load	Share (%)
Wind	33.8	Regional load	76.10
Solar PV	27.4	Export	18.60
Thermoelectric (gas-fired)	10.1	PSHP	5.10
Import	8.7	BESS	0.18
Hydropower	7.8	Corsica spillage	0.02
Biomass	6.2		
Cogeneration	5.8		
BESS	0.2		

227]. Based on this hypothesis, RSE obtained the day-ahead market outcomes[3] for each hour of the year 2030, via simulations of its tool "sMTSIM" [228]. The composition of the generation and load shares, resulting from the simulations, is presented in Table 5.1.

The simulations result in a Sardinian power system characterized by the generation presented in Table 5.2. Below, the details of each plant type are outlined.

II.1 Thermoelectric power plant generation

In total, there are three dispatchable thermoelectric power plant generators in the considered scenario. These are: a 250 MW combined-cycle gas turbine plant (referenced as "Gas turbine 1"), a 80 MW combined-cycle gas turbine (referenced as "Gas Turbine 2"), an equivalent 100 MW cogeneration plant (referenced as "Cogeneration (equivalent)"), and a 550 MW Integrated Gasification Combined Cycle (IGCC) pertaining to the Sarroch refinery. In this scenario, the IGCC is considered out of service, as it is currently not qualified to participate in the frequency regulation services

[3]The 2030 scenario was analyzed via hourly simulations of the day-ahead market with the tool "stochastic Mid-Term SIMulator (sMTSIM)" [220], which calculates the hourly bids of the market by minimizing the cost of the exchanged energy considering a multi-hour optimal power flow, based on a simplified model of the Italian electric system. The tool was not made available to the author.

TABLE 5.2: Types of generators and installed power in the considered 2030 Sardinian scenario.

Generators type	Installed power (MW)
Thermoelectric (gas-fired)	430
Cogeneration	126
Non-dispatchable biomass	65
Hydroelectric (reservoir)	155
Pumped Storage Hydro Power	600
Run-of-river hydro power	19
Dispatchable biomass	20
Battery Energy Storage System	100
Wind generation	2400
Photovoltaic generation	1200
Interconnections	**Rated power (MW)**
SAPEI	1000
SACOI	400

for technical reasons. As such, it would only contribute to the system inertia.

In addition to the aforementioned plants, an equivalent 85 MW biomass-fired plant is considered (referenced as "Biomass (equivalent)").

Regarding the FCR provision:

- cogeneration plants, together with biomass plants are not qualified to perform such a service;
- the rest of the thermoelectric plants have a permanent droop set to 5 %.

11.11 *Hydropower plant generation*

Three hydropower plants have been considered: one equivalent 155 MW hydropower plant (referenced as "Hydropower (equivalent)"), the existing Taloro PSHP ($\pm$255 MW, turbine and pump mode, referenced

as "PSHP Taloro") and a 19 MW Run-of-river (ROR) plant ("ROR hydropower").

In addition, two innovative sPSHPs are assumed to be in operation: the 120 MW plant in Foxi Murdegu (represented by the detailed model presented in Chapter 2) and the 180 MW plant in Cucchinadozza.

Regarding the FCR provision, all the hydropower plants have a permanent droop set to 4 %, except the ROR plant which is not qualified to provide frequency regulation services.

II.III *Energy storage and synchronous condensers*

The generated scenario considers that 100 MW/200 MWh Battery Energy Storage Systems (BESSs) are installed and capable of participating to the frequency regulation services, but as no information is provided about their State Of Charge (SOC) they are considered to not exchange power with the grid.

In addition, two synchronous condenser plants are modeled: one equivalent 2 × 250 MW synchronous condenser in Cordongianos ("Condenser w/o flywheels"), and one equivalent new high inertia synchronous condenser (with flywheels) considering the equipment installed in 2020 in Selargius together with a planned high inertia system in Cordongianos, for a total of 500 MW ("Condenser 2 w/ flywheels"). These systems do not participate in the FCR/FRR services, but contribute to the grid inertia.

The asynchronous motors contribution to the frequency is assumed negligible.

II.IV *HVDC*

The SACOI link is assumed to be modernized with bipolar technology and Line Commutated Current (LCC) power converters, expanding its capacity from the actual 2 × 150 MW to 2 × 200 MW.

The SAPEI HVDC link (2 × 500 MW) already employs bipolar LCC power conversion technology.

The permanent droop for the HVDC links is set to 5 % (as for thermoelectric plants). Power reversal is not allowed, to preserve the equipment. As seen from Table 5.1, Sardinia is a net energy exporter: in any scenario the two HVDC cables are considered to be delivering power to the continent (negative power output).

The margins for the upwards and downwards power reserves are calculated considering that the technical minimum is 10 % of the rated power (due to the LCC technology), for both cables. Moreover, regarding the technical maximum power, a 2 % loss factor is considered, together with a 50 MW spillage to Corsica through the SACOI. As such, the SACOI active power range is 40 MW to 342 MW and the SAPEI 100 MW to 980 MW.

II.V *RES generation*

Four types of non-dispatchable RESs are considered: i) wind power generation, connected in HV; solar PV generation connected in ii) HV, iii) MV, and iv) Low Voltage (LV). The simulation tool RSE employed to build the 2030 scenario does not allow to distinguish between the voltage level of PV generators, hence to quantify the type of downwards regulation, data from 2019 was consulted, for which the share of PV generation in HV and MV was 7.3 % and 55.6 % of the total installed power, respectively [229].

III Simulations

The Sardinian power system model was simulated by including the model of the Foxi Murdegu variable-speed sPSHP in turbine mode, in three cases: non-hybrid (`reference`), optimally hybridized (`optimal`, as per Section 4.III), and optimal with no intentional delay (`fast`, meaning that $T_{lpf,h/b}$ of the `optimal` case are set to 0). Two fault events are condsidered: the first is the loss of 230 MW from Gas Turbine 1, whereas the second is the loss of one of the poles of the SAPEI, exporting 306 MW.

III.I *Underfrequency scenario*

The selected scenario corresponds to hour XVIII of 2030-03-21. This hour is characterized by a low power export from Sardinia to continental Italy: 261 MW through the SAPEI and 85 MW through the SACOI. The regional load corresponds to 1141 MW. During this time, the loss of the Gas Turbine 1 plant results in a step-like generation loss of 230 MW.

Four plants participate in the FCR and FRR services: Gas Turbine 2, Foxi Murdegu sPSHP, and the two HVDC cables. Table 5.3 presents the power system initial operational conditions.

RES generation accounts for 855 MW from wind generation and 73 MW from solar PV generation. The derivative gain for the wind upwards regulation, α is set to 2907 MJ/Hz.

The Foxi Murdegu sPSHP provides synthetic inertia via the power electronics, but this is not modeled as per Equation (5.4), but as the last term of Equation (2.42).

III.II *Overfrequency scenario*

The selected scenario corresponds to hour XII of 2030-11-06. This hour is characterized by a high power export from Sardinia to continental Italy: 612 MW through the SAPEI and 245 MW through the SACOI. The regional load corresponds to 1206 MW. During this time, the loss of one of the SAPEI poles results in a step-like export loss of 306 MW.

As in the previous case, the two HVDC cables, Gas Turbine 2 and the Foxi Murdegu PSHP provide FCR and FRR services. Table 5.4 presents the power system operational conditions.

RES generation accounts for 954 MW from wind generation and 887 MW from solar PV generation. TThe RES generators, participating in the downwards regulation, all have a permanent droop set to 2.6 %.

TABLE 5.3: Power system operational conditions for the underfrequency scenario. Plants that do not participate to the grid's inertia, nor provide regulation, have been omitted.

Plant	P_r (MW)	T_a (s)	P_{gen} (MW)	Upwards reserve (MW)	k_I (MW/Hz)
Gas Turbine 1 (fault plant)	250	15.64	230	0	0
Gas Turbine 2[a]	80	15.64	43	37	32
sPSHP (Foxi Murdegu)[b]	120	–	80	38	60
ROR hydropower	19	8.92	15	0	0
Biomass (equivalent)	85	8.3	85	0	0
Cogeneration (equivalent)	100	8.9	100	0	0
Sarroch IGCC	550	10	0	0	0
Synchronous condenser (w/o flywheel)	500	3	0	0	0
Synchronous condenser (w/ flywheel)	500	14	0	0	0
SACOI HVDC	400	–	−85	45	514.3
SAPEI HVDC	1000	–	−261	161	1285.7

[a]: minimum technical power equal to 30 % of the rated power.
[b]: at the hydraulic conditions specified in Table 3.1 (variable-speed turbine).

Table 5.4: Power system operational conditions for the overfrequency scenario. Plants that do not participate to the grid's inertia, nor provide regulation, have been omitted.

Plant	P_r (MW)	T_a (s)	P_{gen} (MW)	Downwards reserve (MW)	k_I (MW/Hz)
Gas Turbine 2	80	15.64	43	19	32
sPSHP (Foxi Murdegu)[a]	120	-	80	19	60
ROR hydropower	19	8.92	9	0	0
Biomass (equivalent)	85	8.3	85	0	0
Cogeneration (equivalent)	100	8.9	5	0	0
Sarroch IGCC	550	10	0	0	0
Synchronous condenser (w/o flywheel)	500	3	0	0	0
Synchronous condenser (w/ flywheel)	500	14	0	0	0
SACOI HVDC	400	–	−245	514.3	514.3
SAPEI HVDC	1000	–	−612	1285.7	1285.7

[a]: at the hydraulic conditions specified in Table 3.1 (variable-speed turbine).

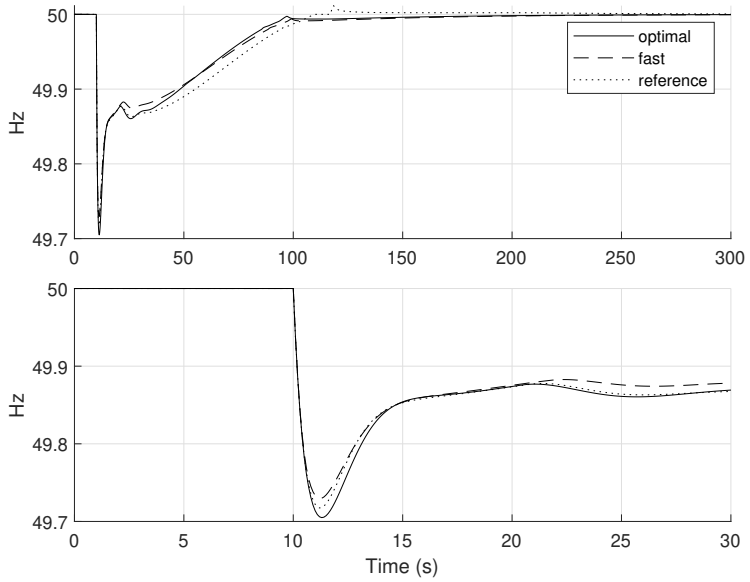

FIGURE 5.2: Grid frequency for the considered underfrequency case (top), with a detail (bottom).

IV RESULTS

The results of both scenarios were obtained by a 900 s simulation of the power system, with a 0.1 s time-step resolution. The fault event is set to trigger at $t = 10$ s.

IV.1 Underfrequency scenario

As soon as Gas Turbine 1 is lost, the frequency drops with an initial Rate Of Change Of post-disturbance Frequency (ROCOF) of 676 mHz/s. As seen from Figure 5.2, in the non-hybridized case the frequency nadir is reachedat 49.717 Hz after 1.2 s; the `optimal` hybridization is associated with a frequency nadir of 49.7050 Hz (after 1.3 s). The `fast` hybridization shows the best performance: the frequency stop decreasing at 49.7296 Hz (after 1.2 s), an improvement of 12.2 mHz with respect to the `referece` case, and 24.6 mHz from the optimal case.

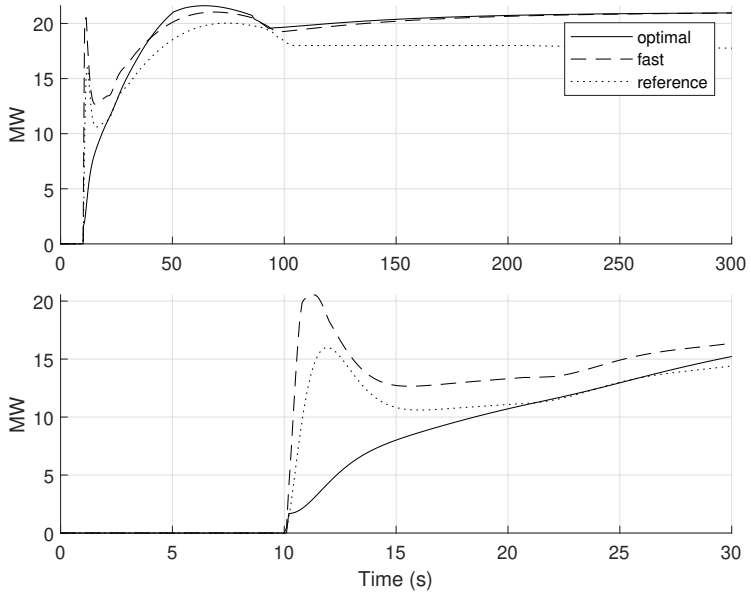

FIGURE 5.3: Foxi Muredgu plant output active power variation for the considered underfrequency case (top), and detail (bottom).

This behavior is due to the intentional delays belonging to the optimal hybridization: the optimization procedure, designed around the plant owner's perspective, favoured a high value of the the PSHP Low-Pass Filter (LPF) time constant (276.57 s), and it is clear from Figure 5.3 that the `optimal` plant (continuous line) avoids the 20 MW power spike in the first seconds, in favor of a smoother power growth. The `fast` plant, on the other hand behaves closer to the `referece`, with a rapid increase in power output right after the fault. The `fast` plant rated power is incremented by the size of the installed BESS and Flywheel Energy Storage System (FESS) (22.8 MW and 2.0 MW respectively): as such the plant must additionally deliver 12.4 MW/Hz for the FCR, resulting in more effective frequency containment.

Examining the power contribution of the devices constituting the HESS, Figure 5.4 illustrates how the intentional delays impact the plant performances. While the `optimal` BESS power reaches a maximum of 17.74 MW

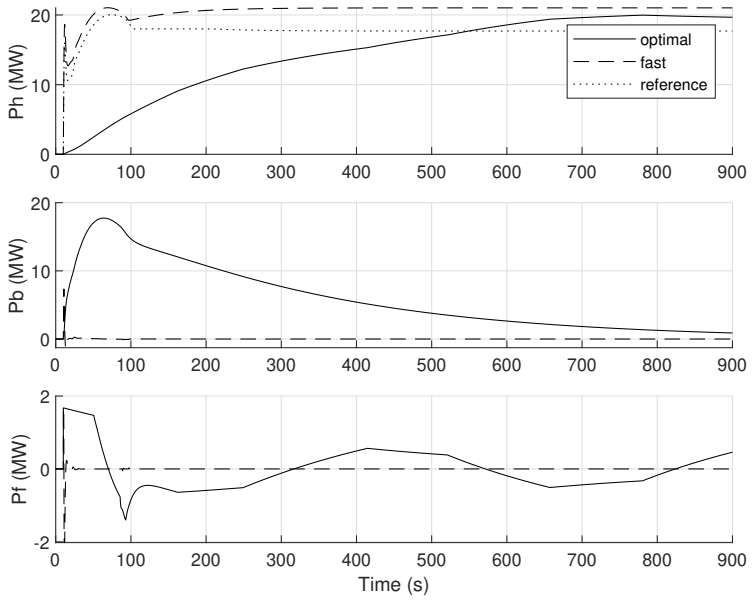

FIGURE 5.4: Foxi Muredgu PSHP (top), BESS (centre), and FESS (bottom) active power output for the considered underfrequency case.

after 53 s from the fault, the `fast` BESS only contributes briefly with up to 10.9 MW, and stops to provide any power after about 5 s. Similarly, the `fast` FESS delivers power shortly after the generation loss (the narrow SOC control bounds cause the FESS power to fluctuate in the `optimal` case). This is mainly for two reasons: the first is that the the PSHP is fast enough to track the frequency excursion, meaning that the BESS and FESS do not need to get involved as the PSHP can manage the regulation necessity, and the second is the impact of the inertial regulation of the wind generators. By taking advantage of the blades inertia, the wind turbines inject into the grid more than 45 MW in 2.9 s (Figure 5.5), effectively reverting the frequency drop and contextually the power gradient from the Foxi Murdegu PSHP. This requires a relatively small power adjustment from the PSHP, that in the absence of intentional delays, can quickly be managed by the PSHP.

The inertial regulation of the wind generators has an additional effect

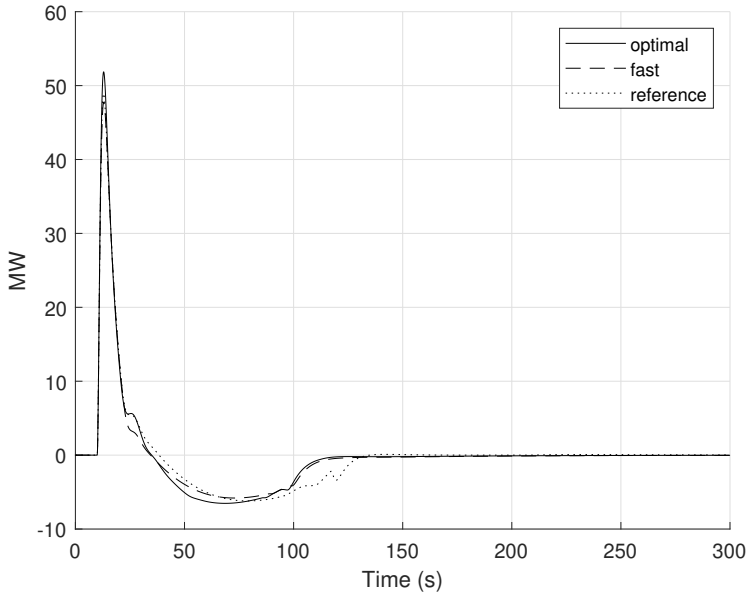

FIGURE 5.5: Wind active power output for the considered underfrequency case.

on the frequency: the rotor blades slow down as a result of converting their kinetic energy into electrical power. At some point they need to be re-accelerated, and therefore the system draws power from the grid (clearly visible in the 40 s to 100 s interval in Figure 5.5). This is the reason why at $t = 22$ s the grid frequency experiences a moderate second frequency drop, before exhibiting an almost linear growing trend. The `optimal` case, delivering less power in the first instants of the fault event, forces the wind to provide more inertial power, forcing said plant to later draw more energy from the grid. At the same time, the `optimal` HESS delivers more energy, and as soon the frequency enters into the deadband zone, the blades are quickly accelerated.

The frequency enters the deadband (Figure 5.2) at $t = 93$ s (`optimal`), $t = 96.8$ s (`fast`) and $t = 102.6$ s (`reference`): the intentional delays of the `optimal` case on one hand reduce the plant capability in contain the frequency excursion (with respect to the other two simulated cases), but on the other hand result in a higher share of energy delivered to the grid,

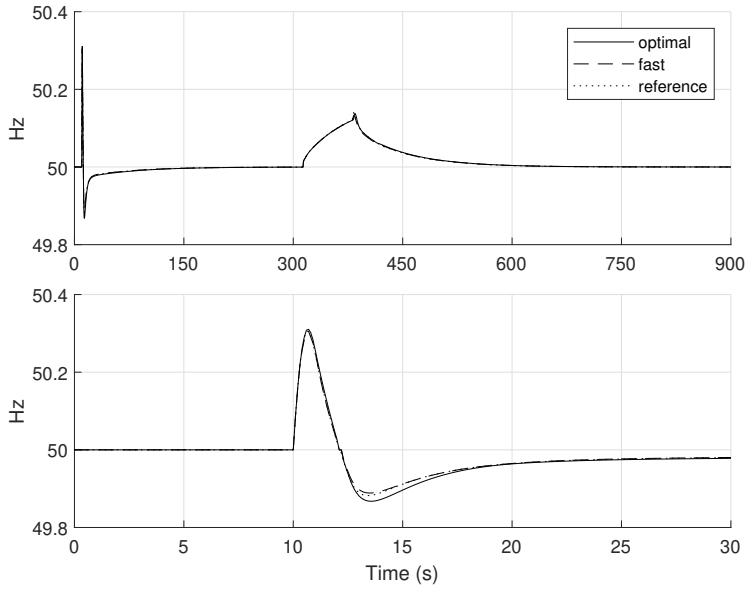

FIGURE 5.6: Grid frequency for the considered overfrequency case (top), and detail (bottom).

thus a quicker frequency restoration.

IV.II *Overfrequency scenario*

Following the loss of one of the SAPEI poles, the frequency spikes with a ROCOF equal to 946.15 mHz/s.

The frequency zenith after the pole loss is reached in 700 ms. The `reference` zenith is equal to 50.3056 Hz, the `optimal` to 50.3105 Hz, and the `fast` 50.3050 Hz (Figure 5.6). As in the previous case, the intentional delay of the `optimal` case reduces the ability of the sPSHP to contain the frequency excursion, even if in this case the impact is smaller in magnitude than in the case of underfrequency (5.05 mHz of difference between `fast` and `optimal`, versus 24.6 mHz).

After 2 s the overfrequency is already null, but the decrease continues, generating an underfrequency that, in the best (`fast`) case reaches 111.3 mHz, and in the worst (`optimal`) 132.4 mHz. This is due to the

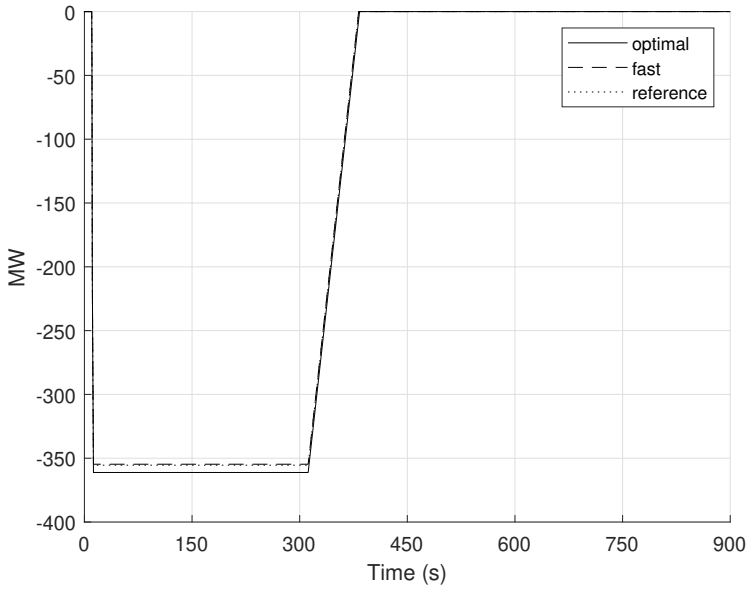

FIGURE 5.7: Combined wind and PV active power output for the considered overfrequency case.

downwards RESs regulation (Figure 5.7). As the overfrequency briefly exceeds the 300 mHz threshold, the downwards regulation of the wind generators, HV PV, and MV PV activates, fully activating at $t = 12.6$ s: by that time their combined power generation dropped by 361.17 MW. The unidirectionality of this regulation action leads to the underfrequency mentioned above.

The RES downwards regulation, according to the Code, must stay active for 300 s, after which it is deactivated with a power ramp of 20 % of the generated power per minute. This power increase triggers a new overfrequency event, culminating in a second zenith at $t = 383.3$ s,`reference` and `fast` cases, peaking at 140.7 mHz (worst case, `reference`) and 132.7 mHz, respectively. The `optimal` zenith 137.9 mHz, occurs at $t = 384.6$ s. Again, the HESS with its increased rated power, is better in containing the frequency increase, especially as this happens more slowly than in case of a tripping event.

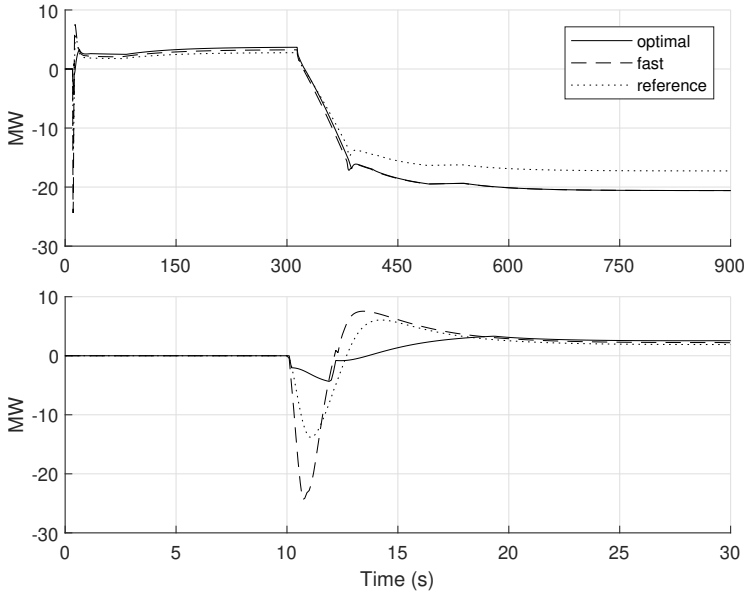

FIGURE 5.8: Foxi Muredgu plant active power output for the considered overfrequency case (top), and detail (bottom).

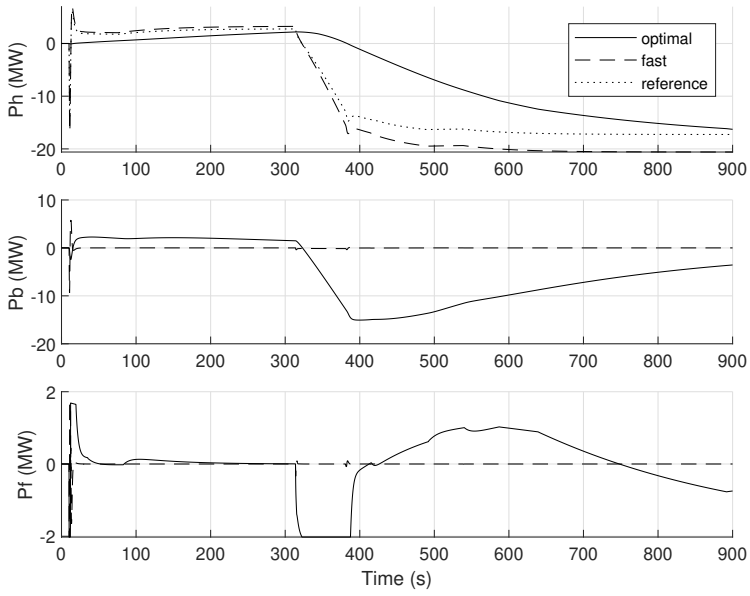

FIGURE 5.9: Foxi Muredgu PSHP (top), BESS (centre), and FESS (bottom) active power output for the considered overfrequency case.

As in the previous case, the HESS in its `optimal` configuration is not fast enough to cope with high frequency frequency fluctuation of this magnitude (in fact the FESS rated power is only 2 MW), as seen from Figure 5.8. On the other hand, again, the `fast` configuration under-utilizes the BESS and FESS devices (Figure 5.9).

v Discussion of the results

This chapter presents the results of the simulation of the Foxi Murdegu variable-speed PSHP, in different cases (non-hybrid, optimally hybridized, and hybridized without intentional delays), included into a model of the 2030 Sardinia power system, considering two tripping events: an underfrequency and an overfrequency, respectively.

The grid model and the scenario were developed and defined by RSE, detailing the energy mix of the 2030 Sardinian power system and the generation/export faults that characterize each event under study.

The optimal HESS, optimized in a way to guarantee the highest return of investment for the plant owner, proves to help stabilizing the grid frequency. The high intentional delay for reducing the PSHP wear and tear results in reducing the capability of the overall plant to track fast and intense frequency excursions. On the other hand, the optimized plant without intentional delays under-utilizes the BESS and FESS, in the simulated cases. It is worth to note that the BESS power converter has been modeled with data taken from the literature. The experimental data sampled for the Supercapacitor Energy Storage System (SC) (see Section 2.v.1) suggests that the power electronics are able to deliver the requested power in the span of tens of milliseconds, hence the real BESS operation (without any intentional delay) could be faster and result in different outcomes. Moreover, a multi-objective optimization problem can be made by merging the TSO and the plant owner's perspectives: finding the optimal control of the hybridization that does not impact the plant performances from the grid point of view, but smooths as much as

possible the PSHP operation.

The wind generation can provide synthetic inertia for upwards regulation, but it has been shown that later on the device needs to draw power from the grid, interfering with the frequency restoration process. Combined wind and PV generaton are effective in providing downwards regulation in case of serious overfrequencies ($\Delta f > 200\,mHz$). Their downwards regulation action is not flexible, as it is mono-directional, and because of its linear deactivation causes a second overfrequency event. In any of these cases, the PSHP contributed to contain the frequency excursions.

It can be said that the results from these simulations, regarding the operation of the Foxi Murdegu HESS, could be expected: a trade-off has to be made in managing a plant, between the priority of the plant owner to smooth the plant operation as much as possible and that of the TSO's to have the fastest possible responses. The optimization process was built around the plant owner's perspective, therefore it is clearly unbalanced in this regard.

A case could be made for the setting in which the plant has been simulated. In this chapter, as well as in Chapter 4, the frequency events were specific, in the sense that the events input signals in the previous chapter, and the power imbalance in this chapter was unique and without noise. The true potential for the proposed (optimal) hybridization may have not been expressed sufficiently given the types of stimuli that were fed to the plant model. Future work, in this sense, should go in this direction, with different data to test the plant in realistic contexts.

List of symbols

Greek letters

	Wind power inertial control derivative gain (MJ/Hz)	α
	Permanent droop (%)	σ
	Angular velocity (rad/s)	ω
Roman letters		
	Apparent power (MV A)	A
	Total secondary regulation band (MW)	BR
	Energy (MJ)	E
	Moment of inertia ($kg\,s^2$)	J
	Frequency (Hz)	f
	Constant of inertia (s)	H
	Allocated FRR (pu)	SB
	AGC integral gain (MW/Hz)	k_{rs}
	Constant	k
	Regulating energy (MW/Hz)	k_I
	AGC signal (%)	$L_{\%}$
	Active power (MW)	P
	Laplacian operator	s
	Starting time (s)	T_a
Subscripts		
	Electrical	e
	Grid	g
	Primary regulation	I
	i-th element	i
	Secondary regulation	II
	Kinetic	k
	Mechanical	m
	Nominal	n
	Rated	r
	Wind power	w

6 Conclusions

In this thesis, the model and assessment of the potential benefits of the hybridization of a seawater Pumped Storage Hydro Power (sPSHP) with Battery Energy Storage System (BESS) and Flywheel Energy Storage System (FESS) was explored.

First, a dynamic model of a variable-speed Pumped Storage Hydro Power (PSHP) – including the characterization of the hydraulic machine via real data – was performed, together with the modeling of BESS and FESS. Two power management strategies were developed, each with its own fundamental objective: the first, Frequency Split (FS), aiming at delivering to each device the most appropriate frequency components of the regulation efforts, the other, Hydro Recharge (HR), which aimed to avoid the PSHP to adjust its power output if the regulation could be performed by the BESS.

Second, a comparative analysis of 100 combinations of BESS and FESS installed powers was performed, in an open-loop simulation framework, simulating one historical hour operation of continental Italy. Depending on the operation mode (variable speed pump-turbine or fixed-speed turbine), and on the power management strategy adopted, the Hybrid Energy Storage System (HESS) proved to be capable to track the frequency error, with lower wear and tear indicators than the non-hybrid case. In particular, the FS strategy proved to be more versatile and reliable for the BESS and variable-speed pump operation.

Third, an optimization procedure was developed to maximize the economic return over the useful life of the hybridization investment. Costs were estimated with publicly available information, and future revenue

schemes and simulation scenarios were provided by Ricerca sul Sistema Energetico (RSE), partner institution in this research project. The results show that the hybridization offers a much higher Net Present Value (NPV) than the standalone PSHP, confirming the FS superiority over the other strategy.

Last, the model was included in a Sardinian power system model, simulated in closed-loop to assess the contribution the HESS could provide in containing the frequency excursions after two different tripping events. In this case, the hybrid plant could provide enhanced regulation only when its operation was not delayed, compared to the optimal solution. This was due to the fact that the optimal plant was such from the point of view of the plant owner, not from the Transmission System Operator (TSO).

This work is the first of its kind to model and develop two coordination strategies between a HESS with more than two technologies. While the fundamental ideas behind the two analysed strategies are not new, their implementation in this framework is original, and the results are worth to be discussed.

The open-loop simulations presented in Chapter 3 have shown that, for the sizes of BESS and FESS considered, more than 50 % of the wear and tear indicators can be had with only 0.5 MW of installed BESS and FESS. This analysis was designed to investigate the impact of relatively small sizes of BESS and FESS, and the results prove that the inclusion of a small-size FESS, in addition to a BESS of similar power rating is beneficial to both the latter and the PSHP. The optimization process in Chapter 4 also employs open-loop simulations, and the solution that was found considers the inclusion of about 23 MW of BESS and 2 MW of FESS. The installed power is significantly higher than the combinations evaluated in Chapter 3. Economic attractiveness was the focus of the optimization: one of the remuneration schemes rewarded high installed BESS powers. If the TSO were to implement different incentives, the optimal hybridization for the plant owner would be much different, based on the same principle of economic attractiveness. These two analyses prove that the choice of

whether to hybridize or not a PSHP, and the choice of the amount of power to install depend both on the priorities of the plant owner, and the framework established by the TSO. Indeed, small BESS and FESS sizes are sufficient to increase the durability (meant as a reduced wear and tear) of the hydraulic machine, but there may be incentives that, to be fully exploited, would require the installation of Energy Storage Devices (ESDs) of greater sizes.

Considering the analysis and results presented in Chapter 5, it is clear that the contribution of the hybridization to the grid frequency stability is relatively small. From this, one could say that the hybridization is mainly in the interest of the plant owner, even if the TSO rewards such investments. This may not be the case for smaller isolated power systems, in which the increased flexibility given by the hybridization may be much more impactful.

There is no simple answer to the question of how to hybridize an existing plant, and this work was not meant to find a definitive answer to such a problem. Nevertheless, this can be meant as a first step to consider multi-ESDs hybrid systems: the developed methodology to coordinate three ESDs can be generalized for any number of storage devices. Future works should go in this direction, analysing different power systems and plants with special focus on the power and energy management strategies, being a core element of hybrid systems. Essential for this work is the proper characterization of electric systems, as this work shows how much the results depend on the type of electric system the plant is simulated into.

In support of the decision about if and how to hybridize a plant, the development of new tools and methods is key. As mentioned above, there are conflicting interests between the parts (TSO and plant owners). Besides new and improved forecasting techniques, to deal with the unpredictability and variability of Renewable Energy Source (RES) generation, multi-objective optimization may find the best design and control of the HESS, satisfying all the actors in this field. Moreover, self-adaptive con-

trol strategies, combining the prediction of a future state of the frequency with the State Of Charge (SOC) control routines and regulation effort split, could demonstrate to be the founding elements of the electric power system of the future.

The results from this work were highly influenced by the lack of available technical and economic data. Much is still unknown (or the information is unavailable) about how much does the provision of frequency regulation services cost, and it is troublesome to gather information about the loads, generators, and the grid frequency in the island of Sardinia in order to reconstruct a typical day operation of that power system, or a set of realistic common events.

This work, in its own small way, attempted to shed some light in the hybridization a PSHP with two more ESDs. Naturally the topic is too wide to be completely explored by one PhD project, but this work provides crucial insight on the effective power management between devices, together with the system behavior under different premises. The author hopes this concept is extended over the next years creating established and, possibly, standardized models and methodologies to support both the plant operator and the regulator in designing a robust decentralized electric system.

Acronyms

AGC	Automatic Generation Control
BEP	Best Efficiency Point
BESS	Battery Energy Storage System
CIEMAT	Centro de Investigaciones Energéticas, Medioambientales y Tecnológicas
DFIG	Doubly Fed Induction Generator
DOD	depth of discharge
ENTSO-E	European Network of Transmission System Operators for Electricity
ESD	Energy Storage Device
FCR	Frequency Containment Reserve
FESS	Flywheel Energy Storage System
FR	Fast Reserve
FRR	Frequency Restoration Reserve
FS	Frequency Split
GA	Genetic Algorithm
GHG	greenhouse gas
GSC	Grid Side Converter
GVO	Guide Vanes Opening
HESS	Hybrid Energy Storage System
HR	Hydro Recharge
HV	High Voltage
HVDC	High Voltage Direct Current
IGBT	insulated gate bipolar transistor

IGCC	Integrated Gasification Combined Cycle
LCA	Life Cycle Assessment
LCC	Line Commutated Current
LPF	Low-Pass Filter
LV	Low Voltage
m.b.	machine-base
MGP	*Mercato del Giorno Prima*, day-ahead market
MV	Medium Voltage
MWFi	Mei-Wang Fluctuation index
NPV	Net Present Value
O&M	Operation and Maintenance
OECD	Organisation for Economic Co-operation and Development
OF	Objective Function
PI	Proportional Integral
PSHP	Pumped Storage Hydro Power
PSO	Particle Swarm Optimization
psp	power set-point
pu	per-unit
PV	Photovoltaic
RES	Renewable Energy Source
ROCOF	Rate Of Change Of post-disturbance Frequency
ROR	Run-of-river
RSC	Rotor Side Converter
RSE	Ricerca sul Sistema Energetico
s.b.	system-base
SC	Supercapacitor Energy Storage System
SOC	State Of Charge
sPSHP	seawater Pumped Storage Hydro Power

TSO	Transmission System Operator
UP	Unità di Produzione
UPM	Universidad Politecnica de Madrid
WTG	Wind Turbine Generator

Bibliography

[1] UNFCCC
Adoption of the Paris Agreement, FCCC/CP/2015/L.9/Rev.1, UNFCCC, 2015.

[2] R. Mechler et al.
Loss and Damage and Limits to Adaptation: Recent IPCC Insights and Implications for Climate Science and Policy, in «Sustainability Science» 15.4 (2020), pp. 1245–1251, doi: 10.1007/s11625-020-00807-9.

[3] Dhakal, S. et al.
2022: Emissions Trends and Drivers, in *IPCC, 2022: Climate Change 2022: Mitigation of Climate Change. Contribution of Working Group III to the Sixth Assessment Report of the Intergovernmental Panel on Climate Change*, Cambridge, UK and New York, NY, USA: Cambridge University Press, 2022.

[4] IEA
Key World Energy Statistics 2021, International Energy Agency, 2021.

[5] IEA
Renewables 2022, Paris: International Energy Agency, 2022.

[6] European Wind Integration Study (EWIS)
Towards a Successful Integration of Large Scale Wind Power into European Electricity Grids, Brussels: European Wind Integration Study, 2010.

[7] P. Kundur, N.J. Balu, and M.G. Lauby
Power System Stability and Control, EPRI Power System Engineering Series, McGraw-Hill Education, 1994.

[8] L. Barelli, G. Bidini, D.A. Ciupageanu, A. Micangeli, P.A. Ottaviano, and D. Pelosi

Real Time Power Management Strategy for Hybrid Energy Storage Systems Coupled with Variable Energy Sources in Power Smoothing Applications, in «Energy Reports» 7 (2021), pp. 2872–2882, DOI: 10.1016/j.egyr.2021.05.018.

[9] D.M. Greenwood, K.Y. Lim, C. Patsios, P.F. Lyons, Y.S. Lim, and P.C. Taylor
Frequency Response Services Designed for Energy Storage, in «Applied Energy» 203 (2017), pp. 115–127, DOI: 10.1016/j.apenergy.2017.06.046.

[10] Johan Morren, Jan Pierik, and Sjoerd W.H. de Haan
Inertial Response of Variable Speed Wind Turbines, in «Electric Power Systems Research» 76.11 (2006), pp. 980–987, DOI: 10.1016/j.epsr.2005.12.002.

[11] *Commission Regulation (EU) 2017/2195 of 23 November 2017 Establishing a Guideline on Electricity Balancing (Text with EEA Relevance)Text with EEA Relevance*, 2022.

[12] *Commission Regulation (EU) 2017/1485 of 2 August 2017 Establishing a Guideline on Electricity Transmission System Operation (Text with EEA Relevance)Text with EEA Relevance*, 2021.

[13] *Balancing and Ancillary Services Markets*, URL: https://docstore.entsoe.eu/about-entso-e/market/balancing-and-ancillary-services-markets/Pages/default.aspx (visited on 02/20/2023).

[14] ENTSO-E and WGAS
Survey on Ancillary Services Procurement Balancing Market Design 2021, 2022, URL: https://eepublicdownloads.blob.core.windows.net/public-cdn-container/clean-documents/mc-documents/balancing_ancillary/2022/2022-06-20_WGAS_Survey.pdf (visited on 02/22/2023).

[15] TERNA
Partecipazione Alla Regolazione Di Frequenza e Frequenza-Potenza, Prescrizione Tecnica Annex A15, TERNA, 2008.

[16] Yogendra Arya and Narendra Kumar

AGC of a Multi-Area Multi-Source Hydrothermal Power System Interconnected via AC/DC Parallel Links under Deregulated Environment, in «International Journal of Electrical Power and Energy Systems» 75 (2016), pp. 127–138, DOI: 10.1016/j.ijepes.2015.08.015.

[17] Haisheng CHEN, Thang Ngoc CONG, Wei YANG, Chunqing TAN, Yongliang LI, and Yulong DING
Progress in Electrical Energy Storage System: A Critical Review, in «Progress in Natural Science» 19.3 (2009), pp. 291–312, DOI: 10.1016/j.pnsc.2008.07.014.

[18] Sergio VAZQUEZ, Srdjan M. LUKIC, Eduardo GALVAN, Leopoldo G. FRANQUELO, and Juan M. CARRASCO
Energy Storage Systems for Transport and Grid Applications, in «IEEE Transactions on Industrial Electronics» 57.12 (2010), pp. 3881–3895, DOI: 10.1109/TIE.2010.2076414.

[19] Nathaniel S. PEARRE and Lukas G. SWAN
Technoeconomic Feasibility of Grid Storage: Mapping Electrical Services and Energy Storage Technologies, in «Applied Energy» 137 (2015), pp. 501–510, DOI: 10.1016/j.apenergy.2014.04.050.

[20] Furquan NADEEM, S. M. Suhail HUSSAIN, Prashant Kumar TIWARI, Arup Kumar GOSWAMI, and Taha Selim USTUN
Comparative Review of Energy Storage Systems, Their Roles, and Impacts on Future Power Systems, in «IEEE Access» 7 (2019), pp. 4555–4585, DOI: 10.1109/ACCESS.2018.2888497.

[21] Umer AKRAM, Mithulananthan NADARAJAH, Rakibuzzaman SHAH, and Federico MILANO
A Review on Rapid Responsive Energy Storage Technologies for Frequency Regulation in Modern Power Systems, in «Renewable and Sustainable Energy Reviews» 120 (2020), p. 109626, DOI: 10.1016/j.rser.2019.109626.

[22] Ababay Ketema WORKU, Delele Worku AYELE, Nigus Gabbiye HABTU, Bimrew Tamrat ADMASU, Getu ALEMAYEHU, Biniyam Zemene TAYE, and Temesgen Atnafu YEMATA
Energy Storage Technologies; Recent Advances, Challenges, and Prospectives, in *Planning of Hybrid Renewable Energy Systems, Electric Ve-*

hicles and Microgrid, ed. by Aashish Kumar Bohre, Pradyumn Chaturvedi, Mohan Lal Kolhe, and Sri Niwas Singh, Singapore: Springer Nature Singapore, 2022, pp. 125–150, DOI: 10.1007/978-981-19-0979-5_7.

[23] CNESA
Energy Storage Industry White Paper 2020 (Beijing: 2020), Beijing: China Energy Storage Alliance, 2020.

[24] REN21
Renewables 2021 Global Status Report, Paris: REN21 Secretariat, 2021.

[25] Hongqing Fang, Long Chen, Nkosinathi Dlakavu, and Zuyi Shen
Basic Modeling and Simulation Tool for Analysis of Hydraulic Transients in Hydroelectric Power Plants, in «IEEE Transactions on Energy Conversion» 23.3 (2008), pp. 834–841, DOI: 10.1109/TEC.2008.921560.

[26] G. Ardizzon, G. Cavazzini, and G. Pavesi
A New Generation of Small Hydro and Pumped-Hydro Power Plants: Advances and Future Challenges, in «Renewable and Sustainable Energy Reviews» 31 (2014), pp. 746–761, DOI: 10.1016/j.rser.2013.12.043.

[27] Shivam Doshi, Anirudh Katoch, Arjun Suresh, Fadil A. Razak, Sagnik Datta, Sameer Madhavan, C. M. Zanhar, and Edison Gundabattini
A Review on Vibrations in Various Turbomachines Such as Fans, Compressors, Turbines and Pumps, in «Journal of Vibration Engineering & Technologies» 9.7 (2021), pp. 1557–1575, DOI: 10.1007/s42417-021-00313-x.

[28] Jun-Won Suh, Seung-Jun Kim, Jin-Hyuk Kim, Won-Gu Joo, Jungwan Park, and Young-Seok Choi
Effect of Interface Condition on the Hydraulic Characteristics of a Pump-Turbine at Various Guide Vane Opening Conditions in Pump Mode, in «Renewable Energy» 154 (2020), pp. 986–1004, DOI: 10.1016/j.renene.2020.03.017.

[29] Ioannis Kougias et al.

Analysis of Emerging Technologies in the Hydropower Sector, in «Renewable and Sustainable Energy Reviews» 113 (2019), p. 109257, DOI: 10.1016/j.rser.2019.109257.

[30] Bjørn W Solemslie, Chirag Trivedi, Einar Agnalt, and Ole G Dahlhaug
Pressure Pulsations and Fatigue Loads in High Head Francis Turbines, in «IOP Conference Series: Earth and Environmental Science» 240 (2019), p. 022039, DOI: 10.1088/1755-1315/240/2/022039.

[31] S Riedelbauch and C Stens
Pump to Turbine Transient for a Pump-Turbine in a Model Test Circuit and a Real Size Power Plant, in «IOP Conference Series: Earth and Environmental Science» 240 (2019), p. 072039, DOI: 10.1088/1755-1315/240/7/072039.

[32] Juan I. Pérez-Díaz, Marcos Lafoz, and Frank Burke
Integration of Fast Acting Energy Storage Systems in Existing Pumped-storage Power Plants to Enhance the System's Frequency Control, in «WIREs Energy and Environment» 9.2 (2019), DOI: 10.1002/wene.367.

[33] Robert Eriksson and Magnus Perninge
Dynamic Performance of the Frequency Containment Reserve – Experience from the Nordic System, in (), p. 7.

[34] José Ignacio Sarasúa, Juan Ignacio Pérez-Díaz, José Román Wilhelmi, and José Ángel Sánchez-Fernández
Dynamic Response and Governor Tuning of a Long Penstock Pumped-Storage Hydropower Plant Equipped with a Pump-Turbine and a Doubly Fed Induction Generator, in «Energy Conversion and Management» 106 (2015), pp. 151–164, DOI: 10.1016/j.enconman.2015.09.030.

[35] Weijia Yang, Per Norrlund, Linn Saarinen, Jiandong Yang, Wencheng Guo, and Wei Zeng
Wear and Tear on Hydro Power Turbines – Influence from Primary Frequency Control, in «Renewable Energy» 87 (2016), pp. 88–95, DOI: 10.1016/j.renene.2015.10.009.

[36] Tomi Makinen, Aki Leinonen, and Markus Ovaskainen
Modelling and Benefits of Combined Operation of Hydropower Unit and Battery Energy Storage System on Grid Primary Frequency Control,

in *2020 IEEE International Conference on Environment and Electrical Engineering and 2020 IEEE Industrial and Commercial Power Systems Europe (EEEIC / I&CPS Europe)*, 2020 IEEE International Conference on Environment and Electrical Engineering and 2020 IEEE Industrial and Commercial Power Systems Europe (EEEIC / I&CPS Europe), Madrid, Spain: IEEE, 2020, pp. 1–6, DOI: 10.1109/EEEIC/ICPSEurope49358.2020.9160666.

[37] Zhigao ZHAO, Jiandong YANG, C.Y. CHUNG, Weijia YANG, Xianghui HE, and Man CHEN
Performance Enhancement of Pumped Storage Units for System Frequency Support Based on a Novel Small Signal Model, in «Energy» 234 (2021), p. 121207, DOI: 10.1016/j.energy.2021.121207.

[38] IEA
Renewables Information: Overview, Paris, 2020.

[39] OCED / IEA
Technology Roadmap Hydropower, in Berlin/Heidelberg: Springer-Verlag, 2012.

[40] Zerui DONG, Jin TAN, Eduard MULJADI, Robert M. NELMS, Antoine ST-HILAIRE, Matthew PEVARNIK, and Mark D. JACOBSON
Developing of Quaternary Pumped Storage Hydropower for Dynamic Studies, in «IEEE Transactions on Sustainable Energy» 11.4 (2020), pp. 2870–2878, DOI: 10.1109/TSTE.2020.2980585.

[41] Soumyadeep NAG, Zerui DONG, Jin TAN, Jinho KIM, Eduard MULJADI, Kwang Y. LEE, and Mark JACOBSON
Impact of Quaternary Pumped Storage Hydropower on Frequency Response of U.S. Western Interconnection with High Renewable Penetrations, in *2022 IEEE Power & Energy Society General Meeting (PESGM)*, 2022 IEEE Power & Energy Society General Meeting (PESGM), 2022, pp. 1–5, DOI: 10.1109/PESGM48719.2022.9916827.

[42] EPRI
Electric Energy Storage Technology Options: A White Paper Primer on Applications, Costs and Benefits, in «Epri» (2010), pp. 1–170.

[43] Oliver SCHMIDT, Sylvain MELCHIOR, Adam HAWKES, and Iain STAFFELL

Projecting the Future Levelized Cost of Electricity Storage Technologies, in «Joule» 3.1 (2019), pp. 81–100, DOI: 10.1016/j.joule.2018.12.008.

[44] Kendall MONGIRD, Vilayanur VISWANATHAN, Patrick BALDUCCI, Jan ALAM, Vanshika FOTEDAR, Vladimir KORITAROV, and Boualem HADJERIOUA
An Evaluation of Energy Storage Cost and Performance Characteristics, in «Energies» 13.13 (2020), p. 3307, DOI: 10.3390/en13133307.

[45] Stefano CASSANO and Fabrizio SOSSAN
Stress-Informed Control of Medium- and High-Head Hydropower Plants to Reduce Penstock Fatigue, in «Sustainable Energy, Grids and Networks» 31 (2022), p. 100688, DOI: 10.1016/j.segan.2022.100688.

[46] Frederic MICHAUD and Gerard ROBERT
Flatness-Based Control of an Hydro Power Plant, in *Melecon 2010 - 2010 15th IEEE Mediterranean Electrotechnical Conference*, Melecon 2010 - 2010 15th IEEE Mediterranean Electrotechnical Conference, Valletta, Malta: IEEE, 2010, pp. 1505–1509, DOI: 10.1109/MELCON.2010.5476253.

[47] Jiri KOUTNIK
Voith Hydro - Hydro Power Plants, AGCS (Munich), 2013.

[48] T. KUWABARA, A. SHIBUYA, H. FURUTA, E. KITA, and K. MITSUHASHI
Design and Dynamic Response Characteristics of 400 MW Adjustable Speed Pumped Storage Unit for Ohkawachi Power Station, in «IEEE Transactions on Energy Conversion» 11.2 (1996), pp. 376–384, DOI: 10.1109/60.507649.

[49] R BESSA, C MOREIRA, B SILVA, J FILIPE, and N FULGÊNCIO
Role of Pump Hydro in Electric Power Systems, in «Journal of Physics: Conference Series» 813 (2017), p. 012002, DOI: 10.1088/1742-6596/813/1/012002.

[50] Igor ILIEV, Chirag TRIVEDI, and Ole Gunnar DAHLHAUG
Variable-Speed Operation of Francis Turbines: A Review of the Perspectives and Challenges, in «Renewable and Sustainable Energy

Reviews» 103.7491 (2019), pp. 109–121, DOI: 10.1016/j.rser.2018.12.033.

[51] José Ignacio Sarasúa, Juan Ignacio Pérez-Díaz, and Blanca Torres Vara
On the Implementation of Variable Speed in Pump-Turbine Units Providing Primary and Secondary Load-Frequency Control in Generating Mode, in «Energies» 8.12 (2015), pp. 13559–13575, DOI: 10.3390/en81212382.

[52] Gabriel Dan Ciocan, Olivier Teller, and Francois Czerwinski
VARIABLE SPEED PUMP-TURBINES TECHNOLOGY, in (2012), p. 10.

[53] N. Sivakumar, Devadutta Das, and N.P. Padhy
Variable Speed Operation of Reversible Pump-Turbines at Kadamparai Pumped Storage Plant – A Case Study, in «Energy Conversion and Management» 78 (2014), pp. 96–104, DOI: 10.1016/j.enconman.2013.10.048.

[54] Edson Bortoni, Zulcy de Souza, Augusto Viana, Helcio Villa-Nova, Ângelo Rezek, Luciano Pinto, Roberto Siniscalchi, Rafael Bragança, and José Bernardes
The Benefits of Variable Speed Operation in Hydropower Plants Driven by Francis Turbines, in «Energies» 12.19 (19 2019), p. 3719, DOI: 10.3390/en12193719.

[55] Giovanna Cavazzini, Juan I. Pérez-Díaz, Francisco Blázquez, Carlos Platero, Jesús Fraile-Ardanuy, José A. Sánchez, and Manuel Chazarra
Pumped-Storage Hydropower Plants: The New Generation, in *Energy Storage*, World Scientific, 2017, pp. 27–80, DOI: 10.1142/9789813208964_0002.

[56] Flávio Oliveira, Arthur Amorim, Lucas Encarnação, Jussara Fardin, Marcos Orlando, Selênio Silva, and Domingos Simonetti
Enhancing LVRT of DFIG by Using a Superconducting Current Limiter on Rotor Circuit, in «Energies» 9.1 (2015), p. 16, DOI: 10.3390/en9010016.

[57] A. Joseph, T. R. Chelliah, R. Selvaraj, and K. Lee

Fault Diagnosis and Fault-Tolerant Control of Megawatt Power Electronic Converter-Fed Large-Rated Asynchronous Hydrogenerator, in «IEEE Journal of Emerging and Selected Topics in Power Electronics» 7.4 (2019), pp. 2403–2416, DOI: 10.1109/JESTPE.2018.2881427.

[58] Juan Ignacio Pérez-Díaz, Giovanna Cavazzini, F. Blázquez, C Platero, J. Fraile-Ardanuy, José Ángel Sánchez-Fernández, and M Chazarra
Technological Developments for Pumped-Hydro Energy Storage, Technical Report, Mechanical Storage Subprogramme, Joint Programme on Energy Storage, European Energy Research Alliance, 2014, pp. 122–122.

[59] Eamonn Lannoye
Renewable Energy Integration: Practical Management of Variability, Uncertainty, and Flexibility in Power Grids [*Book Reviews*], in «IEEE Power and Energy Magazine» 13.6 (2015), pp. 106–107, DOI: 10.1109/MPE.2015.2458758.

[60] Ioannis D. Margaris, Stavros A. Papathanassiou, Nikos D. Hatziargyriou, Anca D. Hansen, and Poul Sorensen
Frequency Control in Autonomous Power Systems With High Wind Power Penetration, in «IEEE Transactions on Sustainable Energy» 3.2 (2012), pp. 189–199, DOI: 10.1109/TSTE.2011.2174660.

[61] José Ignacio Sarasua, Guillermo Martínez-Lucas, Hilel García-Pereira, Gustavo Navarro-Soriano, Ángel Molina-García, and Ana Fernández-Guillamón
Hybrid Frequency Control Strategies Based on Hydro-power, Wind, and Energy Storage Systems: Application to 100% Renewable Scenarios, in «IET Renewable Power Generation» 16.6 (2022), pp. 1107–1120, DOI: 10.1049/rpg2.12326.

[62] Giovanna Cavazzini, Jean-Bernard Houdeline, Giorgio Pavesi, Olivier Teller, and Guido Ardizzon
Unstable Behaviour of Pump-Turbines and Its Effects on Power Regulation Capacity of Pumped-Hydro Energy Storage Plants, in «Renewable and Sustainable Energy Reviews» 94 (2018), pp. 399–409, DOI: 10.1016/j.rser.2018.06.018.

[63] REN21
Renewables 2022 Global Status Report, Paris: REN21 Secretariat, 2022.

[64] Katsuhiro Oshima, Juichiro Kawai, Shiro Otsuka, Toshiro Wada, and Haruo Imano
Development of Pump-Turbine for Seawater Pumped Storage Power Plant, in *Waterpower '99*, Waterpower Conference 1999, Las Vegas, Nevada, United States: American Society of Civil Engineers, 1999, pp. 1–6, DOI: 10.1061/40440(1999)67.

[65] Akitaka Hiratsuka, Takashi Arai, and Tsukasa Yoshimura
Seawater Pumped-Storage Power Plant in Okinawa Island, Japan, in «Engineering Geology» 35.3-4 (1993), pp. 237–246, DOI: 10.1016/0013-7952(93)90012-2.

[66] Dimitris Al. Katsaprakakis, Dimitris G. Christakis, Ioannis Stefanakis, Petros Spanos, and Nikos Stefanakis
Technical Details Regarding the Design, the Construction and the Operation of Seawater Pumped Storage Systems, in «Energy» 55 (2013), pp. 619–630, DOI: 10.1016/j.energy.2013.01.031.

[67] Willett Kempton and Jasna Tomić
Vehicle-to-Grid Power Implementation: From Stabilizing the Grid to Supporting Large-Scale Renewable Energy, in «Journal of Power Sources» 144 (2005), pp. 280–294, DOI: 10.1016/j.jpowsour.2004.12.022.

[68] Alexandre Oudalov, Daniel Chartouni, and Christian Ohler
Optimizing a Battery Energy Storage System for Primary Frequency Control, in «IEEE Transactions on Power Systems» 22.3 (2007), pp. 1259–1266, DOI: 10.1109/TPWRS.2007.901459.

[69] Rahul Walawalkar, Jay Apt, and Rick Mancini
Economics of Electric Energy Storage for Energy Arbitrage and Regulation in New York, in «Energy Policy» 35.4 (2007), pp. 2558–2568, DOI: 10.1016/j.enpol.2006.09.005.

[70] Sekyung Han, Soohee Han, and Kaoru Sezaki

Development of an Optimal Vehicle-to-Grid Aggregator for Frequency Regulation, in «IEEE Trans. Smart Grid» 1 (2010), pp. 65–72, DOI: 10.1109/TSG.2010.2045163.

[71] Meiling YUE, Samir JEMEI, Rafael GOURIVEAU, and Noureddine ZERHOUNI
Review on Health-Conscious Energy Management Strategies for Fuel Cell Hybrid Electric Vehicles: Degradation Models and Strategies, in «International Journal of Hydrogen Energy» 44.13 (2019), pp. 6844–6861, DOI: 10.1016/j.ijhydene.2019.01.190.

[72] Micah S. ZIEGLER and Jessika E. TRANCIK
Re-Examining Rates of Lithium-Ion Battery Technology Improvement and Cost Decline, in «Energy & Environmental Science» 14.4 (2021), pp. 1635–1651, DOI: 10.1039/D0EE02681F.

[73] Jason LEADBETTER and Lukas G. SWAN
Selection of Battery Technology to Support Grid-Integrated Renewable Electricity, in «Journal of Power Sources» 216 (2012), pp. 376–386, DOI: 10.1016/j.jpowsour.2012.05.081.

[74] Holger HESSE, Michael SCHIMPE, Daniel KUCEVIC, and Andreas JOSSEN
Lithium-Ion Battery Storage for the Grid—A Review of Stationary Battery Storage System Design Tailored for Applications in Modern Power Grids, in «Energies» 10.12 (2017), p. 2107, DOI: 10.3390/en10122107.

[75] M. BENINI, S. CANEVESE, D. CIRIO, and A. GATTI
Battery Energy Storage Systems for the Provision of Primary and Secondary Frequency Regulation in Italy, in *2016 IEEE 16th International Conference on Environment and Electrical Engineering (EEEIC)*, 2016 IEEE 16th International Conference on Environment and Electrical Engineering (EEEIC), Florence, Italy: IEEE, 2016, pp. 1–6, DOI: 10.1109/EEEIC.2016.7555748.

[76] Jonas ENGELS, Bert CLAESSENS, and Geert DECONINCK
Combined Stochastic Optimization of Frequency Control and Self-Consumption With a Battery, in «IEEE Transactions on Smart Grid» 10.2 (2019), pp. 1971–1981, DOI: 10.1109/TSG.2017.2785040.

[77] M. Sufyan, N. A. Rahim, M. M. Aman, C. K. Tan, and S. R. S. Raihan
Sizing and Applications of Battery Energy Storage Technologies in Smart Grid System: A Review, in «Journal of Renewable and Sustainable Energy» 11.1 (2019), p. 014105, DOI: 10.1063/1.5063866.

[78] Jan Figgener, Peter Stenzel, Kai-Philipp Kairies, Jochen Linssen, David Haberschusz, Oliver Wessels, Martin Robinius, Detlef Stolten, and Dirk Uwe Sauer
The Development of Stationary Battery Storage Systems in Germany – Status 2020, in «Journal of Energy Storage» 33 (2021), p. 101982, DOI: 10.1016/j.est.2020.101982.

[79] Jun Hou, Ziyou Song, Heath F. Hofmann, and Jing Sun
Control Strategy for Battery/Flywheel Hybrid Energy Storage in Electric Shipboard Microgrids, in «IEEE Transactions on Industrial Informatics» 17.2 (2021), pp. 1089–1099, DOI: 10.1109/TII.2020.2973409.

[80] Gaojun Meng, Qingqing Chang, Yukun Sun, Yufei Rao, Feng Zhang, Yao Wu, and Ling Su
Energy Storage Auxiliary Frequency Modulation Control Strategy Considering ACE and SOC of Energy Storage, in «IEEE Access» 9 (2021), pp. 26271–26277, DOI: 10.1109/ACCESS.2021.3058146.

[81] Tjark Thien, Hendrik Axelsen, Michael Merten, and Dirk Uwe Sauer
Energy Management of Stationary Hybrid Battery Energy Storage Systems Using the Example of a Real-World 5 MW Hybrid Battery Storage Project in Germany, in «Journal of Energy Storage» 51 (2022), p. 104257, DOI: 10.1016/j.est.2022.104257.

[82] Xiaomin Wu, Shaoyi Li, Shengfeng Gan, and Changhui Hou
An Adaptive Energy Optimization Method of Hybrid Battery-Supercapacitor Storage System for Uncertain Demand, in «Energies» 15.5 (2022), p. 1765, DOI: 10.3390/en15051765.

[83] John Wang, Ping Liu, Jocelyn Hicks-Garner, Elena Sherman, Souren Soukiazian, Mark Verbrugge, Harshad Tataria, James Musser, and Peter Finamore

Cycle-Life Model for Graphite-LiFePO4 Cells, in «Journal of Power Sources» 196.8 (2011), pp. 3942–3948, DOI: 10.1016/j.jpowsour.2010.11.134.

[84] Alan MILLNER
Modeling Lithium Ion Battery Degradation in Electric Vehicles, in «2010 IEEE Conference on Innovative Technologies for an Efficient and Reliable Electricity Supply, CITRES 2010» (October 2010 2010), pp. 349–356, DOI: 10.1109/CITRES.2010.5619782.

[85] Daniel-Ioan STROE, Vaclav KNAP, Maciej SWIERCZYNSKI, Ana-Irina STROE, and Remus TEODORESCU
Operation of a Grid-Connected Lithium-Ion Battery Energy Storage System for Primary Frequency Regulation: A Battery Lifetime Perspective, in «IEEE Transactions on Industry Applications» 53.1 (2017), pp. 430–438, DOI: 10.1109/TIA.2016.2616319.

[86] Bolun XU, Alexandre OUDALOV, Andreas ULBIG, Goran ANDERSSON, and Daniel S. KIRSCHEN
Modeling of Lithium-Ion Battery Degradation for Cell Life Assessment, in «IEEE Transactions on Smart Grid» 9.2 (2018), pp. 1131–1140, DOI: 10.1109/TSG.2016.2578950.

[87] Subhashree CHOUDHURY
Flywheel Energy Storage Systems: A Critical Review on Technologies, Applications, and Future Prospects, in «International Transactions on Electrical Energy Systems» 31.9 (2021), DOI: 10.1002/2050-7038.13024.

[88] Xuan Phuong NGUYEN and Anh Tuan HOANG
The Flywheel Energy Storage System: An Effective Solution to Accumulate Renewable Energy, in *2020 6th International Conference on Advanced Computing and Communication Systems (ICACCS)*, 2020 6th International Conference on Advanced Computing and Communication Systems (ICACCS), 2020, pp. 1322–1328, DOI: 10.1109/ICACCS48705.2020.9074469.

[89] S.M. MOUSAVI G, Faramarz FARAJI, Abbas MAJAZI, and Kamal AL-HADDAD

A Comprehensive Review of Flywheel Energy Storage System Technology, in «Renewable and Sustainable Energy Reviews» 67 (2017), pp. 477–490, DOI: 10.1016/j.rser.2016.09.060.

[90] Jorge Torres, Marcos Blanco, Marcos Lafoz, Gustavo Navarro, Jorge Nájera, and Miguel Santos-Herran
Dimensioning Methodology of Energy Storage Systems for Power Smoothing in a Wave Energy Conversion Plant Considering Efficiency Maps and Filtering Control Techniques, in «Energies» 13.13 (2020), p. 3380, DOI: 10.3390/en13133380.

[91] Mustafa E. Amiryar and Keith R. Pullen
A Review of Flywheel Energy Storage System Technologies and Their Applications, in «Applied Sciences» 7.3 (3 2017), p. 286, DOI: 10.3390/app7030286.

[92] M. L. Lazarewicz and A. Rojas
Grid Frequency Regulation by Recycling Electrical Energy in Flywheels, in *IEEE Power Engineering Society General Meeting, 2004.* 2004, 2038–2042 Vol.2, DOI: 10.1109/PES.2004.1373235.

[93] Ioannis Hadjipaschalis, Andreas Poullikkas, and Venizelos Efthimiou
Overview of Current and Future Energy Storage Technologies for Electric Power Applications, in «Renewable and Sustainable Energy Reviews» 13.6 (2009), pp. 1513–1522, DOI: 10.1016/j.rser.2008.09.028.

[94] Yang Jiao and Daniel Månsson
Greenhouse Gas Emissions from Hybrid Energy Storage Systems in Future 100% Renewable Power Systems – A Swedish Case Based on Consequential Life Cycle Assessment, in «Journal of Energy Storage» 57 (2023), p. 106167, DOI: 10.1016/j.est.2022.106167.

[95] A. Buchroithner, A. Haan, R. Pressmair, M. Bader, B. Schweighofer, H. Wegleiter, and H. Edtmayer
Decentralized Low-Cost Flywheel Energy Storage for Photovoltaic Systems, in *2016 International Conference on Sustainable Energy Engineering and Application (ICSEEA)*, 2016 International Conference on Sustainable Energy Engineering and Application (ICSEEA), 2016, pp. 41–49, DOI: 10.1109/ICSEEA.2016.7873565.

[96] Yuehua Cheng, Bin Jiang, Xiaodong Han, and Zhijun Wang
A Life Prediction Model of Flywheel Systems Using Stochastic Hybrid Automaton, in «Electronics» 8.11 (11 2019), p. 1236, DOI: 10.3390/electronics8111236.

[97] J.P. Rouse, S.D. Garvey, B. Cárdenas, A. Hoskin, L. Swinfen-Styles, and W. Xu
A Case Study Investigation into the Risk of Fatigue in Synchronous Flywheel Energy Stores and Ramifications for the Design of Inertia Replacement Systems, in «Journal of Energy Storage» 39 (2021), p. 102651, DOI: 10.1016/j.est.2021.102651.

[98] Yuri V. Makarov, Bo Yang, John G. DeSteese, Shuai Lu, Carl H. Miller, Preben Nyeng, Jian Ma, Donald J. Hammerstrom, and Vilanyur V. Vishwanathan
Wide-Area Energy Storage and Management System to Balance Intermittent Resources in the Bonneville Power Administration and California ISO Control Areas, PNNL-17574, 947483, 2008, PNNL–17574, 947483, DOI: 10.2172/947483.

[99] Maxwell Technologies
2.7V 3000F ULTRACAPACITOR CELL, 2023, URL: https://maxwell.com/wp-content/uploads/2022/11/3003279-EN.3_DS_2.7V-3000F-Cell-BCAP3000-P270.pdf (visited on 02/26/2023).

[100] Joel Schindall
The Charge of the Ultracapacitors, in «IEEE Spectrum» 44.11 (2007), pp. 42–46, DOI: 10.1109/MSPEC.2007.4378458.

[101] Behnam Zakeri and Sanna Syri
Electrical Energy Storage Systems: A Comparative Life Cycle Cost Analysis, in «Renewable and Sustainable Energy Reviews» 42 (2015), pp. 569–596, DOI: 10.1016/j.rser.2014.10.011.

[102] Beacon Power
Operating Plants - Hazle Township, Pennsylvania, URL: https://web.archive.org/web/20221209120625/https://beaconpower.com/hazle-township-pennsylvania/ (visited on 02/27/2023).

[103] M. Benini, S. Canevese, D. Cirio, and A. Gatti

Participation of Battery Energy Storage Systems in the Italian Balancing Market: Management Strategies and Economic Results, in *2018 IEEE International Conference on Environment and Electrical Engineering and 2018 IEEE Industrial and Commercial Power Systems Europe (EEEIC / I&CPS Europe)*, 2018 IEEE International Conference on Environment and Electrical Engineering and 2018 IEEE Industrial and Commercial Power Systems Europe (EEEIC / I&CPS Europe), Palermo: IEEE, 2018, pp. 1–6, DOI: 10.1109/EEEIC.2018.8493701.

[104] Hanis Farhah Jamahori and Hasimah Abdul Rahman
Hybrid Energy Storage System for Life Cycle Improvement, in *2017 IEEE Conference on Energy Conversion (CENCON)*, 2017 IEEE Conference on Energy Conversion (CENCON), Kuala Lumpur, Malaysia: IEEE, 2017, pp. 196–200, DOI: 10.1109/CENCON.2017.8262483.

[105] V. N. Anosov and M. V. Yaroslavtsev
Evaluation of Hybrid Electric Bus Energy Storage Device Capacity, in *2016 11th International Forum on Strategic Technology (IFOST)*, 2016 11th International Forum on Strategic Technology (IFOST), Novosibirsk, Russia: IEEE, 2016, pp. 65–67, DOI: 10.1109/IFOST.2016.7884338.

[106] J.C. Hernández, F. Sanchez-Sutil, F.J. Muñoz-Rodríguez, and C.R. Baier
Optimal Sizing and Management Strategy for PV Household-Prosumers with Self-Consumption/Sufficiency Enhancement and Provision of Frequency Containment Reserve, in «Applied Energy» 277 (2020), p. 115529, DOI: 10.1016/j.apenergy.2020.115529.

[107] Philipp Glücker, Klaus Kivekäs, Jari Vepsäläinen, Panagiotis Mouratidis, Maximilian Schneider, Stephan Rinderknecht, and Kari Tammi
Prolongation of Battery Lifetime for Electric Buses through Flywheel Integration, in «Energies» 14.4 (4 2021), p. 899, DOI: 10.3390/en14040899.

[108] Djamila Rekioua
Storage in Hybrid Renewable Energy Systems, in *Hybrid Renewable Energy Systems*, Cham: Springer International Publishing, 2020, pp. 139–172, DOI: 10.1007/978-3-030-34021-6_4.

[109] *Hydropower | ENGIE Deutschland*, URL: https://www.engie-deutschland.de/en/renewable-energy/hydropower (visited on 03/25/2023).

[110] *VEO Innovation Integrates Energy Storages in Hydropower Plants*, VEO Oy, URL: https://veo.fi/news/veo-innovation-integrates-energy-storages-in-hydropower-plants/ (visited on 03/25/2023).

[111] *New Fortum Batteries Enhance Renewable Energy Capacity*, Fortum, URL: https://www.fortum.com/media/2019/05/new-fortum-batteries-enhance-renewable-energy-capacity (visited on 03/25/2023).

[112] *BlueBattery: Größte Kraftwerks-Batterie Österreichs in Betrieb*, URL: https://www.verbund.com/de-at/ueber-verbund/news-presse/presse/2020/09/17/blue-battery-eroeffnung (visited on 03/25/2023).

[113] ANDRITZ AG
XFLEX HYDRO - Roadmap to More Flexibility for Hydropower Plants, URL: https://www.andritz.com/hydro-en/hydronews/hn35/xflex-hydro (visited on 03/25/2023).

[114] *Fortum Installs Innovative Battery Solution at Landafors Hydropower Plant in Sweden*, Fortum, URL: https://www.fortum.com/media/2021/04/fortum-installs-innovative-battery-solution-landafors-hydropower-plant-sweden (visited on 03/25/2023).

[115] *Hydropower + Batteries = Stable Electricity Supply*, Hydropower + batteries = stable electricity supply, URL: https://www.uniper.energy/news/hydropower--batteries--stable-electricity-supply (visited on 03/25/2023).

[116] *Uniper Investing in More Battery Systems for Hydropower in Sweden*, Uniper investing in more battery systems for hydropower in Sweden, URL: https://www.uniper.energy/news/uniper-investing-in-more-battery-systems-for-hydropower-in-sweden (visited on 03/25/2023).

[117] *In Green Energy Transition Batteries Are Needed More than Ever*, 2022, URL: https://www.helen.fi/en/company/responsibility/

current-topics/blogi/2022/in-green-energy-transition-batteries-are-needed-more-than-ever (visited on 03/25/2023).

[118] *Merus Power Ja Helen Ovat Tehneet Sopimuksen Sähkövaraston Kaupasta Mankalan Vesivoimalaan*, Merus Power, URL: https://www.meruspower.fi/news/merus-powers-energy-storage-system-allows-quick-adjustability-helens-hydropower-plant/ (visited on 03/25/2023).

[119] S. G.Jimmy Ehnberg and Math H.J. Bollen
Reliability of a Small Power System Using Solar Power and Hydro, in «Electric Power Systems Research» 74.1 (2005), pp. 119–127, DOI: 10.1016/j.epsr.2004.09.009.

[120] Dong Jing Lee and Li Wang
Small-Signal Stability Analysis of an Autonomous Hybrid Renewable Energy Power Generation/Energy Storage System Part I: Time-domain Simulations, in «IEEE Transactions on Energy Conversion» 23.1 (2008), pp. 311–320, DOI: 10.1109/TEC.2007.914309.

[121] Joseph Kenfack, François Pascal Neirac, Thomas Tamo Tatietse, Didier Mayer, Médard Fogue, and André Lejeune
Microhydro-PV-hybrid System: Sizing a Small Hydro-PV-hybrid System for Rural Electrification in Developing Countries, in «Renewable Energy» 34.10 (2009), pp. 2259–2263, DOI: 10.1016/j.renene.2008.12.038.

[122] Jon Are Suul, Kjetil Uhlen, and Tore Undeland
Variable Speed Pumped Storage Hydropower for Integration of Wind Energy in Isolated Grids – Case Description and Control Strategies, in NORPIE/2008, Nordic Workshop on Power and Industrial Electronics, June, 2008, p. 8.

[123] M. B. Camara, B. Dakyo, C. Nichita, and G. Barakat
Simulation of a Doubly-Fed Induction Generator with Hydro Turbine for Electrical Energy Production, in *2009 8th International Symposium on Advanced Electromechanical Motion Systems Electric Drives Joint Symposium*, 2009 8th International Symposium on Advanced Electromechanical Motion Systems Electric Drives Joint Symposium, 2009, pp. 1–6, DOI: 10.1109/ELECTROMOTION.2009.5259097.

[124] Bahtiyar Dursun, Bora Alboyaci, and Cihan Gokcol
Optimal Wind-Hydro Solution for the Marmara Region of Turkey to Meet Electricity Demand, in «Energy» 36.2 (2011), pp. 864–872, DOI: 10.1016/j.energy.2010.12.028.

[125] Li Dinglin, Chen Yingjie, Zhang Kun, and Zeng Ming
Economic Evaluation of Wind-Powered Pumped Storage System, in «Systems Engineering Procedia» 4 (2012), pp. 107–115, DOI: 10.1016/j.sepro.2011.11.055.

[126] Getachew Bekele and Getnet Tadesse
Feasibility Study of Small Hydro/PV/Wind Hybrid System for off-Grid Rural Electrification in Ethiopia, in «Applied Energy» 97 (2012), pp. 5–15, DOI: 10.1016/j.apenergy.2011.11.059.

[127] Edgardo D. Castronuovo and João A.Peças Lopes
Optimal Operation and Hydro Storage Sizing of a Wind-Hydro Power Plant, in «International Journal of Electrical Power and Energy System» 26.10 (2004), pp. 771–778, DOI: 10.1016/j.ijepes.2004.08.002.

[128] Stefan Breban, Mehdi Nasser, Arnaud Vergnol, Benoît Robyns, and Mircea M. Radulescu
Hybrid Wind/Microhydro Power System Associated with a Supercapacitor Energy Storage Device - Experimental Results, in «Proceedings of the 2008 International Conference on Electrical Machines, ICEM'08» (2008), pp. 1–6, DOI: 10.1109/ICELMACH.2008.4800026.

[129] Stefanos V. Papaefthymiou and Stavros A. Papathanassiou
Optimum Sizing of Wind-Pumped-Storage Hybrid Power Stations in Island Systems, in «Renewable Energy» 64 (2014), pp. 187–196, DOI: 10.1016/j.renene.2013.10.047.

[130] A.M. Foley, P.G. Leahy, K. Li, E.J. McKeogh, and A.P. Morrison
A Long-Term Analysis of Pumped Hydro Storage to Firm Wind Power, in «Applied Energy» 137 (2015), pp. 638–648, DOI: 10.1016/j.apenergy.2014.07.020.

[131] Xianxun Wang, Yadong Mei, Hao Cai, and Xiangyu Cong

A New Fluctuation Index: Characteristics and Application to Hydro-Wind Systems, in «Energies» 9.2 (2016), p. 114, DOI: 10.3390/en9020114.

[132] Miao Miao, Zhiming Wu, Suhua Lou, and Yongcan Wang
Research on Optimizing Operation of Hybrid PV Power and Pumped Hydro Storage System, in «Energy Procedia» 118 (2017), pp. 110–118, DOI: 10.1016/j.egypro.2017.07.023.

[133] Moein Parastegari, Rahmat Allah Hooshmand, Amin Khodabakhshian, and Amir Hossein Zare
Joint Operation of Wind Farm, Photovoltaic, Pump-Storage and Energy Storage Devices in Energy and Reserve Markets, in «International Journal of Electrical Power and Energy Systems» 64 (2015), pp. 275–284, DOI: 10.1016/j.ijepes.2014.06.074.

[134] Subhojit Dawn, Prashant Kumar Tiwari, and Arup Kumar Goswami
Efficient Approach for Establishing the Economic and Operating Reliability via Optimal Coordination of Wind-PSH-solar-storage Hybrid Plant in Highly Uncertain Double Auction Competitive Power Market, in «IET Renewable Power Generation» 12.10 (2018), pp. 1189–1202, DOI: 10.1049/iet-rpg.2016.0897.

[135] Shahab Karrari, Nicole Ludwig, Giovanni De Carne, and Mathias Noe
Sizing of Hybrid Energy Storage Systems Using Recurring Daily Patterns, in «IEEE Transactions on Smart Grid» 13.4 (2022), pp. 3290–3300, DOI: 10.1109/TSG.2022.3156860.

[136] Akseli Juslin
Complementing a Kaplan Hydropower Turbine with a Battery Energy Storage, 2021.

[137] Mohamed Regad, M'hamed Helaimi, Rachid Taleb, Ahmed M. Othman, and Hossam A. Gabbar
Control of Hybrid Power System Based Renewable Energy Generations Using PID Controller, in «International Journal of Power Electronics and Drive Systems (IJPEDS)» 11.4 (2020), p. 1775, DOI: 10.11591/ijpeds.v11.i4.pp1775-1784.

[138] Mutchimas Kheawcum and Somboon Sangwongwanich

A Case Study on Flywheel Energy Storage System Application for Frequency Regulation of Islanded Amphoe Mueang Mae Hong Son Microgrid, in *2020 17th International Conference on Electrical Engineering/Electronics, Computer, Telecommunications and Information Technology (ECTI-CON)*, 2020 17th International Conference on Electrical Engineering/Electronics, Computer, Telecommunications and Information Technology (ECTI-CON), Phuket, Thailand: IEEE, 2020, pp. 1–4, DOI: 10.1109/ECTI-CON49241.2020.9158108.

[139] Ali Asghar Khodadoost Arani, Gevork B. Gharehpetian, and Mehrdad Abedi
A Novel Control Method Based on Droop for Cooperation of Flywheel and Battery Energy Storage Systems in Islanded Microgrids, in «IEEE Systems Journal» 14.1 (2020), pp. 1080–1087, DOI: 10.1109/JSYST.2019.2911160.

[140] Danilo Laban
Hydro/Battery Hybrid Systems for Frequency Regulation, Msc Thesis, Escola Tècnica Superior d'Enginyria Industrial de Barcelona, 2019.

[141] Jin Tan and Yingchen Zhang
Coordinated Control Strategy of a Battery Energy Storage System to Support a Wind Power Plant Providing Multi-Timescale Frequency Ancillary Services, in «IEEE Transactions on Sustainable Energy» 8.3 (2017), pp. 1140–1153, DOI: 10.1109/TSTE.2017.2663334.

[142] Stalin Munoz Vaca, Charalampos Patsios, and Phil Taylor
Sizing of Hybrid Energy Storage Systems for Frequency Response of Solar Farms in Ecuador, in «2017 IEEE PES Innovative Smart Grid Technologies Conference - Latin America, ISGT Latin America 2017» 2017-January (2017), pp. 1–7, DOI: 10.1109/ISGT-LA.2017.8126749.

[143] Younghyun Kim, Vijay Raghunathan, and Anand Raghunathan
Design and Management of Battery-Supercapacitor Hybrid Electrical Energy Storage Systems for Regulation Services, in «IEEE Transactions on Multi-Scale Computing Systems» 3.1 (2017), pp. 12–24, DOI: 10.1109/TMSCS.2016.2627543.

[144] V. Gevorgian, E. Muljadi, Yusheng Luo, M. Mohanpurkar, R. Hovsapian, and V. Koritarov
Supercapacitor to Provide Ancillary Services, in «2017 IEEE Energy Conversion Congress and Exposition, ECCE 2017» 2017-January (October 2017), pp. 1030–1036, DOI: 10.1109/ECCE.2017.8095900.

[145] Umer Akram and Muhammad Khalid
A Coordinated Frequency Regulation Framework Based on Hybrid Battery-Ultracapacitor Energy Storage Technologies, in «IEEE Access» 6 (2017), pp. 7310–7320, DOI: 10.1109/ACCESS.2017.2786283.

[146] Stalin Munoz Vaca, Charalampos Patsios, and Phil Taylor
Enhancing Frequency Response of Wind Farms Using Hybrid Energy Storage Systems, in «2016 IEEE International Conference on Renewable Energy Research and Applications, ICRERA 2016» 5 (2016), pp. 325–329, DOI: 10.1109/ICRERA.2016.7884560.

[147] Blanca Torres, José Vara, José Ignacio Sarasúa, Juan Moreno, Juan Ignacio Pérez-Díaz, and Marcos Lafoz
Control Strategy and Sizing of a Flywheel Energy Storage Plant for the Frequency Control of an Isolated Wind-Hydro Power System, in «15 th Wind Integration Workshop» (2016).

[148] Iman Naziri Moghaddam and Badrul Chowdhury
Optimal Sizing of Hybrid Energy Storage Systems to Mitigate Wind Power Fluctuations, in «IEEE Power and Energy Society General Meeting» 2016-November (2016), pp. 1–5, DOI: 10.1109/PESGM.2016.7741862.

[149] Feng Guo and Ratnesh Sharma
Hybrid Energy Storage Systems Integrating Battery and Ultracapacitor for the PJM Frequency Regulation Market, in «IEEE Power and Energy Society General Meeting» 2016-November (2016), pp. 1–4, DOI: 10.1109/PESGM.2016.7741867.

[150] Linquan Bai, Fangxing Li, Qinran Hu, Hantao Cui, and Xin Fang
Application of Battery-Supercapacitor Energy Storage System for Smoothing Wind Power Output: An Optimal Coordinated Control Strategy, in «IEEE Power and Energy Society General Meeting» 2016-November (2016), pp. 1–5, DOI: 10.1109/PESGM.2016.7741798.

[151] Chunlian Jin, Ning Lu, Shuai Lu, Yuri V. Makarov, and Roger A. Dougal
A Coordinating Algorithm for Dispatching Regulation Services between Slow and Fast Power Regulating Resources, in «IEEE Transactions on Smart Grid» 5.2 (2014), pp. 1043–1050, doi: 10.1109/TSG.2013.2277974.

[152] Hansang Lee, Byoung Yoon Shin, Sangchul Han, Seyong Jung, Byungjun Park, and Gilsoo Jang
Compensation for the Power Fluctuation of the Large Scale Wind Farm Using Hybrid Energy Storage Applications, in «IEEE Transactions on Applied Superconductivity» 22.3 (2012), pp. 5701904–5701904, doi: 10.1109/TASC.2011.2180881.

[153] Chunlian Jin, Ning Lu, Shuai Lu, Yuri Makarov, and Roger A. Dougal
Coordinated Control Algorithm for Hybrid Energy Storage Systems, in «IEEE Power and Energy Society General Meeting» (2011), pp. 1–7, doi: 10.1109/PES.2011.6039893.

[154] Wei Li, Géza Joós, and Jean Bélanger
Real-Time Simulation of a Wind Turbine Generator Coupled with a Battery Supercapacitor Energy Storage System, in «IEEE Transactions on Industrial Electronics» 57.4 (2010), pp. 1137–1145, doi: 10.1109/TIE.2009.2037103.

[155] Wei Li and Géza Joós
A Power Electronic Interface for a Battery Supercapacitor Hybrid Energy Storage System for Wind Applications, in «PESC Record - IEEE Annual Power Electronics Specialists Conference» (2008), pp. 1762–1768, doi: 10.1109/PESC.2008.4592198.

[156] David Valentín, Alexandre Presas, Mònica Egusquiza, Jean-Louis Drommi, and Carme Valero
Benefits of Battery Hybridization in Hydraulic Turbines. Wear and Tear Evaluation in a Kaplan Prototype, in «Renewable Energy» 199 (2022), pp. 35–43, doi: 10.1016/j.renene.2022.08.117.

[157] Mohammed Ahmed Zabara, Can Berk Uzundal, and Burak Ülgüt

Performance Modeling of Unmanaged Hybrid Battery/Supercapacitor Energy Storage Systems, in «Journal of Energy Storage» 43 (2021), p. 103185, DOI: 10.1016/j.est.2021.103185.

[158] Umer AKRAM, Muhammad KHALID, and Saifullah SHAFIQ
An Innovative Hybrid Wind-Solar and Battery-Supercapacitor Microgrid System—Development and Optimization, in «IEEE Access» 5 (2017), pp. 25897–25912, DOI: 10.1109/ACCESS.2017.2767618.

[159] Mohammed GUEZGOUZ, Jakub JURASZ, Bennaissa BEKKOUCHE, Tao MA, Muhammad Shahzad JAVED, and Alexander KIES
Optimal Hybrid Pumped Hydro-Battery Storage Scheme for off-Grid Renewable Energy Systems, in «Energy Conversion and Management» 199 (2019), p. 112046, DOI: 10.1016/j.enconman.2019.112046.

[160] Yoga ANINDITO, Jannik HAAS, Marcelo OLIVARES, Wolfgang NOWAK, and Jordan KERN
A New Solution to Mitigate Hydropeaking? Batteries versus Re-Regulation Reservoirs, in «Journal of Cleaner Production» 210 (2019), pp. 477–489, DOI: 10.1016/j.jclepro.2018.11.040.

[161] Ning LU, Yuri V. MAKAROV, Mark R. WEIMAR, Frank RUDOLPH, Shashikala MURTHY, Jim ARSENEAUX, Clyde LOUTAN, and S. CHOWDHURY
THE WIDE-AREA ENERGY STORAGE AND MANAGEMENT SYSTEM PHASE II Final Report - Flywheel Field Tests, PNNL-19669, 991592, 2010, PNNL–19669, 991592, DOI: 10.2172/991592.

[162] L. BARELLI, G. BIDINI, F. BONUCCI, L. CASTELLINI, A. FRATINI, F. GALLORINI, and A. ZUCCARI
Flywheel Hybridization to Improve Battery Life in Energy Storage Systems Coupled to RES Plants, in «Energy» 173 (2019), pp. 937–950, DOI: 10.1016/j.energy.2019.02.143.

[163] T. R. AYODELE, A. S. O. OGUNJUYIGBE, and N. O. OYELOWO
Hybridisation of Battery/Flywheel Energy Storage System to Improve Ageing of Lead-Acid Batteries in PV-powered Applications, in «International Journal of Sustainable Engineering» 13.5 (2020), pp. 337–359, DOI: 10.1080/19397038.2020.1725177.

[164] Pawan SESHADRI VENKATESH, Vishnu CHANDRAN, and Sreeram ANIL

Study of Flywheel Energy Storage in a Pure EV Powertrain in a Parallel Hybrid Setup and Development of a Novel Flywheel Design for Regeneration Efficiency Improvement, in SAE WCX Digital Summit, 2021, pp. 2021-01–0721, DOI: 10.4271/2021-01-0721.

[165] V. Gevorgian, E. Muljadi, Yusheng Luo, M. Mohanpurkar, R. Hovsapian, and V. Koritarov
Supercapacitor to Provide Ancillary Services, in *2017 IEEE Energy Conversion Congress and Exposition (ECCE)*, 2017 IEEE Energy Conversion Congress and Exposition (ECCE), Cincinnati, OH: IEEE, 2017, pp. 1030–1036, DOI: 10.1109/ECCE.2017.8095900.

[166] Mohammed Abdulelah Albasheri, Ouahid Bouchhida, Youcef Soufi, Abdelhafidh Moualdia, and Mujammal Mujammal
Control And Power Management of DC Microgrid Based Wind/Battery/Supercapacitor, in *2022 IEEE 2nd International Maghreb Meeting of the Conference on Sciences and Techniques of Automatic Control and Computer Engineering (MI-STA)*, 2022 IEEE 2nd International Maghreb Meeting of the Conference on Sciences and Techniques of Automatic Control and Computer Engineering (MI-STA), Sabratha, Libya: IEEE, 2022, pp. 680–685, DOI: 10.1109/MI-STA54861.2022.9837665.

[167] Yuyan Liu, Zhongping Yang, Xiaobo Wu, Donglei Sha, Fei Lin, and Xiaochun Fang
An Adaptive Energy Management Strategy of Stationary Hybrid Energy Storage System, in «IEEE Transactions on Transportation Electrification» 8.2 (2022), pp. 2261–2272, DOI: 10.1109/TTE.2022.3150149.

[168] Mahmoud M. Mohamed, Helmy M. El Zoghby, Soliman M. Sharaf, and Magdi A. Mosa
Optimal Virtual Synchronous Generator Control of Battery/Supercapacitor Hybrid Energy Storage System for Frequency Response Enhancement of Photovoltaic/Diesel Microgrid, in «Journal of Energy Storage» 51 (2022), p. 104317, DOI: 10.1016/j.est.2022.104317.

[169] Khalid Abdullah Khan, Ammar Atif, and Muhammad Khalid
Hybrid Battery-Supercapacitor Energy Storage for Enhanced Voltage Stability in DC Microgrids Using Autonomous Control Strategy, in

Emerging Trends in Energy Storage Systems and Industrial Applications, Elsevier, 2023, pp. 535–569, DOI: 10.1016/B978-0-323-90521-3.00007-7.

[170] Quanyuan JIANG and Haisheng HONG
Wavelet-Based Capacity Configuration and Coordinated Control of Hybrid Energy Storage System for Smoothing out Wind Power Fluctuations, in «IEEE Transactions on Power Systems» 28.2 (2013), pp. 1363–1372, DOI: 10.1109/TPWRS.2012.2212252.

[171] Jingang HAN, Jean-Frederic CHARPENTIER, and Tianhao TANG
An Energy Management System of a Fuel Cell/Battery Hybrid Boat, in «Energies» 7.5 (5 2014), pp. 2799–2820, DOI: 10.3390/en7052799.

[172] Julio Alberto ALTERACH, Silvia Maria CANAVESE, Antonio GATTI, Marco Raffaele RAPIZZA, Giuseppe STELLA, Roberto CALISTI, Giovanna CAVAZZINI, and Stefano CASARIN
Sviluppo di un modello numerico dinamico di pompaggio idroelettrico ibrido e impostazione metodologica per la localizzazione degli impianti, in (2020).

[173] Julio Alberto ALTERACH, Silvia Maria CANEVESE, Antonio GATTI, Marco Raffaele RAPIZZA, Giovanna CAVAZZINI, and Stefano CASARIN
Modello dinamico ottimizzato del pompaggio ibrido, in (2021).

[174] Massimo MEGHELLA, Julio ALTERACH, Elena GOBBI, Giacomo GARDINI, and Ruggero MARAZZI
Studi e Analisi Di Pre-Fattibilità per l'integrazione Ottimale in Rete Dell'energia Prodotta Da Fonti Rinnovabili Mediante Sistemi Di Pompaggio Marino, Technical report, Ricerca sul Sistema Energetico, 2013.

[175] Julio ALTERACH et al.
Progetto Di Massima e Valutazione Tecnico Economica Di Un Impianto Di Pompaggio e Generazione Marino, Mediante l'utilizzo Di Macchine Reversibili a Giri Variabili. Technical report, Ricerca sul Sistema Energetico, 2014.

[176] Julio ALTERACH, Roberto Maurizio CALISTI, Maria Vittoria CAZZOL, Giuseppe BRUNO, Ruggero MARAZZI, Angelo L'ABBATE, Andrea AMICARELLI, Andrea DANELLI, Francesco CARERI, and Simone SPERATI

Impianto Di Pompaggio Marino: Iniziative per La Fattibilità e l'integrazione Ottimale in Rete, Technical report, Ricerca sul Sistema Energetico, 2015.

[177] TERNA
L'elettricità nelle regioni, TERNA, 2020.

[178] MATLAB
9.13.0.2126072 (R2022b), Natick, Massachusetts: The MathWorks Inc., 2021.

[179] Pierangelo Andreini
Manuale Dell'ingegnere Meccanico, Hoepli Editore, 2002.

[180] M. Hanif Chaudhry
Applied Hydraulic Transients, New York, NY: Springer New York, 2014, doi: 10.1007/978-1-4614-8538-4.

[181] Xianlin Liu and Chu Liu
Eigenanalysis of Oscillatory Instability of a Hydropower Plant Including Water Conduit Dynamics, in «IEEE Transactions on Power Systems» 22.2 (2007), pp. 675–681, doi: 10.1109/TPWRS.2007.895156.

[182] F. P. de Mello et al.
Hydraulic Turbine and Turbine Control Models for System Dynamic Studies Working Group on Prime Mover and Energy Supply Models for System Dynamic Performance Studies, in «IEEE Transactions on Power Systems» 7.1 (1992), pp. 167–179, doi: 10.1109/59.141700.

[183] Juan Ignacio Pérez-Díaz, José Ignacio Sarasúa, and José Román Wilhelmi
Contribution of a Hydraulic Short-Circuit Pumped-Storage Power Plant to the Load-Frequency Regulation of an Isolated Power System, in «International Journal of Electrical Power and Energy Systems» 62 (2014), pp. 199–211, doi: 10.1016/j.ijepes.2014.04.042.

[184] Abdullah Altay, Cem Şahin, İres İskender, Doğan Gezer, and Caner Çakir
A Compensator Design for the Aged Hydro Electric Power Plant Speed Governors, in «Electric Power Systems Research» 133 (2016), pp. 257–268, doi: 10.1016/j.epsr.2015.12.016.

[185] S.P Mansoor, D.I Jones, D.A Bradley, F.C Aris, and G.R Jones
Reproducing Oscillatory Behaviour of a Hydroelectric Power Station by Computer Simulation, in «Control Engineering Practice» 8.11 (2000), pp. 1261–1272, DOI: 10.1016/S0967-0661(00)00068-X.

[186] Ana Fernández-Guillamón, Eduard Muljadi, and Angel Molina-García
Frequency Control Studies: A Review of Power System, Conventional and Renewable Generation Unit Modeling, in «Electric Power Systems Research» 211 (2022), p. 108191, DOI: 10.1016/j.epsr.2022.108191.

[187] German Ardul Munoz-Hernandez, Sa'ad Petrous Mansoor, and Dewi Ieuan Jones
Modelling and Controlling Hydropower Plants, Advances in Industrial Control, London: Springer London, 2013, DOI: 10.1007/978-1-4471-2291-3.

[188] Jan Machowski, Zbigniew Lubosny, Janusz W Bialek, and James R Bumby
Power System Dynamics: Stability and Control, John Wiley & Sons, 2020.

[189] E. Kopf and S. Brausewetter
Control Strategies for Variable Speed Machines - Design and Optimization Criteria, in «Hydro» (figure 1 2005).

[190] Linn Saarinen, Per Norrlund, and Urban Lundin
Field Measurements and System Identification of Three Frequency Controlling Hydropower Plants, in «IEEE Transactions on Energy Conversion» 30.3 (2015), pp. 1061–1068, DOI: 10.1109/TEC.2015.2425915.

[191] Weijia Yang, Jiandong Yang, Wencheng Guo, Wei Zeng, Chao Wang, Linn Saarinen, and Per Norrlund
A Mathematical Model and Its Application for Hydro Power Units under Different Operating Conditions, in «Energies» 8.9 (2015), pp. 10260–10275, DOI: 10.3390/en80910260.

[192] Weijia Yang and Jiandong Yang

Advantage of Variable-Speed Pumped Storage Plants for Mitigating Wind Power Variations: Integrated Modelling and Performance Assessment, in «Applied Energy» 237 (2019), pp. 720–732, DOI: 10.1016/j.apenergy.2018.12.090.

[193] Weijia YANG, Per NORRLUND, Linn SAARINEN, Jiandong YANG, Wei ZENG, and Urban LUNDIN
Wear Reduction for Hydropower Turbines Considering Frequency Quality of Power Systems: A Study on Controller Filters, in «IEEE Transactions on Power Systems» 32.2 (2017), pp. 1191–1201, DOI: 10.1109/TPWRS.2016.2590504.

[194] Chirag TRIVEDI, Bhupendra GANDHI, and Cervantes J. MICHEL
Effect of Transients on Francis Turbine Runner Life: A Review, in «Journal of Hydraulic Research» 51.2 (2013), pp. 121–132, DOI: 10.1080/00221686.2012.732971.

[195] Olivier PACOT, Thomas de COLOMBEL, Claire SEGOUFIN, Joachim DELANNOY, Sebastian LEGUIZAMON, João DELGADO, Miguel ROQUE, and Cécile MÜNCH-ALLIGNÉ
EFFECT OF THE VARIABLE SPEED ON THE HYDRAULIC BEHAVIOR OF THE CANIÇADA FRANCIS TURBINE, in (2021), p. 15.

[196] J. YANG, G. PAVESI, S. YUAN, G. CAVAZZINI, and G. ARDIZZON
Experimental Characterization of a Pump–Turbine in Pump Mode at Hump Instability Region, in «Journal of Fluids Engineering» 137.5 (2015), p. 051109, DOI: 10.1115/1.4029572.

[197] Andreas JOSSEN
Fundamentals of Battery Dynamics, in «Journal of Power Sources» 154.2 (2006), pp. 530–538, DOI: 10.1016/j.jpowsour.2005.10.041.

[198] ADAM NIESLONY
Rainflow Counting Algorithm, MATLAB Central File Exchange, 2020, URL: https://www.mathworks.com/matlabcentral/fileexchange/3026-rainflow-counting-algorithm (visited on 12/26/2020).

[199] Dominique FRANÇOIS, André PINEAU, and André ZAOUI

Mechanical Behaviour of Materials, Vol II: Viscoplasticity, Damage, Fracture and Contact Mechanics, Springer Netherlands, 1998.

[200] Jorge Torres, Pablo Moreno-Torres, Gustavo Navarro, Marcos Blanco, and Marcos Lafoz
Fast Energy Storage Systems Comparison in Terms of Energy Efficiency for a Specific Application, in «IEEE Access» 6 (2018), pp. 40656–40672, DOI: 10.1109/access.2018.2854915.

[201] Jorge Torres, Gustavo Navarro, Marcos Blanco, Mariano González-de-Soto, Luis García-Tabares, and Marcos Lafoz
Efficiency Map to Evaluate the Performance of Kinetic Energy Storage Systems Used with Renewable Generation, in *2018 20th European Conference on Power Electronics and Applications (EPE'18 ECCE Europe)*, IEEE, 2018, P–1.

[202] Gustavo Navarro Soriano
Modelado y Dimensionado de Un Sistema de Almacenamiento Basado En Supercondensadores Para La Integración En Red de Energías Renovables, PhD thesis, Universidad Politécnica de Madrid, 2022, DOI: 10.20868/UPM.thesis.70483.

[203] Helix Power
Regenerative Braking Using Flywheels, Proceedings of the NY-BEST Energy Storage Technology Conference (Syracuse, NY, USA), 2016.

[204] R. Boyle and J. Kure-Jensen
Fixed Costs of Providing Ancillary Services from Power Plants: Reactive Supply and Voltage Control, Regulation and Frequency Response, Operating Reserve - Spinning, TR-107270-V5, Palo Alto, CA: EPRIGEN, 1997, p. 58.

[205] J. Stein
Cost of Providing Ancillary Services from Power Plants Operating Reserve - Spinning, TR-107270-V4, EPRI, 1997.

[206] *Cost of Providing Ancillary Services from Power Plants - Volume 1: A Primer*, TR-107270-V1, EPRI, 1997.

[207] *Cost of Providing Ancillary Services From Power Plants - Regulation and Frequency Response*, TR-107270-V2, EPRI, 1997, p. 88.

[208] Cliff W Hamal and Arun Sharma
Adopting a Ramp Charge to Improve Performance of the Ontario Market, in (2006), p. 53.

[209] TERNA
Progetto Pilota Servizio di regolazione ultra-rapida di frequenza (" Fast Reserve ") Relazione di accompagnamento, Relazione di accompagnamento, TERNA, 2019, pp. 1–8.

[210] ARERA
Approvazione Del Regolamento, Predisposto Da Terna S.p.A., Ai Sensi Della Deliberazione Dell'Autorità 300/2017/R/Eel, Relativo al Progetto Pilota per l'erogazione Del Servizio Di Regolazione Ultra-Rapida Di Frequenza, URL: https://www.arera.it/it/docs/20/200-20.htm (visited on 01/18/2022).

[211] TERNA
Progetto Pilota Fast Reserve – Esiti Asta - Terna spa, URL: https://web.archive.org/web/20230322130850/https://www.terna.it/it/sistema-elettrico/pubblicazioni/news-operatori/dettaglio/esiti-asta-Fast-reserve (visited on 03/22/2023).

[212] ARERA
ARERA - Regime Transitorio per Il Trattamento Economico Dell'energia Erogata Dalle Unità Di Produzione per La Regolazione Primaria Di Frequenza, URL: https://www.arera.it/it/docs/14/066-14.htm (visited on 03/22/2023).

[213] ARERA
ARERA - Trattamento Economico Dell'energia Erogata Dalle Unità Di Produzione per La Regolazione Primaria Di Frequenza, URL: https://www.arera.it/it/docs/13/231-13.htm (visited on 03/22/2023).

[214] TERNA
Specifiche tecniche per la verifica e valorizzazione del servizio di regolazione primaria di frequenza, Versione per consultazione Annex A73, TERNA, 2013.

[215] TERNA
Codice di trasmissione, dispacciamento, sviluppo e sicurezza della rete - Capitolo 4: Regole per il dispacciamento, URL: https://www.terna.it/it/sistema-elettrico/codici-rete/codice-rete-italiano (visited on 03/22/2023).

[216] Guido Ardizzon, Giovanna Cavazzini, and Giorgio Pavesi
Adaptive Acceleration Coefficients for a New Search Diversification Strategy in Particle Swarm Optimization Algorithms, in «Information Sciences» 299 (2015), pp. 337–378, DOI: 10.1016/j.ins.2014.12.024.

[217] Michael Angelo A. Pedrasa, Ted D. Spooner, and Iain F. MacGill
A Novel Energy Service Model and Optimal Scheduling Algorithm for Residential Distributed Energy Resources, in «Electric Power Systems Research» 81.12 (2011), pp. 2155–2163, DOI: 10.1016/j.epsr.2011.06.013.

[218] Masoud Sharafi and Tarek Y. ELMekkawy
Multi-Objective Optimal Design of Hybrid Renewable Energy Systems Using PSO-simulation Based Approach, in «Renewable Energy» 68 (December 2014), pp. 67–79, DOI: 10.1016/j.renene.2014.01.011.

[219] Rabindra Kumar Sahu, Sidhartha Panda, and G. T. Chandra Sekhar
A Novel Hybrid PSO-PS Optimized Fuzzy PI Controller for AGC in Multi Area Interconnected Power Systems, in «International Journal of Electrical Power and Energy Systems» 64 (2015), pp. 880–893, DOI: 10.1016/j.ijepes.2014.08.021.

[220] Deepak Kumar Gupta, R. Naresh, and Amitkumar Vidyakant Jha
Automatic Generation Control for Hybrid Hydro-Thermal System Using Soft Computing Techniques, in «2018 5th IEEE Uttar Pradesh Section International Conference on Electrical, Electronics and Computer Engineering, UPCON 2018» (2018), pp. 1–6, DOI: 10.1109/UPCON.2018.8597013.

[221] Roberto Marconato
Sistemi elettrici di potenza, Milano: CLUP, 1984.

[222] Marco Raffaele Rapizza, Adriano Iaria, and Diego Cirio
Regolazioni Innovative Dell'eolico: Impatto Sulla Stabilità Di Frequenza, in «Energia Elettrica» 2 (2020), pp. 37–51.

[223] TERNA
Centrali Eoliche Condizioni generali di connessione alle reti AT Sistemi di protezione regolazione e controllo, Guida Tecnica Annex A.17, TERNA, 2018.

[224] TERNA
Impianti Di Produzione Fotovoltaica Requisiti Minimi per La Connessione e l'esercizio in Parallelo Con La Rete AT, Guida Tecnica Annex A.68, TERNA, 2012.

[225] TERNA
Regolazione tecnica dei requisiti di sistema della generazione distribuita, Guida Tecnica Annex A.70, 2012.

[226] Ministero dello Sviluppo Economico
Strategia Energetica Nazionale, 2017.

[227] Lanati, F., Gelmini, A., Moneta, D., Viganò, G, Iaria, A, and Rapizza, M. R.
Studi a Supporto Della Governance Dei Sistemi Elettrici, 18001055, Milano: RSE, Ricerca di Sistema, 2018.

[228] D. Siface, M. T. Vespucci, and A. Gelmini
Solution of the Mixed Integer Large Scale Unit Commitment Problem by Means of a Continuous Stochastic Linear Programming Model, in «Energy Systems» 5.2 (2014), pp. 269–284, doi: 10.1007/s12667-013-0107-z.

[229] Alessio Agrillo, Vincenzo Surace, and Paolo Liberatore
Solare Fotovoltaico - Rapporto Statistico 2019, Gestore dei Servizi Energetici S.p.A., 2020.